JAERI-M
5564

Annual Report of JAERI Thermonuclear Fusion Laboratory

(covering the period April 1, 1972
—March 31, 1973)

February 1974

Thermonuclear Fusion Laboratory

日本原子力研究所
Japan Atomic Energy Research Institute

この報告書は，日本原子力研究所が JAERI-M レポートとして，不定期に刊行している研究報告書です．入手，複製などのお問合わせは，日本原子力研究所技術情報部（茨城県那珂郡東海村）あて，お申しこしください．

JAERI-M reports, issued irregularly, describe the results of research works carried out in JAERI. Inquiries about the availability of reports and their reproduction should be addressed to Division of Technical Information, Japan Atomic Energy Research Institute, Tokai-mura, Naka-gun, Ibaraki-ken, Japan.

JAERI-M 5564

Annual Report of the JAERI Thermonuclear Fusion Laboratory

(covering the period April 1, 1972 - March 31, 1973)

Thermonuclear Fusion Laboratory, Tokai, JAERI

(Received January 21, 1974)

Activities in Thermonuclear Fusion Laboratory for the period of April 1972 to March 1973 are described. During the period, the JFT-2 tokamak was brought into operation, as scheduled, and hot plasma confinement was achieved. In the JFT-1 hexapole, plasma loss processes and low-frequency fluctuations were investigated The design of a tokamak with a teardrop-shaped cross-section with an axisymmetric divertor (JFT-2a) was completed and construction of the device was started. Theoretical studies were also made of the equilibrium of a free-boundary toroidal plasma, the influence of impurity ions and surrounding neutral gases on the tokamak confinement, and thermal stability and control of a reactor "core plasma".

核融合研究室年報（昭和47年度）

日本原子力研究所東海研究所核融合研究室

（1974年1月21日受理）

核融合研究室における昭和47年度の研究進行状況をまとめたものである。この期間，JFT－2装置の運転が開始され，高温プラズマの閉じ込めについて満足すべき成果が得られた。JFT－1では，プラズマの損失過程，低周波不安定性が詳しく調べられた。軸対称ダイバータを備えた涙滴型断面トカマクの設計が完了し，装置（JFT－2a）の建設が始められた。これらと平行してプラズマ平衡の自由境界問題，不純物イオンおよび中性ガスのトカマク閉じ込めにおよぼす影響，“炉心”プラズマの熱的安定性と制御の問題などについて理論的研究が進められた。

CONTENTS

Preface

During the period covered by the third annual report*, the successful operation of the JFT-2 tokamak is first to be mentioned. The machine was completed in March, 1972, and after repairing some initial troubles and measuring the machine characteristics, plasma of electron and ion temperature of 700 eV and 210 eV, respectively and density of (1-2) x 10^{13} cm^{-3} was confined with the energy confinement time of 20 ms, in February, 1973. As for more detailed information of the plasma, we have to wait for laser scattering experiment, scheduled in the fall of 1973.

A brief summary of the activities in this period is as follows. Plasma confinement in JFT-1, a toroidal hexapole, was studied. Improvements of JFT-1 were made on two points: 1) a symmetric shell was installed inside the vacuum chamber to reduce the field errors due to the asymmetry of induced wall currents, 2) the outer hoops were changed to new ones of smaller cross-sections to increase the available flux around the hoops. After these improvements, anomaly in diffusion coefficient near the outer hoop reduced significantly. Collisionless drift waves were identified and the interpretation of the observed mode transition in poloidal mode number was made in comparison with linear theory with slab geometry.

After the completion of JFT-2, we encountered some troubles (vacuum leaks, outgassing from the wall and limiter, trouble in turbo-molecular pumps etc.). Trouble hunting was really a time-consuming job due to inconvenience in assembling and disassembling, which is inevitable in a fat tokamak of medium size like JFT-2. But after this initial trouble, JFT-2 has been operating reliably with no accidental shutdown longer than a week since November, 1972. Compared to the JFT-2 machine itself, preparation of diagnostic systems is rather delayed by budgetary and man-power reasons.

Design of a tokamak with a teardrop-shaped cross-section with an axisymmetric divertor was completed. In the course of the design, equilibrium and stability of noncircular plasma of one and two dimensions were investigated and techniques of the evaporation of gold onto copper shell were critically tested. An apparatus based on this design will be constructed in 1974.

Computer codes of non-linear kink, tearing and dissipative drift instabilities were developed. Behaviour of impurity ions in the plasma and "gas insulation" were studied. A tokamak with noncircular cross-section was also studied theoretically.

Study of thermal stability and control of reactor "core plasma" was completed as a general theoretical consideration. A series of papers on this study was awarded a Prize of Atomic Energy Society of Japan (Ohta, Yamato and Mori).

(S. Mori)

*The first annual report is JAERI-M 4564 and the second one JAERI-M 5029.

I. TOROIDAL CONFINEMENT EXPERIMENTS

1. JFT-1

S. Arizono, T. Nagashima, H. Ohtsuka,
T. Shiina, S. Tamura and H. Yamato*

1.1 Introduction

As mentioned in the previous annual report (JAERI-M 5029), improvements of the JFT-1 magnetic field were made by installing a toroidal conducting shell inside the vacuum chamber to reduce the field asymmetry due to induced wall currents, and by replacing the outer hoops by new ones of smaller cross-sections to increase the available magnetic flux around them. Our main emphasis has been on understanding plasma loss processes in JFT-1, especially the influence of the field asymmetry and of obstacles in the plasma. We have also emphasized studies of low-frequency fluctuations in the microwave-produced plasma. In the following sections these experiments will be described separately.

1.2 Plasma loss processes

(1) Possible causes of plasma loss

Confinement experiments in JFT-1 have been made, in this period, putting an emphasis on investigation of two possible causes of anomalous plasma transport. One of these causes we considered is magnetic field errors produced by inhomogeneity of induced wall current; disturbance in the wall currents due to various portholes of the vacuum chamber will cause the destruction of the azimuthal symmetry of the magnetic field. The effect of field errors on the plasma confinement have been studied in several internal ring devices[1),2),3),6)]. Some of those experiments[1),3)] have pointed out that an azimuthally asymmetric error field affects to a considerable extent the plasma confinement properties. Therefore, the introduction of an azimuthally symmetric conducting shell (Fig. 1) is expected to improve the symmetry of the magnetic field and to reduce the anomalous loss in the hexapole device.

---

*On leave from The Research and Development Center, Tokyo Shibaura Electric Co., Ltd.

Another possible cause of the anomalous loss is an obstacle-induced plasma convection. Our device has twenty supports in total. These supports will induce azimuthal inhomogeneity of plasma potentials and this will probably cause the enhancement of plasma loss by forming convective flows. To study the effect of existing supports experimentally, a model support was introduced into the plasma and subsequent changes in the plasma were investigated.

(2) Effect of a toroidal conducting shell

The results of the experiment is summarized bellow.

1) Azimuthal distribution of loss fluxes: azimuthal inhomogeneity of loss fluxes still exists.

2) Loss ratio versus magnetic field strength (Fig. 2): the loss ratio to the hoop is considerably reduced with the increase of the magnetic field strength.

3) Confinement time τ calculated by $\tau = (\frac{1}{N}\frac{dN}{dt})^{-1}$, and perpendicular confinement time $\tau_\perp = \frac{\Gamma_{11}+\Gamma_\perp}{\Gamma_\perp}$ where Γ_{11} and $\Gamma_\perp$ are the parallel and the perpendicular loss fluxes, respectively (Fig. 3): $\tau_\perp$ is slightly improved, whereas no improvement in the overall confinement time τ is observed.

4) Effective diffusion coefficients $<D>$'s estimated from the density gradient and the loss fluxes (Fig. 4): $<D>$'s near the inner hoop and near the wall show no apparent change, but considerable decrease in $<D>$'s are observed near the outer hoop.

In summary, the introduction of the conducting shell seems to cause no appreciable change in the overall plasma behavior, while the reduction of the cross-section of the outer hoops contributed significantly to reduce the particle loss to the hoop. The experiment was made with microwave-produced hydrogen plasma with $n \sim 3 \times 10^{10}$ cm^{-3} and $T_e \sim 0.5$ eV.

(3) Support-induced convection

The experimental arrangement is shown in Fig. 5. The model support used in this experiment was 10 mm-diam. stainless steel rod, which was introduced on the outer hoop surface penetrating the plasma confinement region. A brief summary of the experimental results is as follows.

1) Floating potential across and along the model support: a charge separation electric field due to the average grad B drift is observed across the model support.

2) Enhanced loss fluxes by the model support: in the downstream side with

respect to the ion grad B drift the enhancement is stronger than in the upstream side.

3) Floating potential at the separatrix across the model support: the floating potential near the support at the separatrix is found to be slightly less negative; namely, an azimuthal electric field arises across the support at the separatrix where no grad B drift is present.

4) Density profile along the model support: a shift of the plasma density profile occurs in the direction of E x B flow where E is the electric field mentioned above. This is also in agreement with the observed enhancement of the loss fluxes.

Combining these results, we can image consistently a support-induced convection as shown in Fig. 6. This experiment was carried out mainly with helium plasma with $n \sim 10^{11}$ cm^{-3} and $T_e \sim 2$ eV.

(4) Conclusion

The effect of the field error produced by the inhomogeneous wall currents on the plasma confinement seems to be insignificant in the hexapole device. As to the convective loss, a support-induced convection loss was found experimentally. A similar experiment has been made in the Wisconsin toroidal octupole[4),5)]. The result of both experiments agrees qualitatively with each other, but the interpretation was made in a different way. A convection by an azimuthal electric field has also been observed in our additional error field experiment[6)].

(H. Ohtsuka, S. Tamura and H. Yamato)

1.3 Fluctuation studies

(1) Collisionless drift waves*

Low-frequency fluctuations of drift type are observed in the hexapole. It is shown that mode transition of poloidal mode number occurs at a critical toroidal field superimposed on the hexapole field as the toroidal field is increased.

A hydrogen plasma is produced by the electron resonance heating in the hexapole[7)]. The density n_0 on the separatrix is 2×10^{10} cm^{-3}, with the decay constant 0.8 msec, and the electron temperature T_e is 0.7 eV at 0.4 msec after the heating power is turned off. The ion temperature T_i is estimated to be ~ 0.1 eV from a calculation of the ion heating by Coulomb collisions and simultaneous

cooling by charge exchange. The average hexapole field on the stability limit line is 460 G. The magnitude of superimposed toroidal field is measured to be $B_T = 44.2\, I_T/R$ (G), where I_T (A) is a toroidal-coil current and R (cm) is the major radius. The maximum shear parameter in the present experiment is $\Theta = i/\kappa L_s = 3.7 \times 10^{-3}$ in the wall region where the fluctuations are localized ($\kappa = \nabla n_0/n_0$).

Fluctuations varying nearly sinusoidally in time are observed only in the region where the density falls off towards the wall. The amplitude is maximum ($\sim$12 %) where the density gradient is maximum with $\nabla n_0/n_0 = 3.2\ \mathrm{cm}^{-1}$, while it is nearly constant along a flux line. The spatial properties of the waves are studied by measuring the relative phase difference of the probe signals at various positions. The observed frequency and azimuthal wavelength are shown in Figs. 7 and 8 as a function of toroidal field. Three branches of curves are obtained with the addition of B_T to the hexapole field. Using three probes on the same flux line, poloidal mode number n is found to be constant in each branch and observed to be n = 1 without B_T and successively n = 0, -1, and -2 with increasing B_T. The jumps of the frequency (see Fig. 7) and the azimuthal wavelength (see Fig. 8) are accompanied by these mode transitions in the poloidal mode number. The parallel and perpendicular wavelengths are determined from the observed azimuthal wavelength and poloidal mode number as shown in Fig. 9 (a) and (b). The wave behaviours in the ($\lambda_{\parallel}\kappa$, $k_\perp \rho_i$) plane with and without B_T are summarized in Fig. 10, where $\lambda_{\parallel} = 2\pi/k_{\parallel}$ and the ion Larmor radius ρ_i is 1 mm. The solid circle represents the wave without B_T. Open circles, rectangles, and triangles are the modes with n = 0, -1, and -2, respectively. Also shown are the stable and unstable regions of the collisionless drift wave and contour lines of constant growth rate, $\gamma = \omega_I/\kappa v_{thi}$, where ω_I is the imaginary part of the frequency ω and v_{thi} is the ion thermal velocity ($T_e/T_i = 10$, $\nabla T_e = 0$; by Brossier[8]). The potential fluctuation $\tilde{\phi}$ is detected with a high impedance probe. The amplitude satisfies the relationship $\tilde{n}_0/n_0 = e\tilde{\phi}/KT_e$ within a factor of 2 as expected from an electrostatic mode. The observed wave characteristics in the plasma rest frame are summarized in Table I. The correction of $\vec{E}_0 \times \vec{B}$ plasma rotation due to a radial electric field $\vec{E}_0$ is made. The Doppler shift of the frequency is less than 30 %. These observations are consistent with those expected for the density-gradient-driven drift wave.[9] Collisional effects may not be negligible in the range of the ratio of electron-ion collision frequency to wave frequency, ν_{ei}/ω = 1-5, in the present experiment.[10] However, the observed drift wave is likely a collision-

less mode since the stabilization with increasing B_T can be explained by ion Landau damping of a collisionless mode, but not by viscosity stabilization of a collisional mode.

Figure 11 compares the experimental dispersion relation with the theoretical ones; the upper dashed line predicted qualitatively for a $\beta = 0$ plasma in the multipole configuration[11] and the solid curve calculated for a $T_e = T_i$ plasma with slab geometry.[12] The open and closed circles represent the waves with and without B_T, respectively. With the addition of B_T to the hexapole field the wave jumps to a smaller $k_\perp \rho_i$ with a frequency drop. The observed decreases in ω and $k_\perp$ with the addition of B_T are seen to be consistent with those expected from the dispersion curve. The waves with and without B_T are in the same mode and are likely to be density-gradient-driven collisionless drift waves.

As to the mode transition of poloidal mode number n, it is assumed, in anology with other results,[13),14)] that a mode with a given n becomes dominant if it has a larger growth rate than those of the other modes. The dashed lines in Fig. 10 are calculated from the boundary condition imposed on $k_\parallel$ and $k_\perp$ of the modes with $n = 1$ and $n = 0$ for $I_T = 2$ A. The mode that appears first with the addition of B_T is expected to be the mode with $n = 0$ from the curve. Further successive mode transitions of $n = 0, -1, -2, \cdots$ are predicted to occur with increasing B_T. These theoretically predicted results agree qualitatively with the experimental results. It is observed that the amplitude of the fluctuation in each branch tends to decrease as B_T is increased. The stabilization in each branch with increasing B_T is likely due to ion Landau damping in the collisionless regime,[12),14)] because under the condition $\omega < \omega_{*e}$ a decreasing ratio of $v_\parallel / v_{thi}$ with B_T is found 5-6, near the transition region, which is in reasonable agreement with a theoretical value of 2.6[14].

In the above discussions we have neglected the effect of magnetic shear since the maximum shear parameter is 3.7×10^{-3} which is smaller than a theoretical value required for shear stabilization of drift waves[15] at least by a factor of 10.

An estimate of plasma loss due to the fluctuation indicates that the drift wave is responsible for part of the wall loss ($\lesssim$30 % of the total loss)[7], although no dependence of the confinement time on the fluctuation amplitude is observed within experimental errors.

(T. Nagashima, S. Arizono and T. Shiina)

---

*Phys. Rev. Letters 31, 82 (1973).

(2) A localized mode

Another type of mode, localized around the points of maximum of unfavourable magnetic curvature or of maximum magnetic field, is also observed in the hexapole. The frequency in the laboratory frame is in the range of 100-140 kHz for ECRH-hydrogen plasmas with $n_0 = 2 \times 10^{10}$ cm^{-3}, $T_e = 0.7$ eV, $T_i \simeq 0.1$ eV and neutral density is equal to 2×10^{12} cm^{-3}. The radial profile of the fluctuation amplitude is peaked near the point of the maximum density gradient towards the wall.

The profile of the fluctuation along a field line, studied using a multiple probe system at several points simultaneously, is a standing wave that has loops at maxima of the unfavourable magnetic curvature or at maxima of the hexapole field (Fig. 12). The fluctuations at P and Q are 180 degrees out of phase, while in phase at Q and R. The observed wave characteristics in the plasma rest frame are summarized in Table II.

A possible instability which is localized in the unfavourable curvature is a drift balooning instability.[9),12),16)] In the hexapole geometry, however, drift wave cannot be localized in the unfavourable curvature, since the maximum of $\kappa + b$ corresponds to a minimum of the magnetic field where $\kappa = 2\ \partial \ln B / \partial \ln n_0$, $b = k_\perp{}^2 T_e / M\Omega_i{}^2$. Other possibilities are an electron trapped particle mode[11),12),17)] and a mode represented by the branch (j) in Ref. (11), a residually unstable positive energy wave. Observations made so far are consistent with the mode of the branch (j), but more detailed comparison, for example, comparison of observed amplitude distribution with theoretical prediction is required to confirm the identity.

(S. Arizono, T. Nagashima and T. Shiina)

Referemces

1) M. Yoshikawa, et al.: Gulf-GA-A12006 (January, 1971).
2) M. Okabayashi and R. Freeman : Phys. Fluids 15, 1346 (1972).
3) T. Jernigan, R. Prater and D. M. Meade : Phys. Fluids 14, 1235 (1971).
4) H. Forsen, et al. : Plasma Physics and Controlled Nuclear Fusion Research, 1969, Vol. I, p.313 (IAEA, Vienna, 1969).
5) J. A. Schmidt and G. L. Schmidt : Phys. Fluids 13, 1351 (1970).
6) S. Tamura, et al. : in Proceedings of Fifth European Conference on Controlled Fusion and Plasma Physics, Grenoble, August 21-25, 1972, Vol. I, 94, and JAERI-M 5029 (October, 1972).

7) S. Tamura, et al. : Plasma Physics and Controlled Nuclear Fusion Research, 1971, Vol. I, p. 75 (IAEA, Vienna, 1971).

8) P. Brossier : EURATOM-Commissariat à l'Energie Atomique Report No. EUR-CEA-FC-565 (1970).

9) N.A. Krall and M.N. Rosenbluth : Phys. Fluids 8, 1488 (1965).
P.A. Rutherford and E.A. Frieman : Phys. Fluids 11, 569 (1968).
P. Brossier, et al. : Phys. Rev. Letters 26, 124 (1971).

10) D. K. Bhadra : Phys. Fluids 14, 977 (1971).

11) R. J. Hastie and J. B. Taylor : Plasma Physics 13, 265 (1971).

12) S. Yoshikawa : in "Methods of Experimental Physics" edited by H. R. Griem and B. Lovberg, Vol. 9, Part A, Academic, 319 (1970).

13) H. W. Hendel, et al. : Phys. Rev. Letters 18, 439 (1967).
H. W. Hendel, et al. : Phys. Fluids 11, 2426 (1968).

14) P. A. Politzer : Phys. Fluids 14, 2410 (1971).

15) J. D. Jukes : Phys. Fluids 7, 1468 (1964).
P. H. Rutherford and E. A. Frieman : Phys. Fluids 10, 1007 (1967).
L. D. Pearlstein and H. L. Berk : Phys. Rev. Letters 23, 220 (1969).
M. Mishin : Soviet Phys. JETP 32, 1218 (1971).

16) B. Coppi, et al. : Phys. Rev. Letters 29, 190 (1968).

17) P. Rutherford, et al. : Plasma Physics and Controlled Nuclear Fusion Research, 1969, Vol. I, p. 367 (IAEA, Vienna, 1969).
B. Coppi, et al. : Phys. Rev. Letters 21, 1055 (1968).

TABLE I. Measured wave characteristics in the plasma rest frame.

I_T (A)	0	2-80
Frequency (kHz)	59	19-39
Perpendicular wavelength (cm)	2.0-3.2	3.6-8.7
Perpendicular phase velocity $v_\perp$ (10^5 cm/sec)	1.2-2.7	0.7-3.4
ω / ω_{*e}	0.7-0.9	0.5-0.8
$k_\perp \rho_i$	0.21-0.3	0.09-0.18
Propagation	Electrons	Electrons
Parallel wavelength (cm)	80	89-749
Parallel phase velocity $v_\parallel$ (10^6 cm/sec)	4.7-6.8	1.7-29
$v_\parallel / v_{the}$	0.1-0.14	0.04-0.6
Phase difference $\Delta_\Psi = \Psi(\tilde{n}) - \Psi(\tilde{\phi})$ (deg)	71 ± 27	94 ± 51

TABLE II. Measured wave characteristics of the localized mode in the plasma rest frame.

Frequency (kHz)		130
Perpendicular wavelength (cm)		0.7
Perpendicular phase velocity $v_\perp$ (10^5 cm/sec)		0.91
ω / ω_{*e}		0.6
Propagation		Electrons
Parallel wavelength (cm)		80
Phase difference $\Delta_\Psi = \Psi(\tilde{n}) - \Psi(\tilde{\phi})$ (deg)		19 ± 26
$b = k_\perp^2 (kT_i / M\Omega_i^2)$	at field maximum	0.02
	at field minimum	3.9
$\kappa = 2(\partial \ln B / \partial \ln n_0)$	at field maximum	0.1
	at field minimum	-0.6

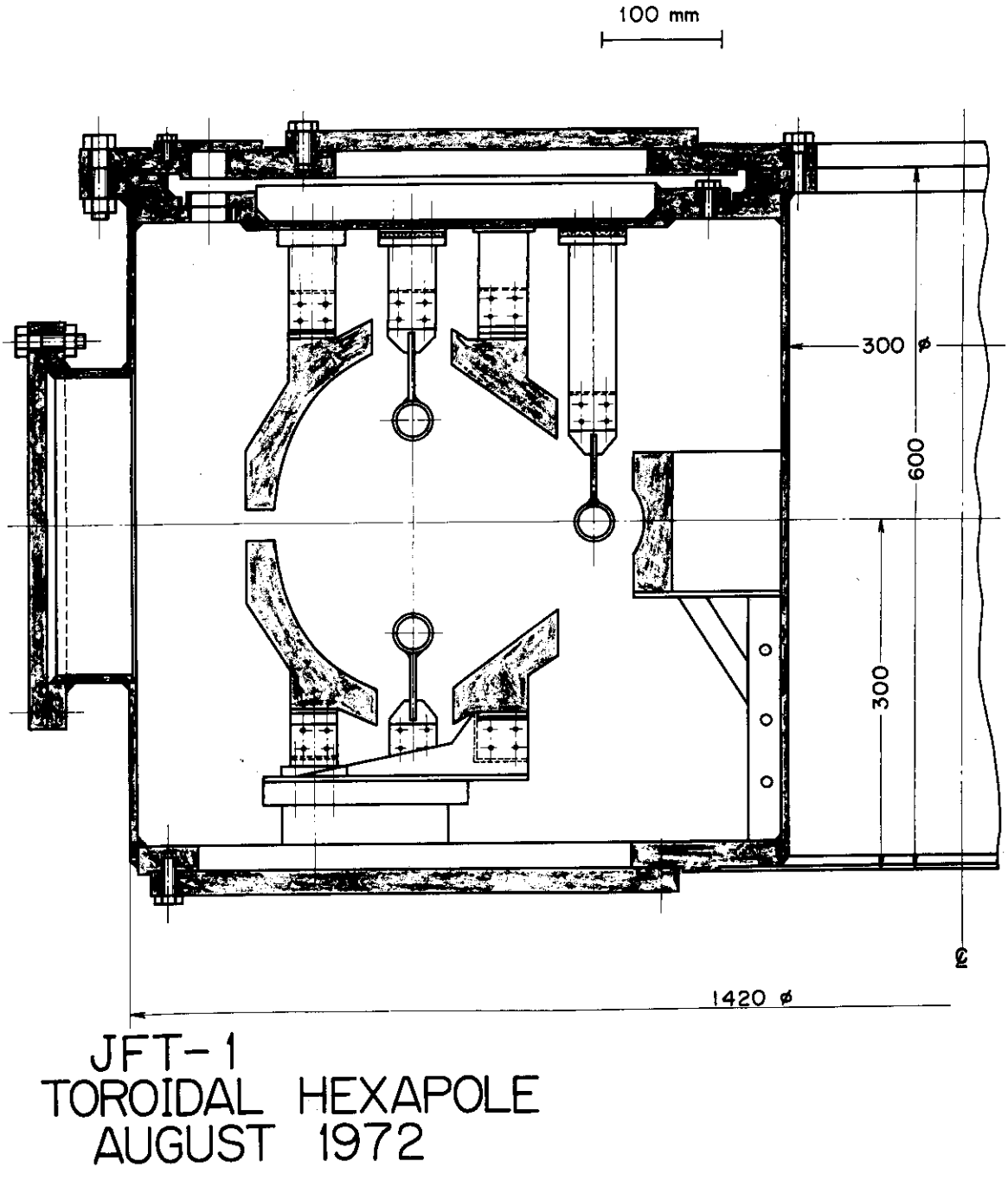

Fig. 1 Cross-sectional view of the JFT-1 device. A toroidal conducting shell is installed inside the vacuum chamber.

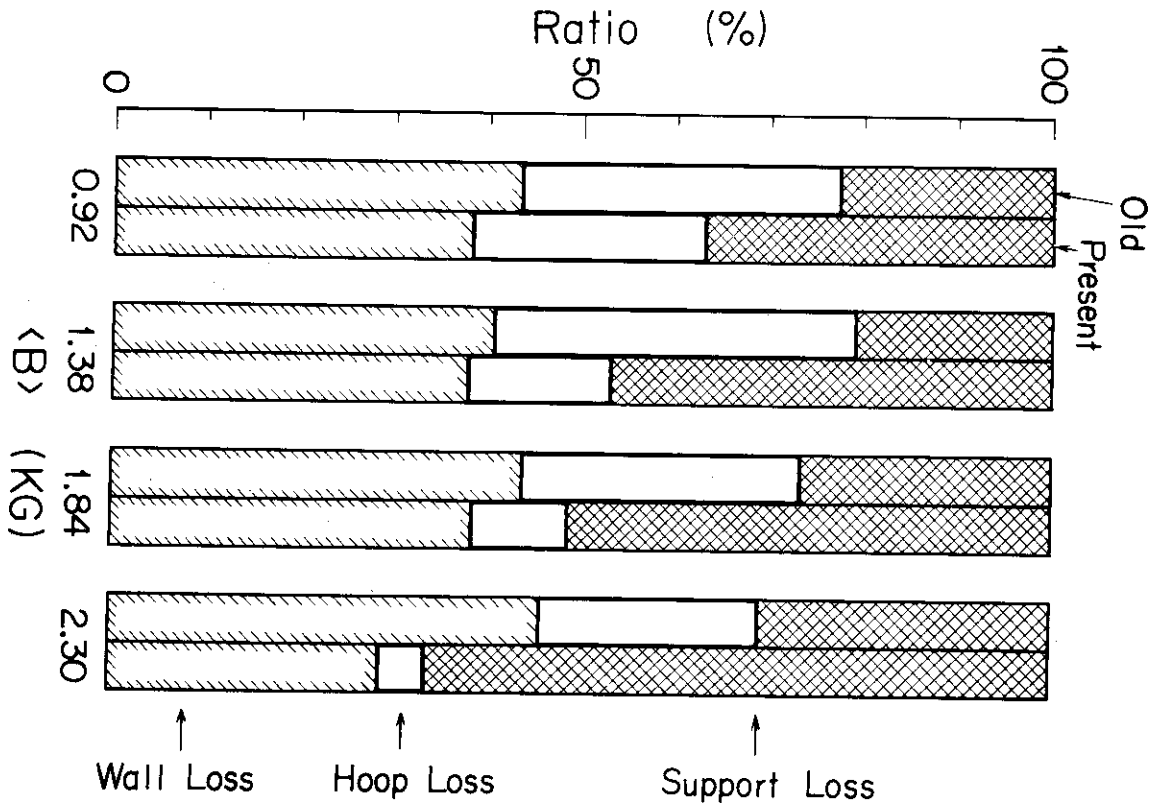

Fig. 2 Loss ratio vs. magnetic field strength.

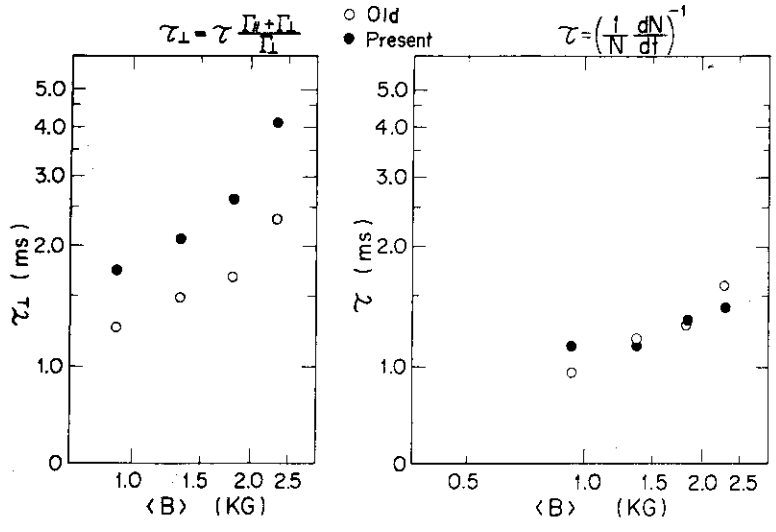

Fig. 3 (a) Overall confinement time $\tau = \left(\frac{1}{N}\frac{dN}{dt}\right)^{-1}$ vs. magnetic field strength. Time variations of the plasma density N are estimated from the support loss current.
(b) Perpendicular confinement time $\tau_\perp = \tau \frac{\Gamma_\parallel + \Gamma_\perp}{\Gamma_\perp}$, where $\Gamma_\parallel$ and $\Gamma_\perp$ are the parallel and the perpendicular loss fluxes, respectively.

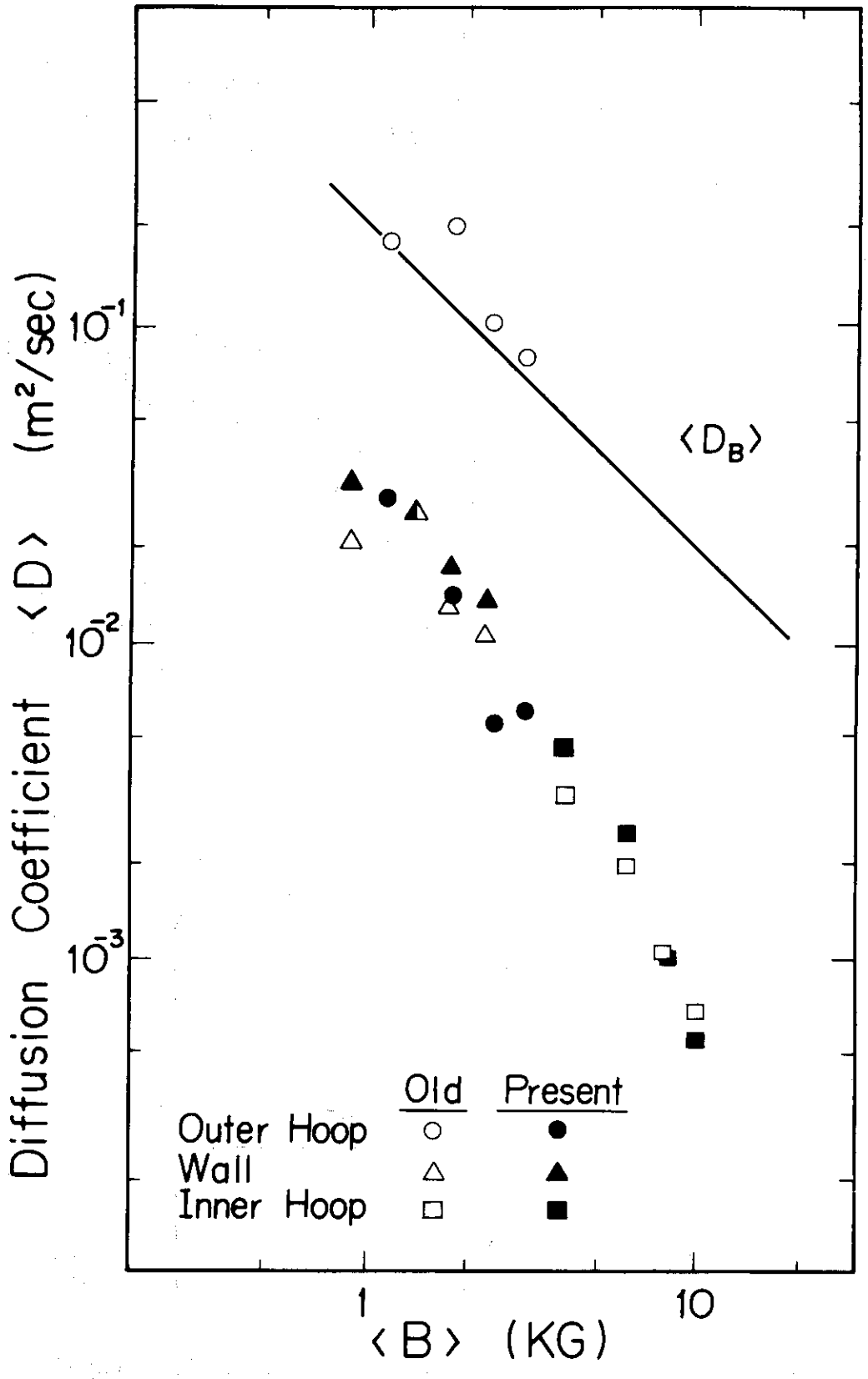

Fig. 4 Effective diffusion coefficients $<D>$ obtained from the relation $\Gamma = <D> \frac{dN}{dx}$. $<D_B>$ indicates the Bohm diffusion coefficient.

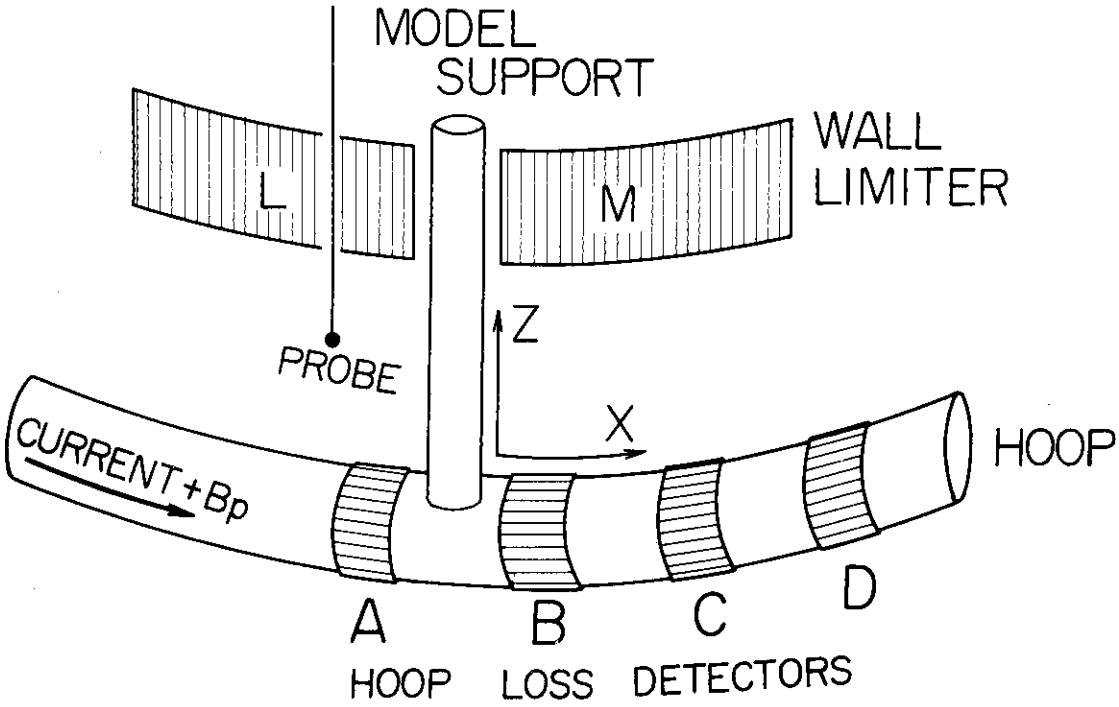

Fig. 5 Arrangements for the model support experiments. The origin of the local coordinates (X,Z) is set at the point of contact of the model support with the hoop. The separatrix lies at Z = 11 mm.

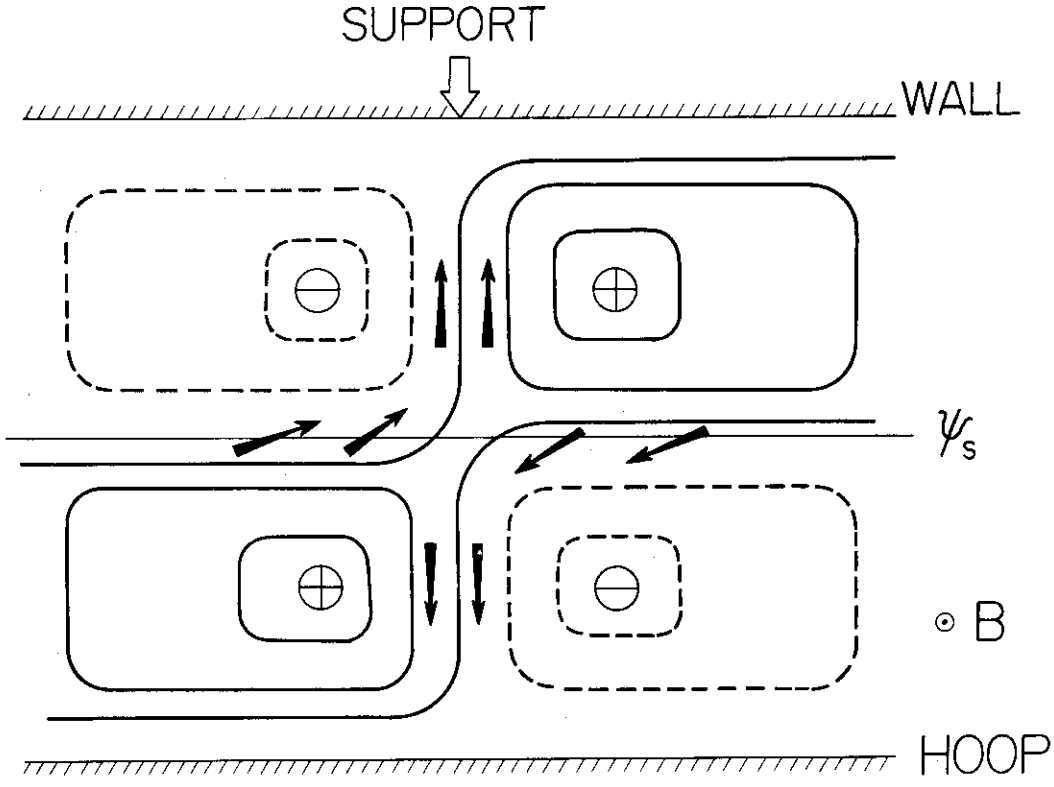

Fig. 6 Schematic diagram of a support-induced convection. Arrows indicate the direction of the enhanced flow. Contour lines represent enhanced potentials.

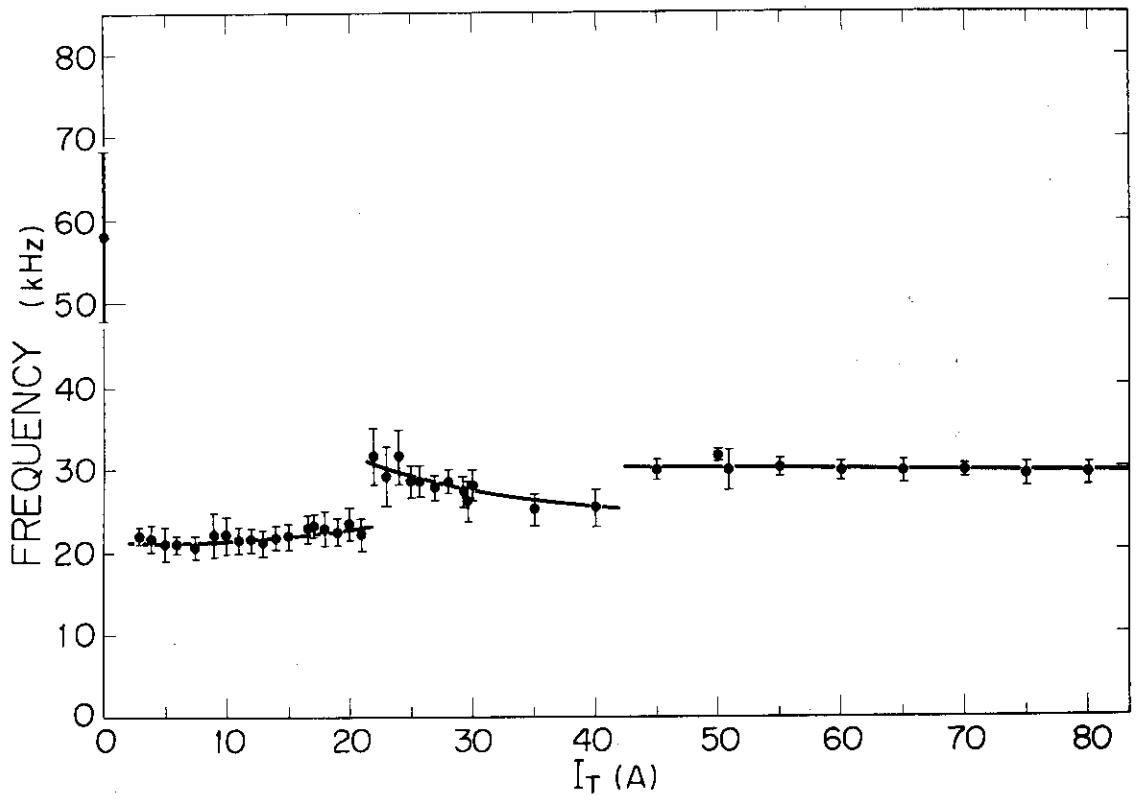

Fig. 7 Observed frequency of the wave in the laboratory frame as a function of toroidal field.

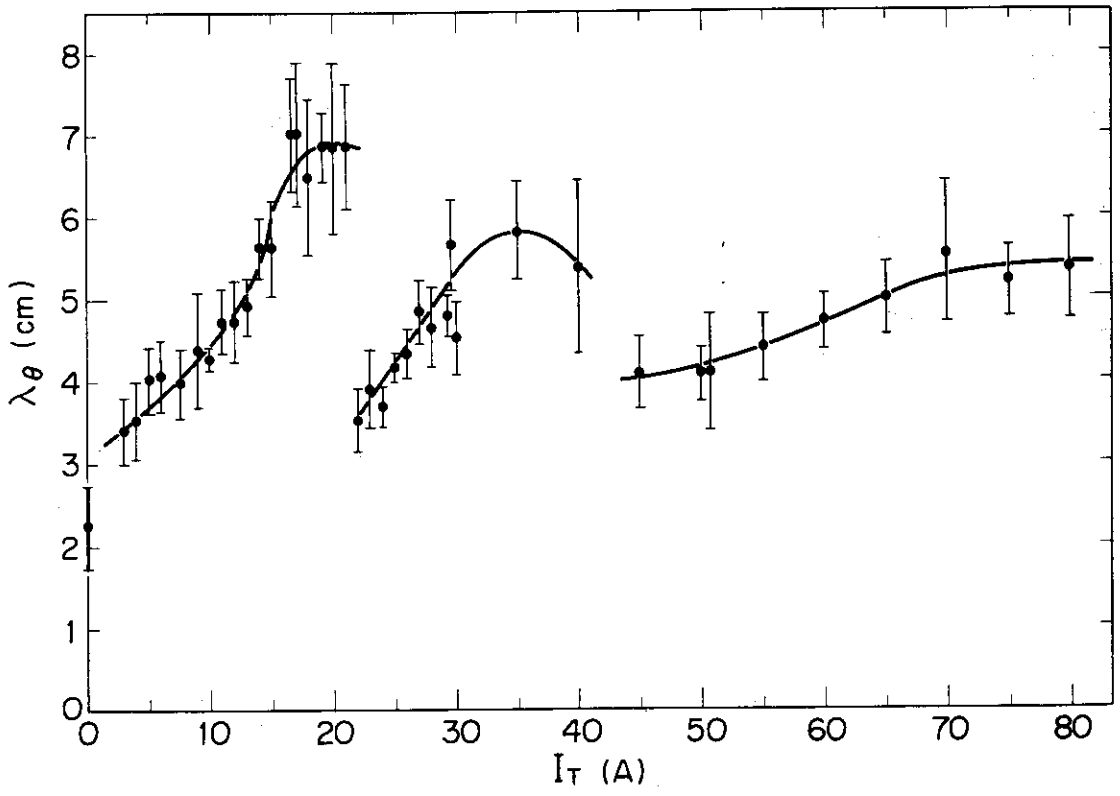

Fig. 8 Observed azimuthal wavelengths as a function of toroidal field.

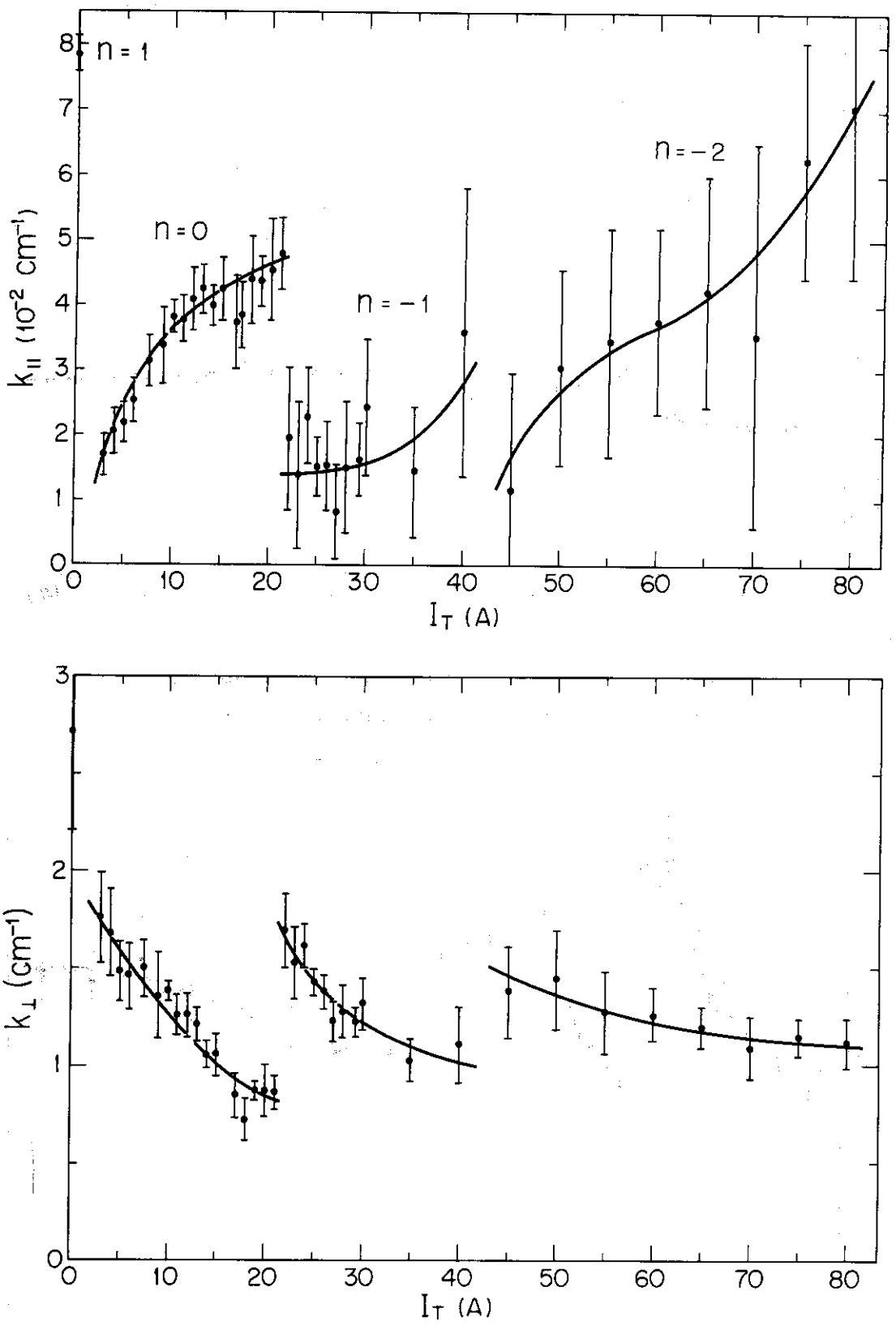

Fig. 9 Observed parallel (a) and perpendicular (b) wavelengths versus toroidal field.

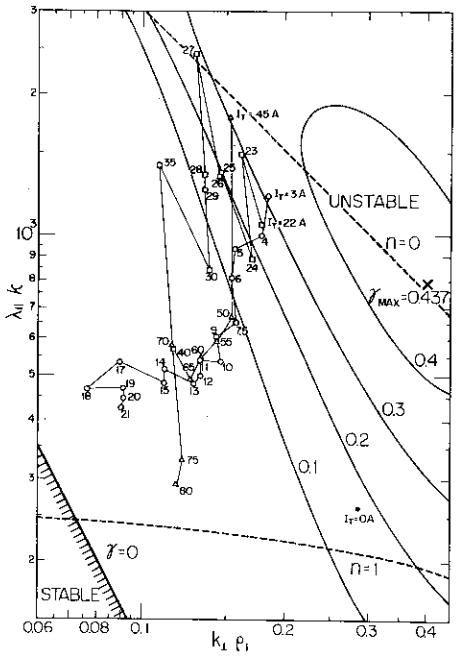

Fig. 10 Wave behaviors in the $(\lambda_{/\!/}\kappa, k_\perp \rho_i)$ plane when the toroidal field is increased from I_T=0 A. Also shown is the stable and unstable regions of the collisionless drift wave and contour lines of constant growth rates, $\gamma = \omega_I / \kappa v_{thi}$ for T_e/T_i=10 and ∇T_e =0, where ω_I is the imaginary part of the frequency ω and v_{thi} is the ion thermal velocity (Ref. 8). The dashed lines are calculated from the boundary condition imposed on $k_{/\!/}$ and $k_\perp$ of the modes with n=1 and n=0 for I_T=2 A.

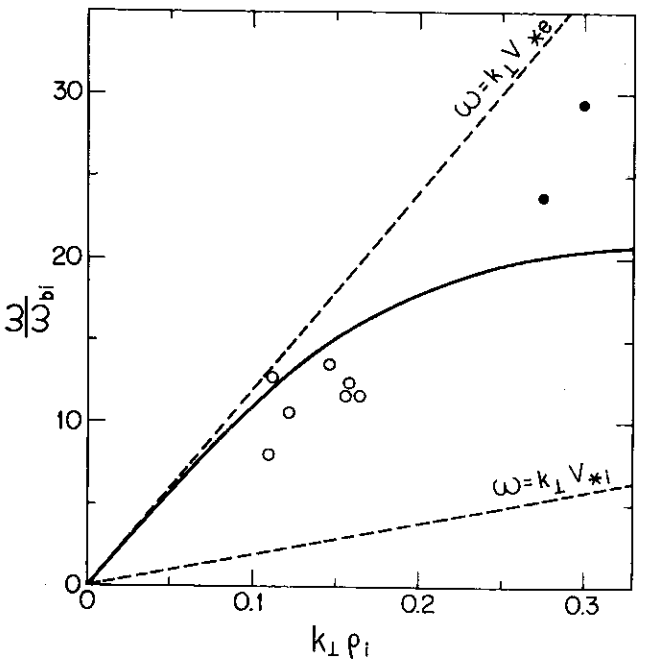

Fig. 11 Experimental dispersion curve. The open and closed circles represent the n=0 and n=1 mode, respectively. The upper dashed line is the dispersion curve predicted qualitatively for a β =0 plasma in the multipole configuration (Ref. 11) and the solid curve is calculated for a T_e=T_i plasma of a slab geometry (Ref. 12). Here, the ion bounce frequency ω_{bi} is defined as ω_{bi}= v_{thi}/L_0.

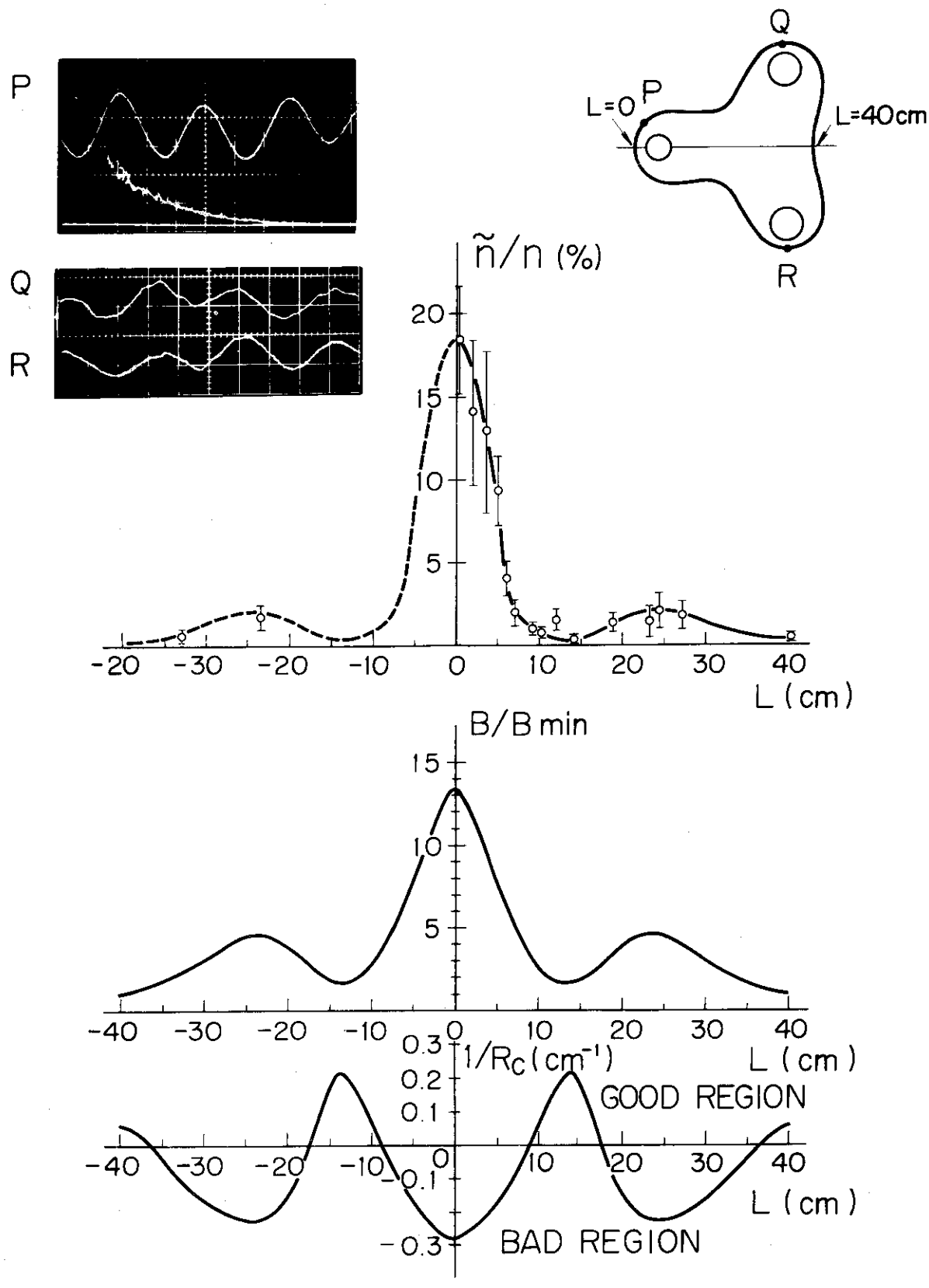

Fig. 12 Profile of the localized mode along the field line.

2. JFT-2 (fat tokamak)

T. Arai, N. Fujisawa, A. Funahashi, K. Inoue, S. Itoh, S. Kasai, S. Kunieda, M. Maeno, T. Matoba, S. Matsuda, T. Sugawara*, T. Ohga, K. Toi, M. Ohta, N. Suzuki, T. Takeda, T. Tazima, and K. Yokokura

2.1 Introduction

The preliminary experiments were continued for about a month after the completion of the device in March, 1972. The plasma current was, however, small as 70 kA and the electron temperature was very low as 20 eV due to impurities from the wall[1]. After the preliminary experiments the measurements of the uniformity of various magnetic fields and the improvement of the vacuum systems, especially the cleaning of the inner surface of the vacuum chamber were carried out intensively for about six months. At the end of this reporting period, we eventually attained a high plasma current of up to 175 kA with low loop voltage of about 0.4 V after the repetition of high current discharges (50 - 100 kA) of about 4,000 times.

Major results are summarized below.

The shift of the current channel from the shell axis is measured with magnetic probes. During the discharge the horizontal displacement is nearly constant; the vertical displacement, on the contrary, increases gradually. The horizontal component of the external magnetic field derived from the measurement of the vertical motion of the plasma column is constant during the discharge and is proportional to the toroidal field strength. This indicates that the horizontal error field is due to imperfection in the toroidal coils. The average value of the error field is 10 G for the toroidal field of 10 kG.

With a compensation field in opposition to the error field, the current duration time of the discharge is considerably elongated and reaches up to 800 msec in some cases. The duration time is typically about 200 msec without the compensation field.

Evaluation of energy confinement has been made for hydrogen discharges. The behaviour of the plasma is found to be classified into two groups. In the first group, the safety factor at the edge of the limiter falls to two and in that

*On leave from The Research and Development Center, Tokyo Shibaura Electric Co., Ltd.

case violent fluctuations appear in the loop voltage. In the second group, the safety factor is greater than two during the discharge, and the current and voltage behave comparatively quiet. Figure 1 shows the typical waveform of loop voltage and plasma current. In this figure the case 1 belongs to the first group as classified above, and the case 2 and 3 to the second. The latter cases have been studied mainly.

The plasma energy is measured with diamagnetic loop, and the ion temperature with charge-exchanged neutral energy analyzer. Our values of the poloidal beta are a little lower than the T3-A and ST values as shown in Fig. 2. The ion temperature is shown in Fig. 3 with the data of other tokamaks. The energy confinement time $\tau_E = W(Q_{in} - dW/dt)$ is calculated using the power input due to ohmic-heating $Q_{in} = I_p (V_{loop} - L\, dI_p/dt)$ and the plasma energy W. The scaling law for the energy confinement time obtained empirically in the other tokamaks is shown in Fig. 4 together with our present results. This figure indicates that the scaling law still holds even for the plasma radius as large as 23 cm.

In the following sections the diagnostics, the uniformity of the magnetic fields, the effect of the discharge cleaning, the dynamic limiter and the numerical simulation of tokamak discharges are described.

(S. Itoh and T. Sugawara)

2.2 Diagnostics

(1) Diamagnetic measurement

The total plasma energy is measured with two-turn diamagnetic loops located inside the conducting shell. One of the loops is used through the low-pass filter for the compensation of the slowly varying component of the longitudinal magnetic flux. The cut-off frequency of the filter is selected to attenuate sufficiently the high frequency component due to the plasma. The balancer circuit is adjusted so that the output signal is null on switching the filter off.

As an example, the diamagnetic flux $\Delta\phi$ is shown in Fig. 6 together with loop voltage V and plasma current I_p measured with electromagnetic diagnostic instruments[2]. It is seen from the figure that the diamagnetic flux is about 6.5×10^{-4} Wb at 100 msec after the breakdown. The poloidal beta β_p, the perpendicular energy $E_\perp$ and the energy confinement time τ_E are about 0.2, 150 J/m and 18 msec as shown in Fig. 7.

(M. Maeno, T. Matoba, T. Sugawara)

〔Figure 7 shows that the maximum values of β_p and τ_E are 0.2 and 18 msec, respectively. It is, however, shown recently by closer examination of the experimental data that those of β_p and τ_E are found to be 0.28 and 25 msec, respectively. The above value of β_p is in agreement with that obtained by using the measured values of conductivity electron temperature, ion temperature and electron density (July, 1973).〕

(2) Ion-temperature measurement by the charge-exchanged neutrals

The neutral particle energy analyzer designed and constructed in 1971 - 1972 was calibrated to obtain the relation between absolute sensitivity and energy in order to measure the energy distributions of ions in the JFT-2 device. For the calibration, an atomic hydrogen beam source consisting of an rf ion source with an einzel lens, a momentum analyzer, and a neutralizing cell with a hydrogen gas in it, was connected to the neutral particle energy analyzer. In this combination, it was necessary to know the absolute intensity of the neutral beam entering the particle analyzer, which was measured by the following two methods. One for the particles with energies above a few keV is called the indirect method, and the other for the particle energies of 0.3～4 keV is called the direct method. In the former, the neutral beam intensity is assumed to be equal to the difference in intensity between the beam through the evacuated cell and the gas filled one, at the entrance of the neutral particle energy analyzer, for an ion beam of the same intensity entering the neutralizing cell. In this method, the charge stripping and neutralizing cross sections of atomic hydrogens and protons in a nitrogen gas, as well as the analyzer sensitivity, are measured by changing pressure of the nitrogen gas. The value obtained are in good agreement with those reported by other workers[4,5]*.

In the latter method, the neutral beam intensity is calculated from the measured value of the secondary electron current produced by impingement of the neutral beam on the target of a Faraday cage. The secondary electron emission coefficient for hydrogen atoms used in this calculation is assumed to be equal to the coefficient for protons measured with the Faraday cage. In Fig. 8, the values obtained for the copper surface are shown together with those by C.F. Barnett and J.A. Ray[6]. The calibrated efficiency of the atom-ion conversion cell of the neutral particle energy analyzer to be installed to the JFT-2 device is in good agreement with the design value calculated from the

*The authors tabulated and showed in figures these cross sections in JAERI-M 4734.

two-component differential equations, in which two kinds of particles with charge states 0 and 1 are assumed. Experiments on the calibration were completed by November 1972.

In December 1972, the neutral particle analyzer was installed to observation box B-1 of the JFT-2 device. In the experimental program of JFT-2, the first measurement of ion temperature was made in February and the second in March 1973. Owing to the severe background produced by X-rays from the discharge, it first appeared difficult to detect the neutral particle signals. In the first experiment, however, the signals of neutral particle counting were distinguished from those of X-rays, by means of the difference in shape of the distribution between the pulse heights, and the ion temperature at 74-75 ms after the breakdown was calculated to be about 150 eV from the measured counting averaged over about 40 shots of discharges, which were made at a filling pressure 10^{-4} torr of H_2 and B_t = 10 kG. In this measurement, it was confirmed that the filling pressure 6.2×10^{-4} torr of N_2 in the atom-ion conversion cell where calibration was made, had influence on the partial pressure of the residual gas in JFT-2 only within 15%.

In the second measurement, an improved lead shield against the X-rays was used. All the discharges for which measurements were made were the case 2 (Fig. 1), in the classification of the operating conditions of JFT-2. All the signals including those due to the X-rays were counted at various settings of the energy analyzer voltage. Subtracting the background from the total countings, the reliable energy distributions of neutrals entering the analyzer could be obtained. The background countings, wholly due to X-rays from the discharge, were given without applying potentials to the electrodes of electrostatic energy analyzer. The ion temperature thus obtained at 74-76 and 84-86 ms of the discharge were calculated to be about 200 eV averaged over 120 shots of discharges. Figure 9 shows the relation between the relative number of ions proportional to the exponential function and the energy; which indicates the existence of two different ion temperatures. The higher temperature probably corresponds to the hot central part of the discharge.

(S. Yano*, H. Shirakata* and K. Takahashi*)

(3) Electron density measurements with 4-mm microwaves

Electron densities are measured with the interferometric method using 4-mm

*Ionized Gas Laboratory, Division of Physics

microwaves at the position by 90 degrees away from the limiter in the toroidal direction. The waves are focused by quartz lenses to improve spatial resolutions. These lenses are also used for vacuum seals of the microwave ports. There are eight vertical wave-paths with regular intervals of 60 mm. The transmitting and receiving horns are moved horizontally to determine density profile.

The average electron densities $\bar{n}_e$ measured at 100 msec after the breakdown of the case 2 discharges are plotted against the positions of the wave-paths in Fig. 10. The lenses of the center and its adjacent paths have often become opaque by sputtering of the materials of the wall and/or the dynamic limiter and the densities along the corresponding paths cannot be determined. Also shown in Fig. 10 is the density profile of $n_e(r) = n_{e0}(1-r^4/b^4)$ (b: liner radius) except the region near the limiter. The maximum central density n_{e0} is also inferred to be 1.4×10^{13} cm^{-3} from the best-fit curve (solid line) as shown in Fig. 10. Figure 11 shows the time-variation of the central density n_{e0} determined by the above-mentioned method. It is found from this figure that the density is nearly constant during the plasma duration except the initial stage of discharge.

(A. Funahashi and S. Kasai)

(4) Spectroscopic measurement

For the discharge cleaning condition (see 2.4), spectral intensities of neutral hydrogen H_β, carbon and oxygen atoms or ions were measured by a 25 cm visible monochrometer, and from the photographic measurements by a 50 cm normal incidence VUV monochrometer, spectra of emitting lines over the wavelength range of 1220 - 2000 A were obtained. These measurements were made at the position by 90 degrees away from the molybdenum limiter in the toroidal direction.

Typical oscillograms of spectral intensities of H_β, singly ionized carbon and oxygen ions (CII, OII) are shown in Fig. 12. Figure 13 shows the change in H_β line intensity with respect to the shot number. The intensity of this line decreases rapidly with the shot number up to about 3,000 shots of discharges. On the other hand, from the photographic measurements, it is found that the resonance lines of λ 1548 Å of CIV, λ 1403 Å of SiIV are emitted and ionic lines of metals (Fe, Ni and Cr) are extended over the ranges of 1430 - 1490 Å and 1580 - 1660 Å.

(S. Kasai and A. Funahashi)

(5) X-ray measurement

The measurement of X-ray radiation from a hot plasma is important to obtain useful imformation on plasma parameters. The electron temperature T_e and the number of runaway electrons can be estimated from the continuum spectrum of Bremsstrahlung radiation from the plasma. The methods of measurement and the results of the preliminary experiments are briefly summarized bellow.

(i) Soft X-ray measurement (2 keV~ 100 keV)

Si(Li) semiconductor detector with a cryogenic system is employed to measure the X-ray energy spectrum in the range from several keV to about 100 keV. The low energy limit is determined from the thickness of the entrance window made of beryllium foil. Output signals are processed with a multichannel pulse-height-analyzer. This method is suitable for the accurate measurement of X-ray energy spectrum, but several hundred shots of discharges are necessary to measure it. The system will be completed in October 1973.

(ii) Hard X-ray measurement ($>$50 keV)

In a tokamak plasma with joule heating, hard X-ray radiation occurs frequently at the limiter by impacts of runaway electrons. The hard X-ray penetrates the shell of aluminium of 30 mm thick. The measurements of the hard X-ray were carried out with a set of an NaI scintillator and a photo-multiplier. The results are shown in Figs. 14 and 15. The number of runaway electrons and the energy of them increase with time monotonically in comparatively stable discharges, but in other discharges saturation phenomena appear in some time after the breakdown.

The X-ray dose was measured outside the toroidal coils with pocket dosimeters. The distribution of the dose in the toroidal direction is shown in Fig. 16. From this measurement, it is concluded that the source of the hard X-ray is located at the limiter and that it is radiated strongly forward. The maximum X-ray dose exceeds 200 mrem/shot, which is the upper limit of a pocket dosimeter, in case of a long current duration. Dependence of the dose on discharge parameters will be studied in the next stage of experiments.

(iii) Absorption method

The absorption method is applied to evaluate the electron temperature T_e. Foils of beryllium of 20~500 μm thick are chosen for the absorber because of its low energy absorption edge. An apparatus is designed so that absorbers of five kinds of thickness may be changeable without breaking the vacuum. A detector set consists of a plastic scintillator and a photomultiplier. This system has been prepared and will be used in the next stage.

(N. Suzuki and T. Matoba)

(6) Ruby laser scattering measurement

The Q-switched ruby laser, the sequenced pulse delay system, the optical system and the photo-detector system were ordered in May, and the observation box was ordered in June, 1972. We took delivery of all of the equipments in March, 1973. Figure 17 shows the schematic diagram of the apparatus[7].

It is scheduled that examinations of the equipments are to be made in the first two months in the next reporting period and then intensity of stray light is to be measured in order to confirm the feasibility of Thomson scattering measurement. The experiment will be made in a regular way from August, 1973.

(T. Matoba and A. Funahashi)

(7) Measurement of current distribution by means of high energy particles

This work is the continuation of the one described in the previous annual report[8], in which basic problems in the α -particle probing of a current distribution in the axisymmetric toroidal plasma column were elucidated. In this reporting period, numerical analyses of the α -particle orbits, preliminary test of a semiconductor detector which will be used for detection of the α -particle, and the planning of production of ^{210}Po α -source were performed. The basic investigation of the α -particle probing of a current distribution in the axisymmetric toroidal plasma column was summarized in Ref. 9). The results of the numerical analyses of the α -particle orbits and design of the experimental arrangement to apply the method to JFT-2 were summarized in a JAERI-M report[10].

The preliminary test of the semiconductor detector was performed, especially with the view to studying the performance of the detector subject to the strong light flash which arises at the initial phase of the tokamak discharge and it was concluded that the detector could be used for the measurement of current distribution by the α -particles. A manual for the production of ^{210}Po α -source was established. Preliminary test of the ^{210}Po α -source production will be conducted before long.

(S. Kawasaki*, K. Inoue, and T. Takeda)

(8) Bolometer measurement

The movable probe holder which can be moved forward and backward in the range of 0 - 600 mm was prepared for a bolometer and other sensors. The

---

*Visiting scientist on leave from Kanazawa University.

order will be placed for the detector of the bolometer shortly.

(T. Matoba and H. Shirakata*)

(9) Measurement of the electrical conductivity distribution

We are preparing an apparatus to measure the electrical conductivity distribution in JFT-2 by the method of superimposing a small sinusoidal voltage on the main loop voltage. The important point of this method is to estimate the A.C. impedance of a plasma from measurement of the response of the plasma for the superimposed sinusoidal component.

The primary circuit of the present current transformer of JFT-2 is shown in Fig. 18. The small sinusoidal voltage is excited through the inductor with low resistance by several kinds of capacitor blocks. It is required that the sinusoidal components should not disturb the plasma and the frequencies should be about an order of magnitude higher than that of the main discharge. Under this fundamental consideration the capacitances and charging voltage of these capacitor blocks are determined. The waveform of voltage superimposed on the main loop voltage is shown in Fig. 19, which was obtained by the preliminary experiments in JFT-2. The frequencies ranging from about 50 Hz to 1.25 kHz were examined experimentally.

In JFT-2 it is planned to measure the electron temperature distribution using laser scattering method and its apparatus is on the stage of adjustment for applying to JFT-2. Therefore, it is expected that the effective charge distribution of the JFT-2 plasma may be estimated from the electrical conductivity distribution assuming that the conductivity varies with electron temperature as $\sigma_p \propto T_e^{3/2}$. The current density distribution may also be evaluated on the assumption that the current density is proportional to the electrical conductivity.

(K. Toi, T. Matoba and S. Itoh)

(10) Data processing system

Concerning the automatic data processing systems of JFT-2, "the data acquisition system"[8] was brought to completion, and the detailed design study of "the data processing system"[11] and preparation of the final specification of the system were carried out in this reporting period.

The data acquisition system is a small scale automatic data processing system prepared for the JFT-2 research program and we had set up two

*Ionized Gas Laboratory, Division of Physics.

purposes in designing the system. Firstly, we should process the input signals with comparatively low frequency by the system and secondly, for the preparation of the data processing system, we should be able to make effective use of our experience obtained during construction of the data acquisition system. By using the data acquisition system analogue signals from 8 magnetic probes (rogowskii coils, probes for the measurement of plasma displacement etc.) are converted to 8-bit digital signals and stored in a 16-kByte core memory of a TOSBAC-40 computer. Controlling parameters, conversion rates of the signals and various kinds of physical constants are given as input parameters through a teletypewriter and the output data are displayed in a graphical form and recorded by a set of a Sony-Tektronix Graphic Display and a Hard Copy Unit. The block diagram of the system is shown in Fig. 20.

The design of "the data processing system" was reexamined on the basis of the experience obtained during the construction of the data acquisition system and the experimental studies of the JFT-2 plasmas. In the first period of the JFT-2 experiment it was found that the plasma duration time exceeded the design value considerably. Therefore the design value of the data acquisition time was changed from 100 msec to 1200 msec. The basic ideas of designing "the data processing system" are as follows. At first, in principle all the electrical signals from the diagnostic devices for the JFT-2 experiments should be analogue-to-digital converted, processed and displayed within 2 min. of the pause of plasma discharge which follows the data acquisition time. The definite description of the above-mentioned signals is presented in Ref. 11. Secondly, practicably many kinds of input signals obtained from the diagnostic devices equipped at a time should be processed simultaneously. For this purpose 8 "input ports" which are adequate to various characteristics of the input signals and about 100 input channels are provided for the system. The fastest sampling rate of the AD converters is 0.5 event/μ sec. At the maximum operating rate the system is operated every 2 min. in accordance with the maximum operating rate of the JFT-2. The processed data are presented every 2 min. through 2 sets of the Graphic Display and the Hard Copy Unit. A simplified block diagram of the system is shown in Fig. 21.

(T. Takeda, N. Suzuki and S. Matsuda)

2.3 Measurements of magnetic fields

The equilibrium of a plasma confined in a tokamak device with an iron core is obtained by vertical magnetic field generated by currents induced in a conducting shell, by additional vertical field produced by external coils and by leakage magnetic field from the iron core. These magnetic fields were measured on the JFT-2 device to examine the absolute strength of the fields and the effect of gaps in the shell. Some results of model experiments on these fields and the methods of measurements are presented in Refs. (12), (13), (14). We summarize here the results of measurements made on the JFT-2 device.

(1) D.C. vertical field (B_{VD})

The results of measurements of D.C. vertical field with a Hall probe are shown in Fig. 22. The distribution of the strength of B_{VD} field along the major radius is in good agreement with a calculation in which no iron core is present. A small deviation from the calculation seems to be due to the effects of the ion core and the shielding plate. The uniformity of the toroidal distribution of B_{VD} field is found to hold within ± 1 % owing to the presence of the shielding plate.

(2) Pulsed vertical field (B_{VP})

The results of measurements of pulsed vertical field with magnetic probes are consistent with the results of the model experiments. The strength of B_{VP} field is weakened near the gaps in the shell and the decay time of B_{VP} field varies with the distance along the toroidal direction from the gap. At the gap the decay time of the field is nearly the same as that of the B_{VP} coil current, but at the middle of the shell between the gaps it is approximately 10 times longer than that at the gap. This result indicates that the decay time of the image current in the shell is to be estimated by the relation $\tau \approx \mu\sigma \frac{\delta}{2} \cdot \frac{\ell}{2}$ rather than $\tau \approx \mu\sigma (\frac{\delta}{2})^2$. Here δ is the thickness of the shell and ℓ is the minor radius of it. These results are shown in Figs. 23 and 24.

(3) Vertical field produced by the shell and by the iron core

The vertical field produced by the shell and the vertical component of the leakage field from the iron core were measured separately or in combination by a pick up coil with a special form which does not pick up the magnetic field due to plasma current. A ring conductor of aluminium with minor diameter of 25 mm was placed at the center of the cross-section of the shell to simulate the plasma current. The results are shown in Fig. 25. The strength of the vertical

field of the shell is ~ 180 G/100 kA at the middle of the shell between the gaps, but it is weakened near the gap to about 40 % of this value. The vertical field from the iron core is ~ 220 G/100 kA when no shell is present and it is in the same direction as the field due to the shell. As a result, the nonuniformity in the toroidal distribution of the field of the shell is compensated by the penetration of the leakage field from the iron core through the shell gaps. Thus the resultant vertical field is found to be uniform within about 10 % in the toroidal direction. It is noted that the strength of the vertical field due to the iron core is in the same order of magnitude as that due to the shell and it takes an important part for maintaining the plasma column in equilibrium.

(N. Suzuki, T. Ohga and S. Matsuda)

2.4 Effect of discharge cleaning

(1) Vacuum system

The vacuum system is shown in Fig. 26. The vacuum vessel consists of 4 liners connected by 3 diagnostic boxes and an evacuation box. The liners are made of stainless steel bellows of 0.6 mm thickness, whose major and minor radii are 900 mm and 300 mm, respectively. The evacuation box has a window of 66 x 600 mm^2 and is connected to the manifold, through which the vessel are evacuated.

All the elements are cleaned with aceton and the surfaces of the boxes are scraped off with the glass beads spray. The liners are baked up to 200 ^{o}C by induction heating, and the boxes and the high-vacuum conduit pipes are baked up to 100 ^{o}C by oil.

The pumping system consists of turbomolecular pumps (TMP), sputter ion pumps (SIP), bulk getter pumps (BGP), oil rotary pumps, sorption pumps and liquid nitrogen traps, as shown in Fig. 26. The SIP is used for the conservation of the apparatus.

The working gas of hydrogen purified through the palladium film is continuously introduced into the vessel, whose pressure is adjusted to 10^{-3}~ 10^{-4} torr by evacuating only with the TMP.

(2) Conditioning by discharge cleaning

The vacuum vessel is evacuated with 3 TMP's. The ultimate pressure of 3.0 x 10^{-7} torr and the total outgassing rate of 1.1 x 10^{-4} torr.l/sec are obtained after 20 hours baking. About 2000 shots of discharges from the

1900th shot to the 4100th are carried out for the conditioning.

The conditioning discharges are made under the following condition; the filling pressure of the hydrogen gas P_f is 1.0×10^{-4} torr, the toroidal magnetic field B_t is 7 kG, the plasma current I_p is 40~120 kA and the repetition time of discharges t_r is 1.5 min. In the case of the measurement of impurities, the discharge condition is the following; $P_f = 1.0 \times 10^{-4}$ torr, B_t = 10 kG, I_p = 50~200 kA and t = 2 min.

A number of impurities are desorbed and created by particle bombardment during discharges. The ratio of the mass to the charge of impurities (M/e) is measured by the quadrupole-type mass analyzer installed in the manifold. Figure 27 shows all the impurities for M/e from 1 to 50 at the 1920th and the 4174th shots. It is remarkable that hydrocarbons C_mH_n (M/e = 12m+n) except for carbon (M/e=12), water (M/e=18) and nitrogen and/or carbon monoxide (m/e=28) appear at the early stage of the conditioning. These hydrocarbons are seemed to be produced from the working gas and the carbon due to oils which contaminate the surfaces. Disappearance of the oxgen (M/e=32) at the 4174th shot suggests that most molecules of M/e=28 are carbon monoxides, which is supported by the spectroscopic measurement.

Figure 28 illustrates the time evolution of impurities. The characteristic decreasing rate indicates the pumping speed of 250 1/sec. This contains the evacuation of the TMP and the sorption on the surfaces. Very small difference between M/e=28 peaks before and after discharges at the 4174th shot suggests that the working gas contains the carbon monoxide.

The changes of some impurities before and after discharges are shown in Fig. 29. It is noticeable that methan and its cracking (M/e = 16, 15) slowly decrease compared with the water and the M/e = 28 molecules.

The electron temperature of the plasma increases rapidly with the decrease of impurities. At the beginning of the conditioning the temperature is only 6 eV, but at the 4200th shot it reaches to 300 eV, as shown in Fig. 30.

Usually the conditioning is performed with discharges of 50~60 Hz or glow discharges. On the other hand, the repetition time of our discharges is 1.5 min as previously mentioned, but discharge current is relatively large compared with the usual ones. In our case, therefore, the energy of bombardment particles is large, and the efficiency per shot of discharges in removing impurities seems to be better.

(3) Summary

1) Impurities are decreased to considerably low level by the discharge cleaning.
2) A number of hydrocarbons are produced in the hydrogen discharges.
3) Methane and its cracking are left persistently.
4) The repetition time of discharges is longer than the pumping out time, but discharges of large current are effective in removing impurities.

(N. Fujisawa, T. Sugawara, K. Toi, T. Matoba, S. Kasai and S. Itoh)

2.5 Dynamic limiter

The dynamic limiter was installed to JFT-2 in January 1972. As shown in Fig. 31, its driving system is divided into the upper and the lower part. The compressed air at a pressure of about 10 kg/cm^2, regulated by the pressure regulator, is stored in cylindrical tanks of 30 litres. As the triggering time of fast-acting 4-way valves is adjustable, both limiters are removed simultaneously after the breakdown of a discharge.

The performance test of the driving system showed a good agreement with the results of a full scale model described in the previous annual report[8]. The final and average velocities are 8.3 m/sec and 5.1 m/sec, respectively for a stroke of 10 cm at a cylinder pressure of 10 kg/cm^2.

Immeadiately after the limiters are removed, its supporting members, especially the magnetic shielding plates and cylinder supporting plates, begin to vibrate. The deformation of above members, however, is less than 400 μm at a cylinder pressure of 10 kg/cm^2, and no vibration of the liner and limiter box is observed.

Shortly, a series of experiments with the dynamic limiter will be made to make clear the effect of limiter on the plasma stability and equilibrium.

(M. Ohta, T. Ohga and S. Kunieda)

2.6 Numerical simulation of JFT-2 plasma

Previously we wrote a computer code to simulate space-time evolution of a tokamak plasma[15]. By the code we calculated the behavior of plasma

parameters on the basis of the published data of the T-3 and the ST tokamaks and examined the results by comparing them with those calculated by the codes of other institutes. In our work we adopted two-fluids model keeping the fluid density fixed. To compare the experimental data with theoretically predicted ones and to conjecture the values of the plasma parameters which cannot be measured because of lack of an appropriate diagnostic method, it is necessary to have a fluid code based on more realistic plasma model. For this reason we improved the computer code as follows. We added the particle balance equation to the previous code by taking the particle diffusion, ionization and charge exchange processes into account. Generally speaking, the objective differential equations are non-linear and, in the previous work, we transformed them into the difference equations and linearized the equations by taking only the zeroth order term with respect to the transport coefficients into account. We included, however, the first order term in this work. One of the distinctions of the JFT-2 device is that it has a fast-acting removable limiter (a dynamic limiter). To simulate the plasma behavior after triggering the motion of the dynamic limiter, the code was improved so that one could calculate the plasma parameters in a system with moving boundary.

In the previous code the set of the difference equations was formulated by the implicit method and in coding the new program, we incorporated the following points. Firstly, the differential equations were linearized as mentioned already. Secondly, to save the computational time the recursion formula[16] was used for solving the linear simultaneous equations. Thirdly, the above-mentioned formulation of the difference equations was carried out automatically by automatic coding program written in IBM PL/I (or FORTRAN) FORMAC language. The program is similar to the one reported by Rosen and Okabayashi[17]. The automatic coding program was checked for a very simple diffusion equation which simulated penetration of an electric field into a cylindrical plasma column and it was found that the program worked satisfactorily. This program proves, however, its merit when it is used for more complicated system where some linearizations are inevitable. From this point of view it is very useful to apply the program for the simulation code of the kind described here. Until the end of this reporting period only a preliminary check of the whole program was completed.

(T. Takeda and S. Itoh)

References

1) S. Itoh, et al. : in Proceedings of Fifth European Conference on Controlled Fusion and Plasma Physics, Grenoble, August 21-25, 1972, vol.I, p.3 and vol. II, p.231.
2) M. Maeno, et al. : JAERI-M 5204 (March, 1973) (in Japanese).
3) S. Itoh, et al. : in Proceedings of Third International Symposium on Toroidal Plasma Confinement, Garching, March 26-30, 1973, Paper B4.
4) S.K. Allison : Revs. Modern Phys. 30, 1137 (1958).
5) C.F. Barnett, J.A. Ray and J.C. Thompson : ORNL-3113, Revised, August 1964.
6) C.F. Barnett and J.A. Ray : Nuclear Fusion 12, 65 (1972).
7) T. Matoba, A. Funahashi, and S. Itoh : in Proceedings Japan-US Seminar "Laser Interaction with Matter" Kyoto, September 24-29, 1972, p.413.
8) JAERI Thermonuclear Fusion Laboratory : JAERI-M 5029 (October, 1972).
9) S. Kawasaki and K. Inoue : Nuclear Fusion 12, 387 (1972).
10) S. Kawasaki, K. Inoue, and T. Takeda : JAERI-M 5146 (February, 1973).
11) JAERI Thermonuclear Fusion Laboratory : JAERI-M 4564 (September, 1971).
12) N. Fujisawa, et al. : JAERI-M 4688 (February, 1972) (in Japanese).
13) T. Ohga and S. Matsuda : JAERI-M 4784 (February, 1972) (in Japanese).
14) S. Matsuda, et al. : JAERI-M 5021 (October, 1972) (in Japanese).
15) T. Tazima, T. Takeda, and S. Itoh : JAERI-M 4941 (August, 1972) (in Japanese).
16) R.D. Richtmeyer and K.W. Morton : "Difference Methods for Initial-Value Problems" 2nd ed. Interscience, 198 (1967).
17) B. Rosen and M. Okabayashi : Nuclear Fusion 13, 3 (1973).

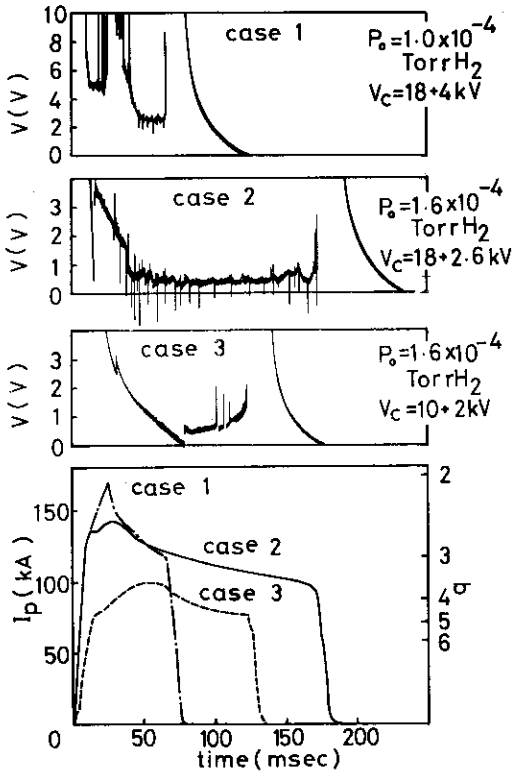

Fig. 1 Typical wave form of loop voltage and plama current. Case 1: Charging voltages of the first and the second banks (V_{C1} and V_{C2}) are 18 kV and 4 kV, respectively. The DC vertical magnetic field (B_{VD}) is 150 G and the filling pressure (P_0) is 1.0 x 10^{-4} torr. Case 2: V_{C1}=18 kV, V_{C2}=2.6 kV, B_{VD}=133 G and P_0=1.6 x 10^{-4}torr. Case 3: V_{C1}= 10 kV, V_{C2}=2 kV, B_{VD}=109 G and P_0= 1.6 x 10^{-4}torr.

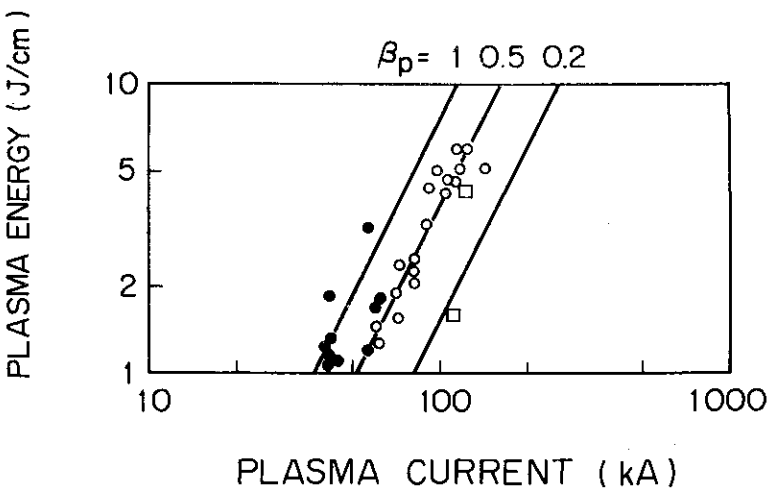

Fig. 2 The plasma energy versus the Ohmic-heating current. Open and black dots are the T-3A and the ST data, respectively. Squares donote the present data.

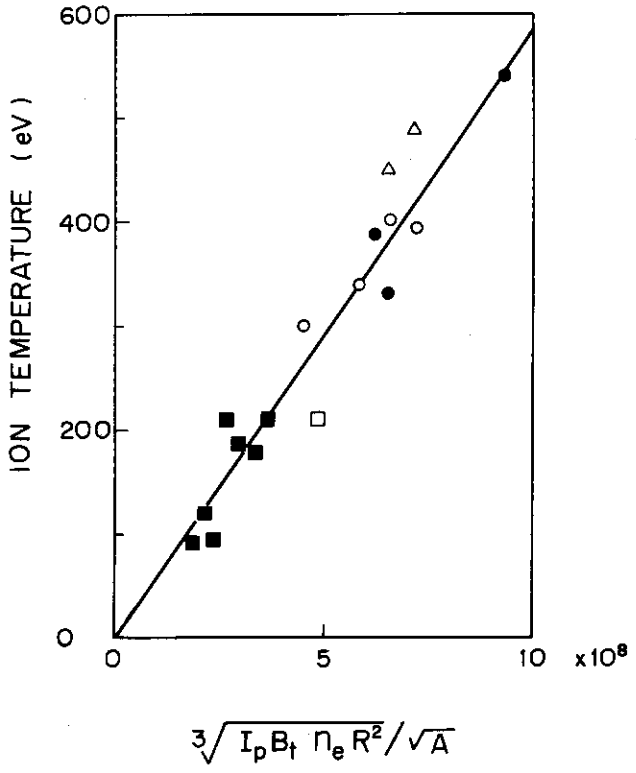

Fig. 3 The maximum ion temperature. Open squares denote the present data. Others are T-4 (△), T-3A (○, ●) and TM-3 (□).

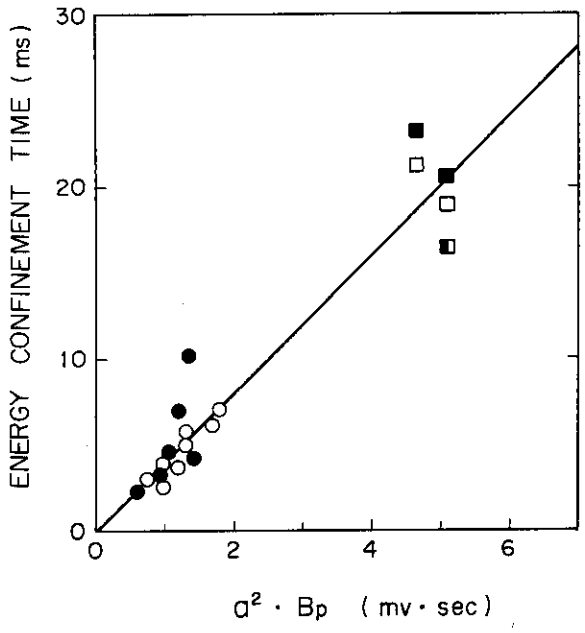

Fig. 4 Energy confinement time τ_E versus $a^2 B_p$ where a is the plasma radius and B_p is the poloidal magnetic field at the edge of the plasma. Open and black dots are the T-3 and the ST data, respectively. Squares denote the present data. The values of normalized internal inductance are derived from the horizontal displacement and the poloidal beta (◨), or assumed to be 1/2 (■) and 1 (□).

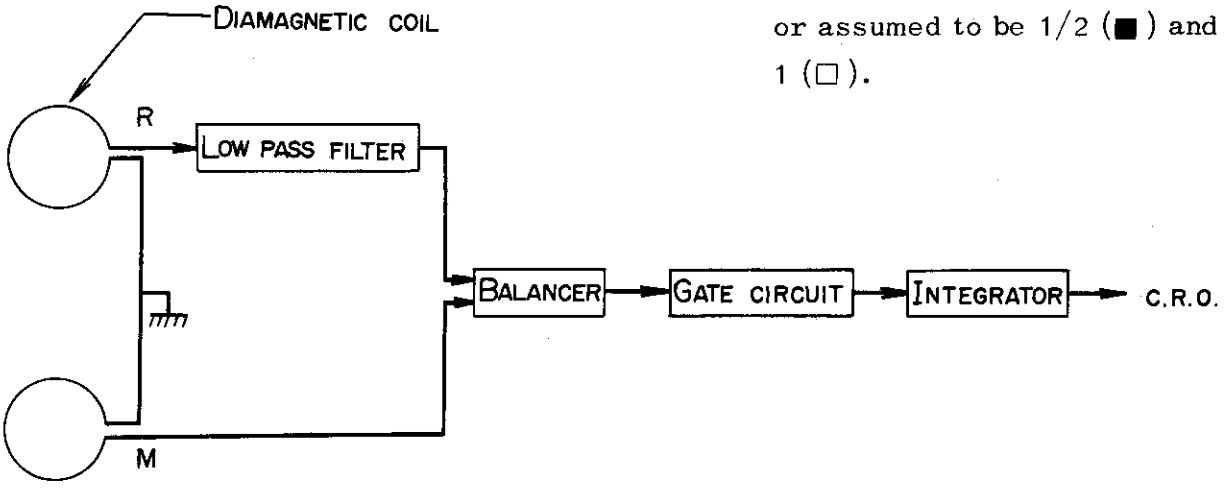

Fig. 5 Block diagram of the diamagnetic measurement.

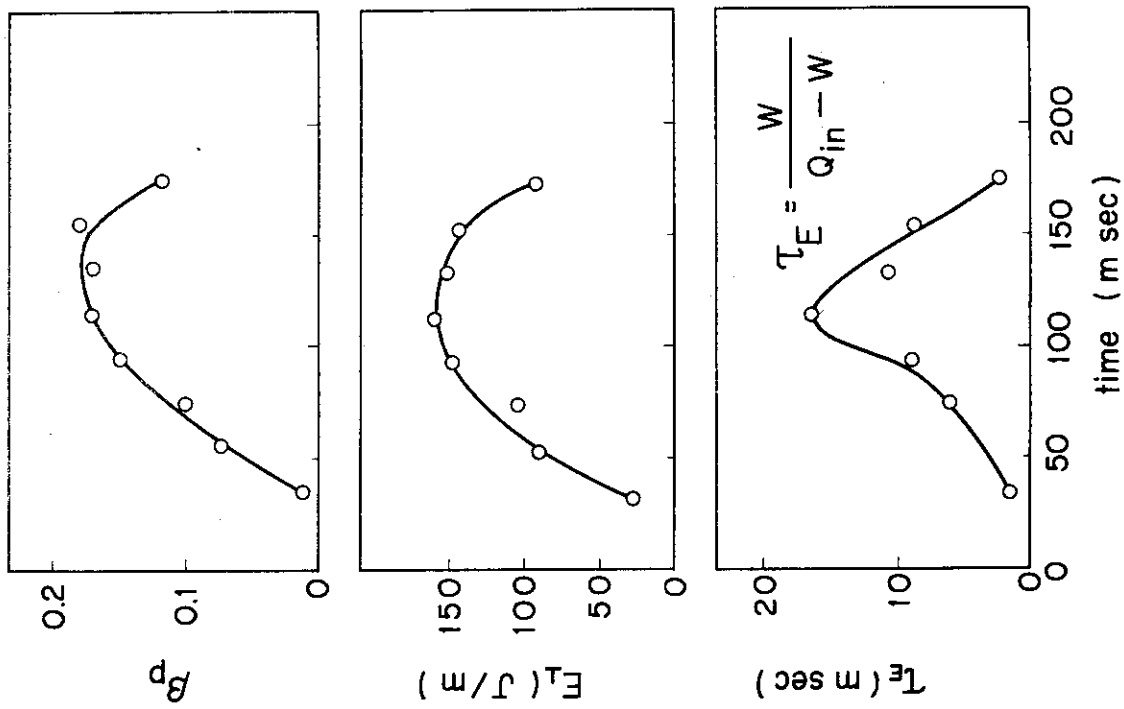

Fig. 7 Time dependence of β_p, E and τ_E.

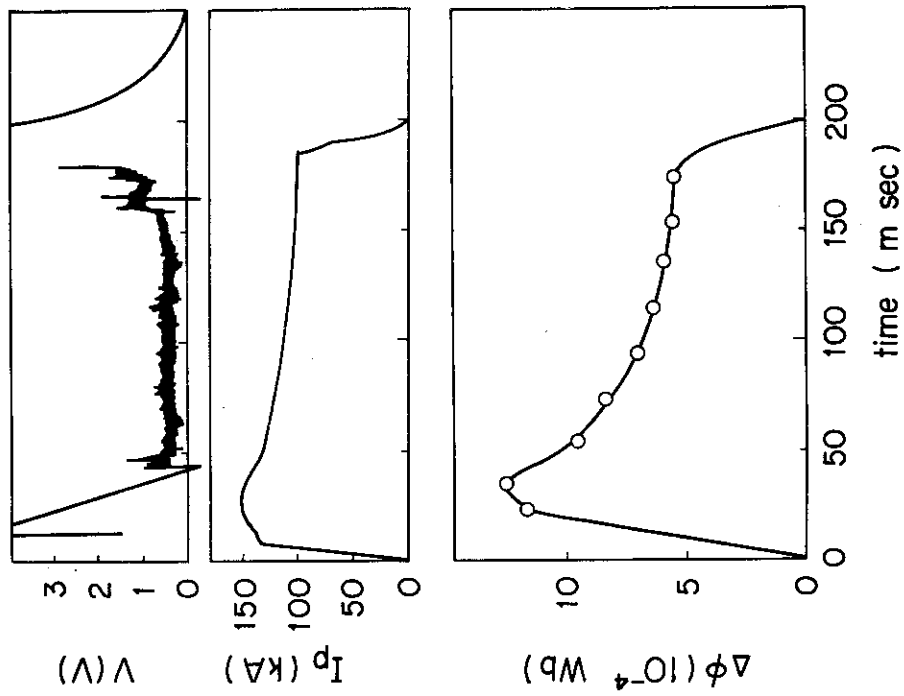

Fig. 6 Time dependence of V, I_p and $\Delta\phi$.

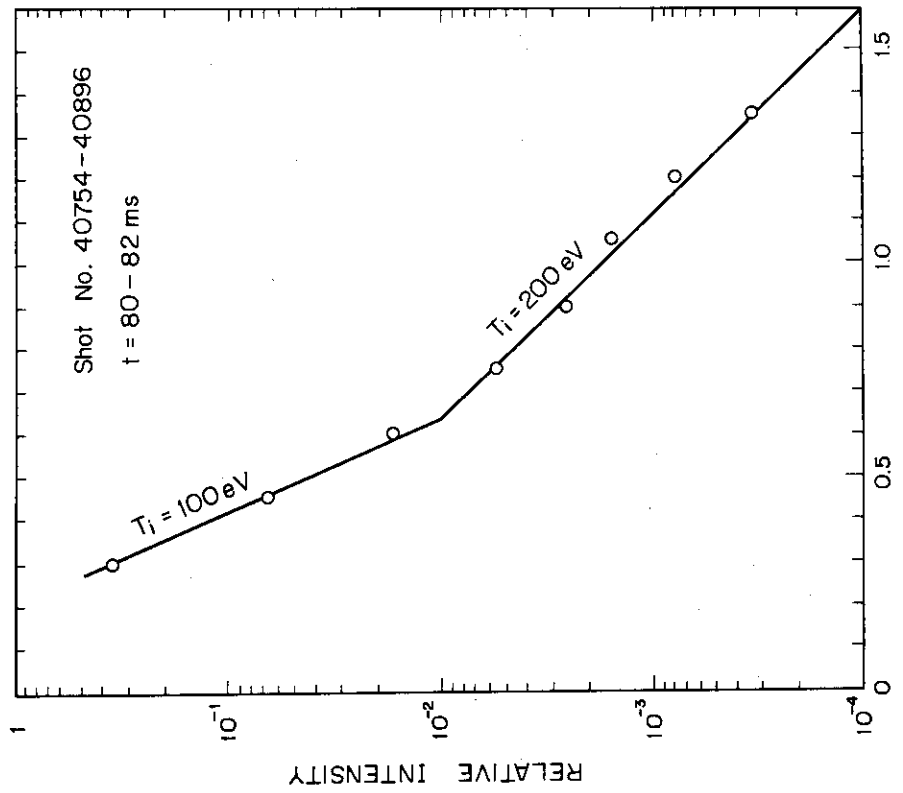

Fig. 9 Relative intensity vs. energy for obtaining the ion temperature from the slope of curve.

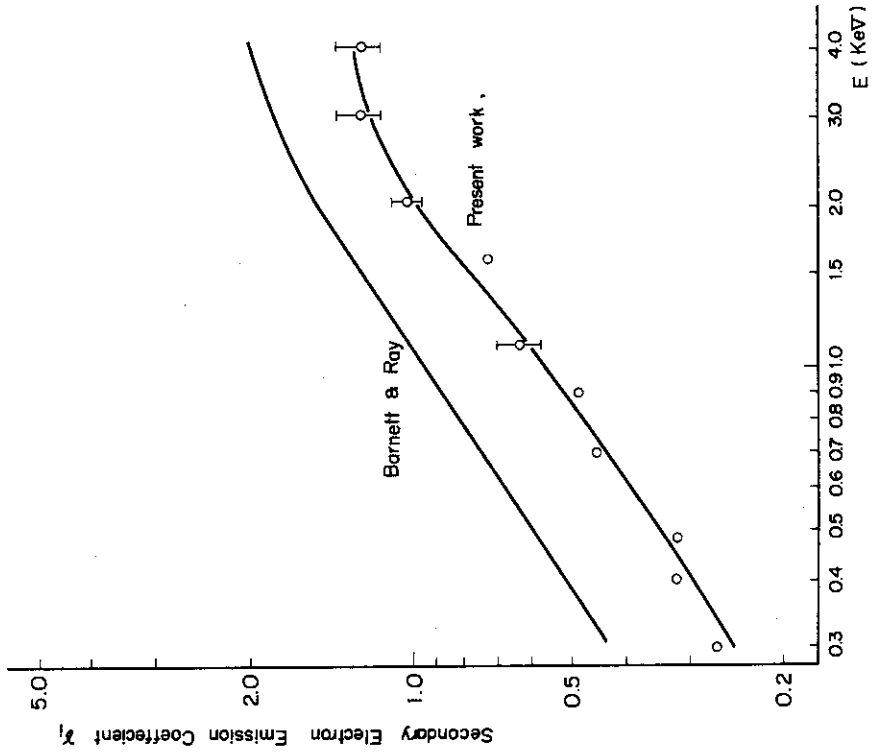

Fig. 8 Secondary electron emission coefficient γ_i for H^+ incident on copper surface with an angle of 90 degree. The difference in two curves is probably due to the difference in surface conditions.

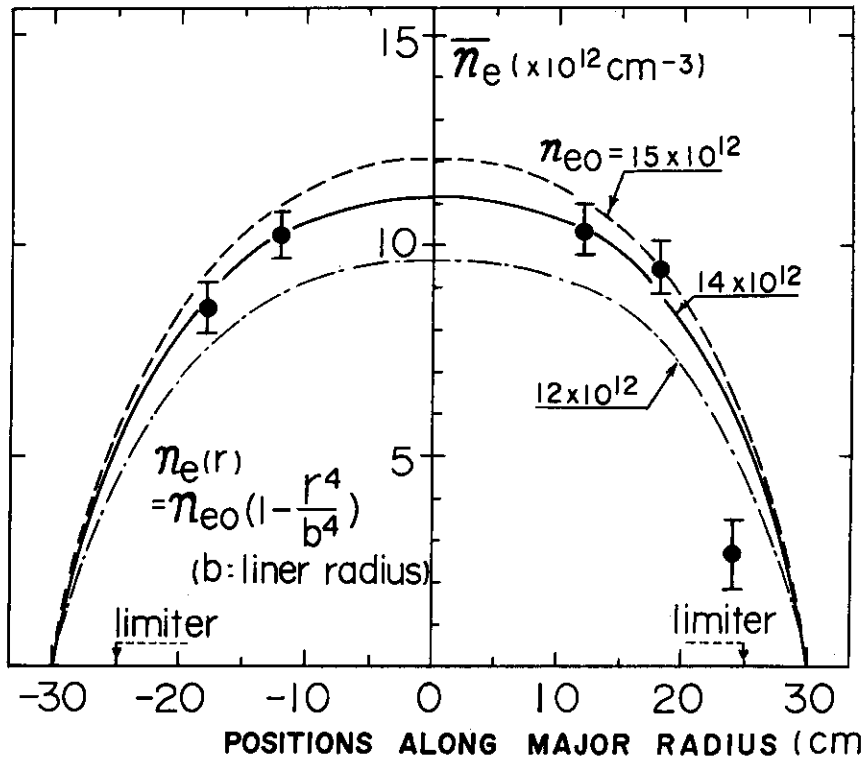

Fig. 10 Measured average electron densities $\bar{n}_e$(t=100 msec) versus the positions of wave-paths. (dotted line: n_{e0}=1.5 x 10^{13} cm^{-3}, solid line: 1.4 x 10^{13}, and dot-dash-line: 1.2 x 10^{13})

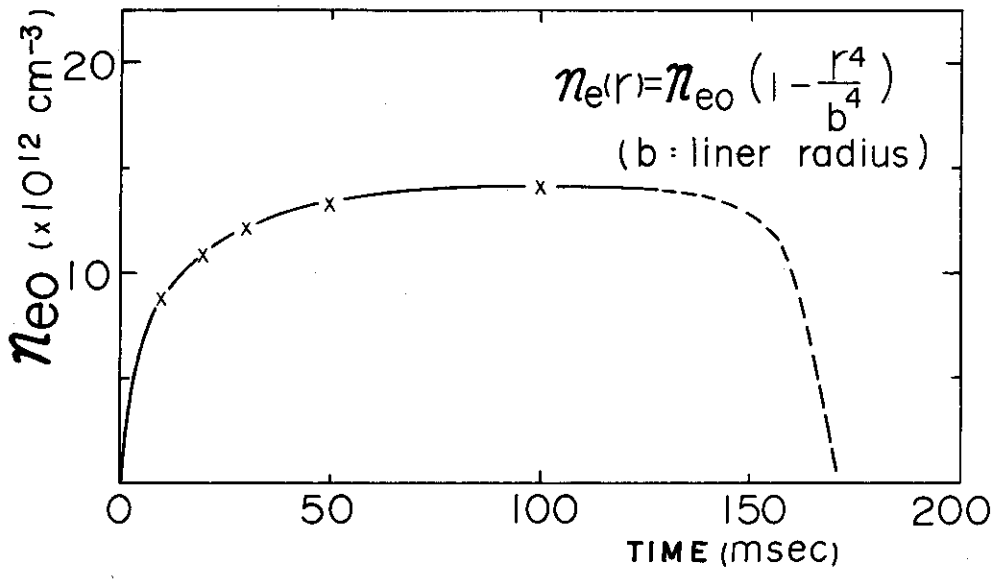

Fig. 11 Time-variation of maximum, central electron density n_{e0}.

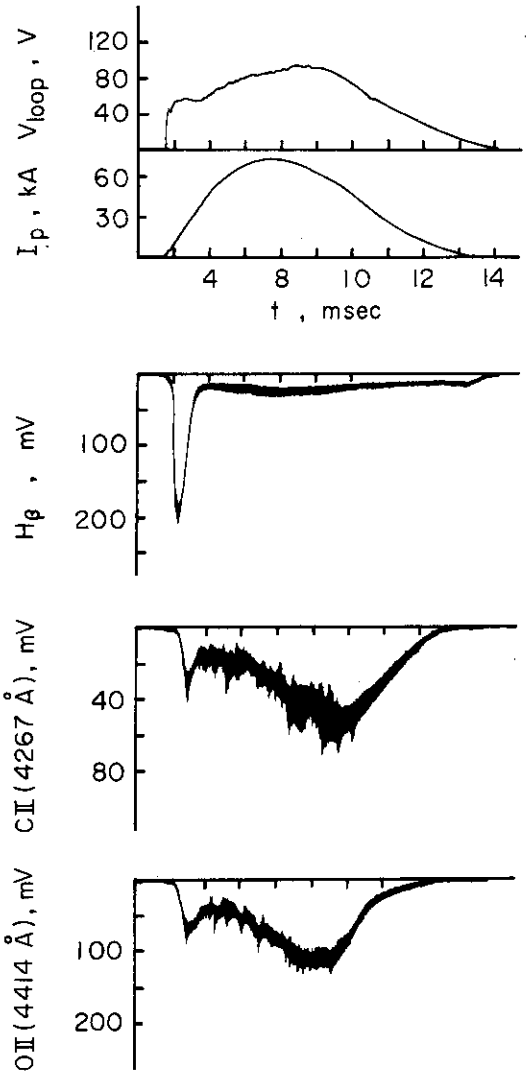

Fig. 12 Typical oscillograms of I_p, V_{loop}, H_β , CII and OII after about 2400 shots of discharge cleaning.

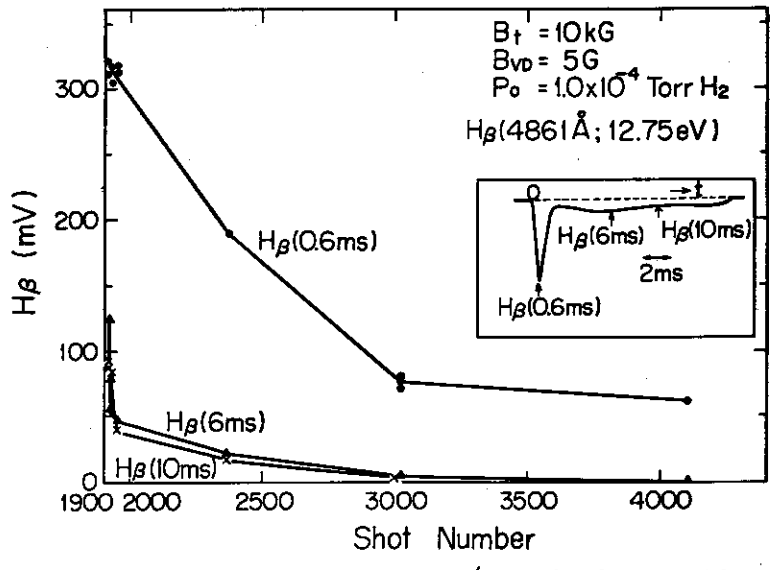

Fig. 13 H_β line intensities (t=0.6, 6, and 10 msec) versus shot number.

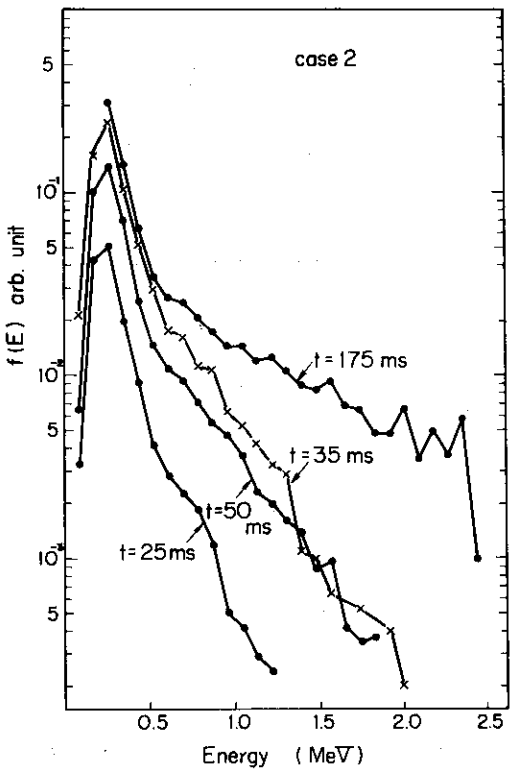

Fig. 14 Energy spectrum of hard X-ray in the Case 2 discharge. Correction to the slit of Pb and to the detecting efficiency of NaI is made. The current duration time is about 200 msec.

Case2: P_f=1.6 x 10^{-4} torr H_2 (with ECRH pre-heating), V=18 kV (400 μF) +2.6 kV (10200 μF), B_{VD}=133 G, B_{VP}= 120 G and B_t=10 kG.

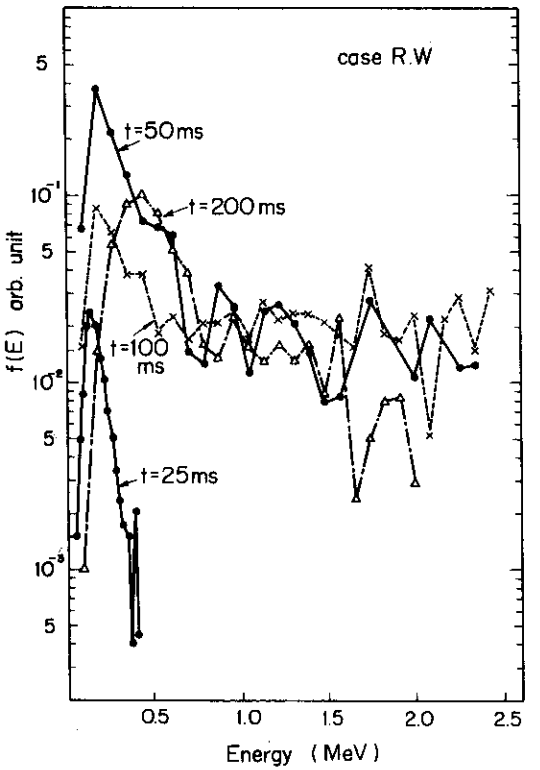

Fig. 15 Energy spectrum of hard X-ray in the Case R.W. discharge. No correction is made. The current duration time is about 800 msec.

Case R.W.: P_f=0.8 x 10^{-4} torr H_2 (with ECRH pre-heating), V=18 kV (400 μF) + 4.0 kV (10200 μF), B_{VD} =133 G, B_{VP} =120 G and B_t=10 kG.

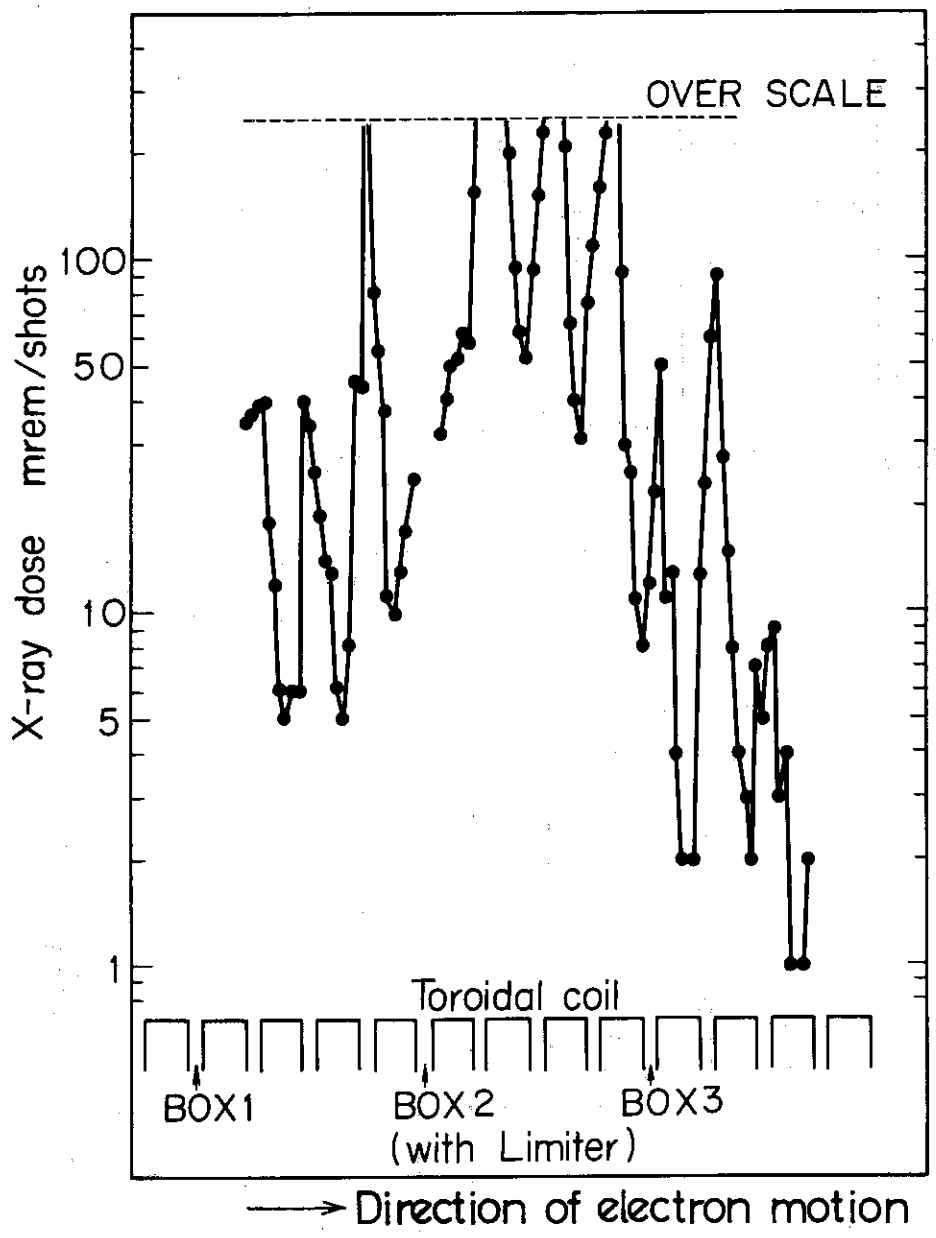

Fig. 16 Toroidal distribution of X-ray dose measured with pocket dosimeters outside the toroidal coils. R=170 cm, z=0 cm. Dose behind the toroidal coils is one order smaller than that in the face of the limiter.

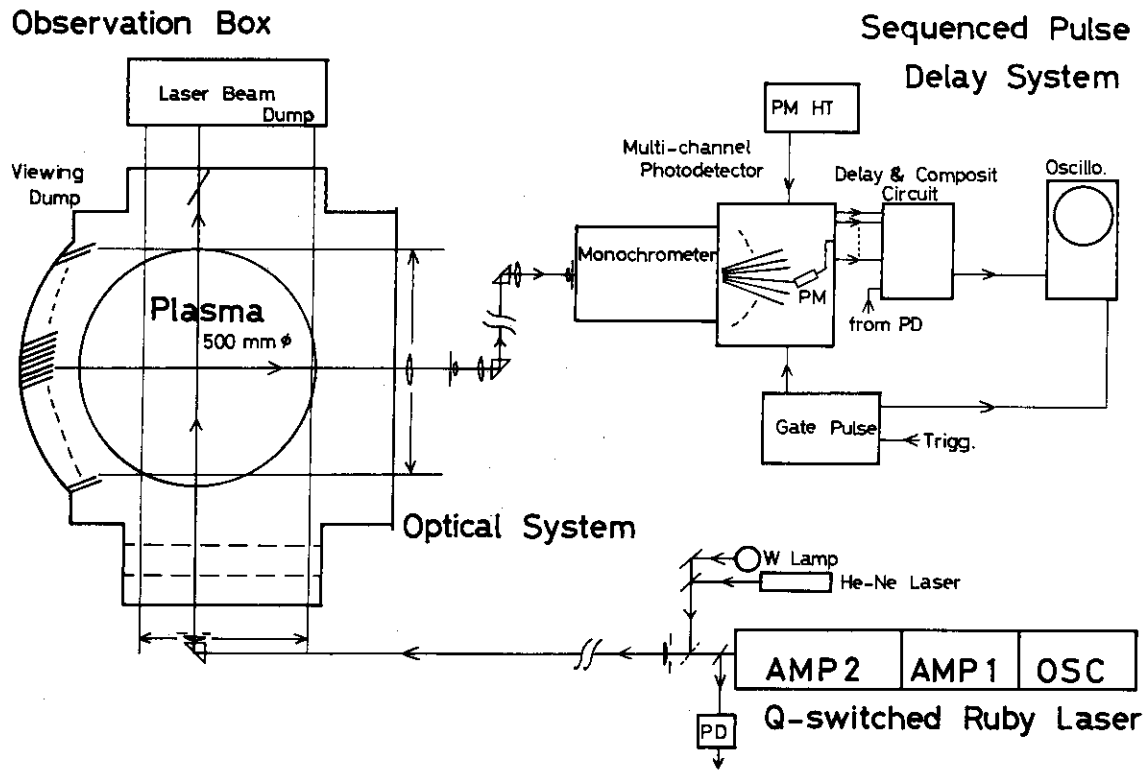

Fig. 17 Schematic diagram of the laser scattering experiment on JFT-2.

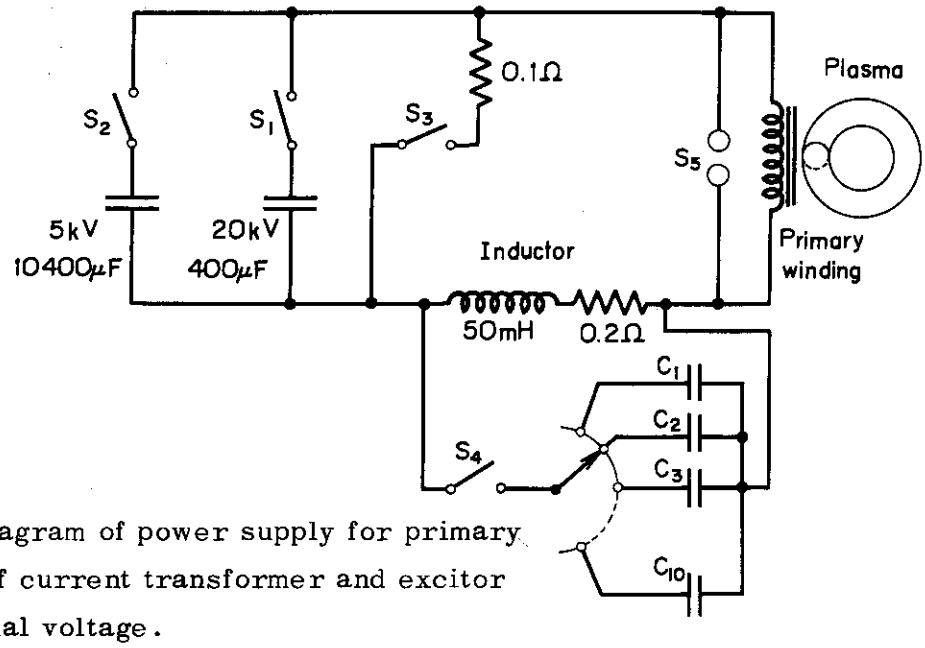

Fig. 18 Circuit diagram of power supply for primary windings of current transformer and excitor of sinusoidal voltage.

S_1, S_2, S_3: Ignitrons

S_4: Air gap switch for exciting the sinusoidal voltage.

S_5: Air gap for protecting the primary windings.

C_1, C_2, ..., C_{10}: 600 μF —— 0.02 μF, 200 V —— 10 kV.

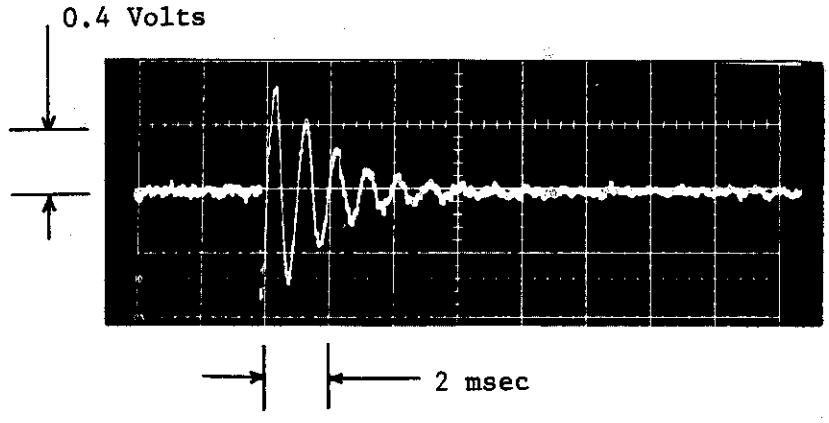

Fig. 19 Typical waveform of voltage superimposed on the main loop voltage. Frequency components lower than 1 kHz and higher than 3 kHz are eliminated by the band-pass filter.

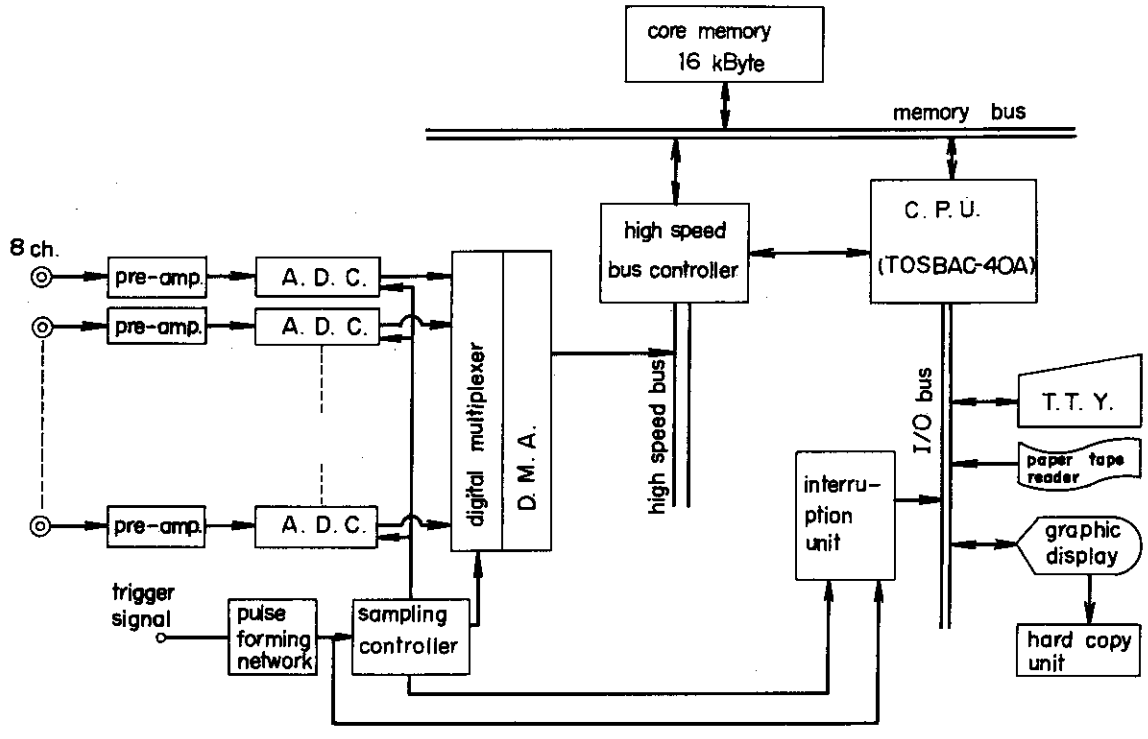

Fig. 20 Block diagram of the data acquisition system.

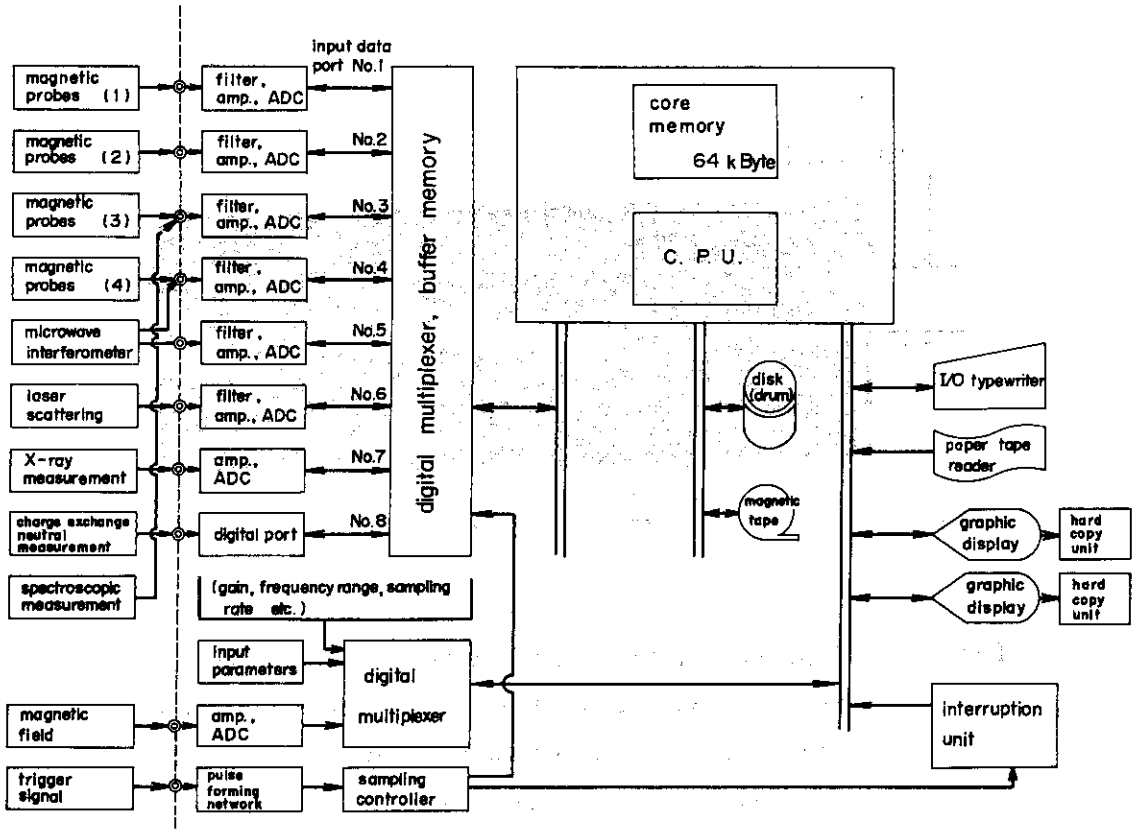

Fig. 21 Simplified block diagram of the data processing system.

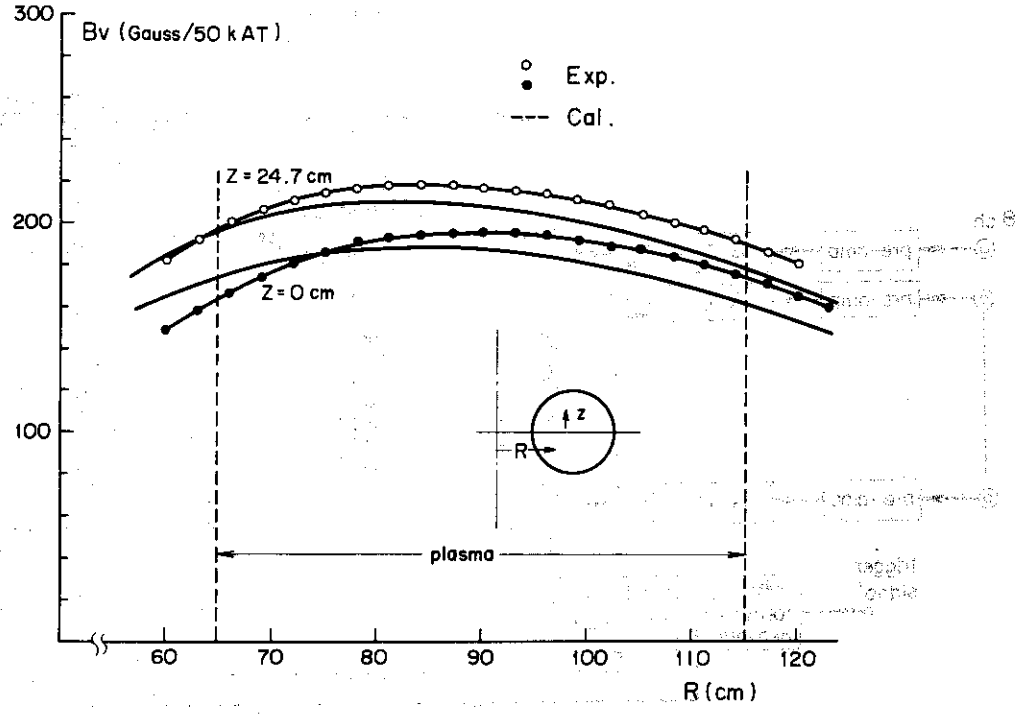

Fig. 22 Radial distribution of the D.C. vertical magnetic field comparing experimental data with a simplified calculation in which no iron core is present.

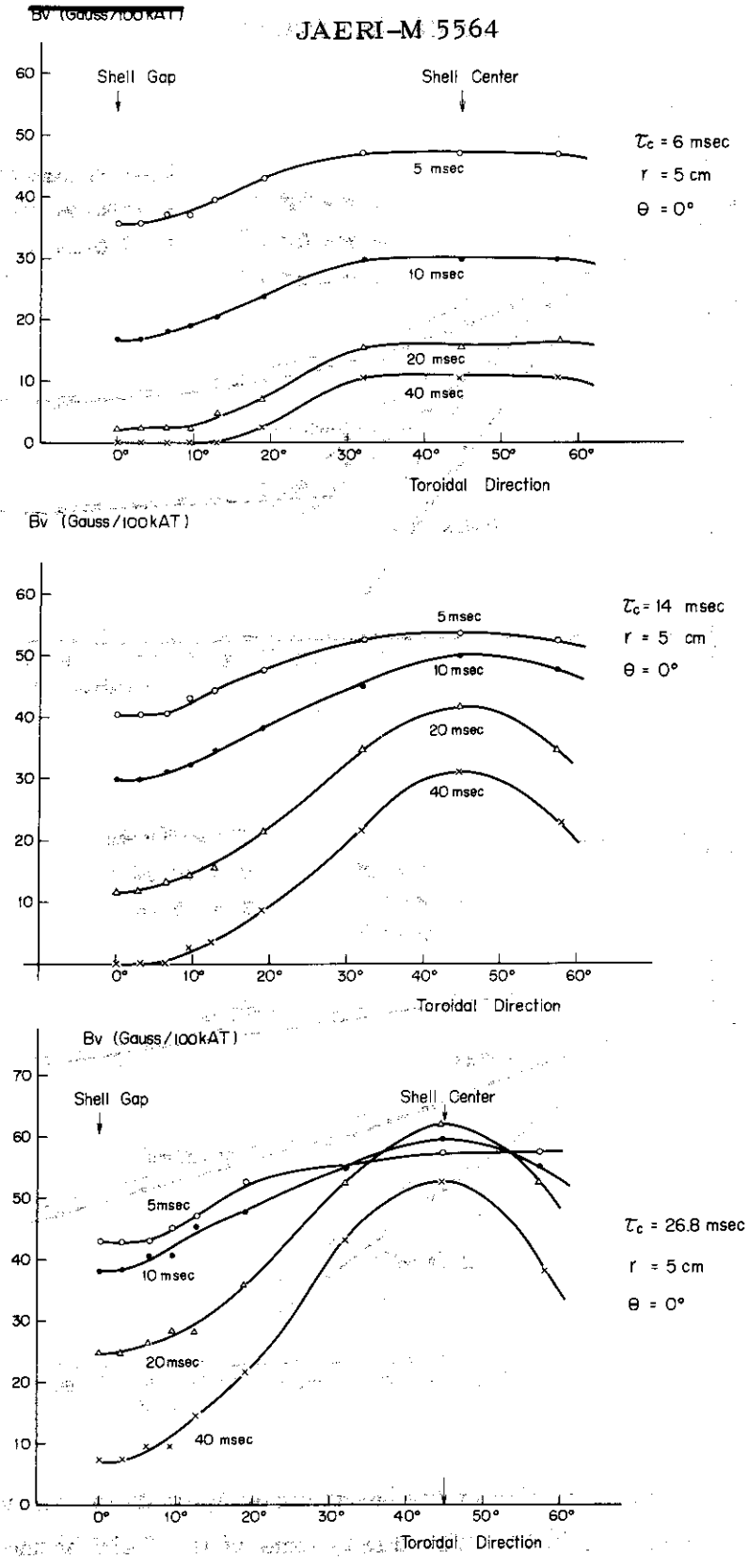

Fig. 23 Toroidal distribution of the vertical component of the pulsed vertical magnetic field with time measured at r=5 cm and $\theta = 0^{o}$ for various current decay times(τ_c).
(a) τ_c=6 msec, (b) τ_c=14 msec and (c) τ_c= 26.8 msec.

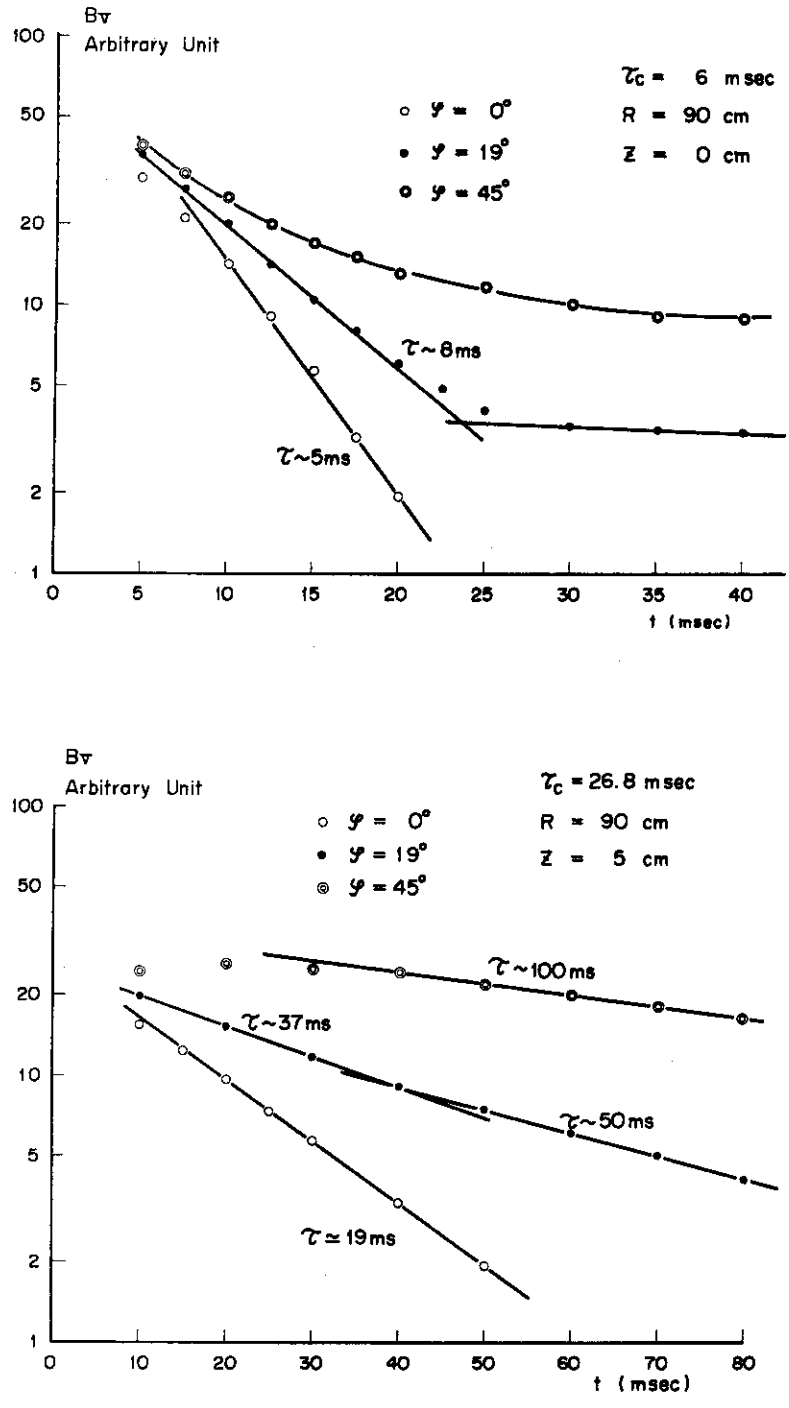

Fig. 24 Time behavior of the vertical component of the pulsed vertical field. The decay time of the field at the gap nearly equals to that of the coil current, while at the middle of the shell it becomes long with time. τ_c is the decay time of the coil current. (a) τ_c=6 msec and (b) τ_c=26.8 msec.

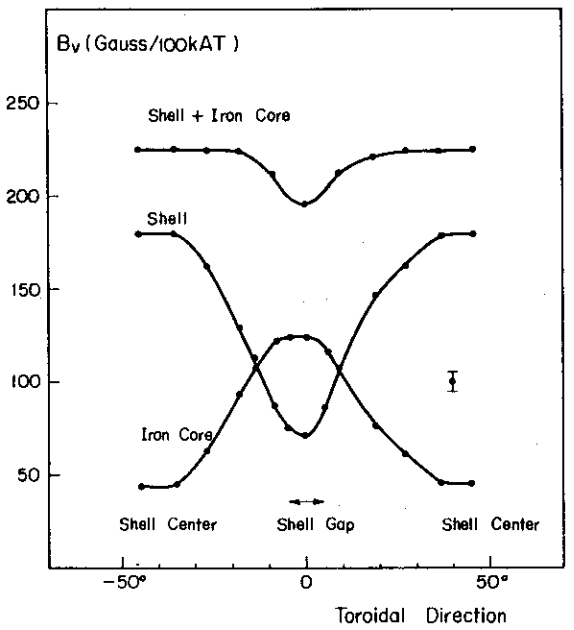

Fig. 25 Toroidal distribution of the vertical field due to the shell and the iron core averaged over the area of the pick up coil. The magnetic field of the shell is weakned at the gaps in the shell but the leakage magnetic field from the iron core penetrates inside the shell through the gaps.

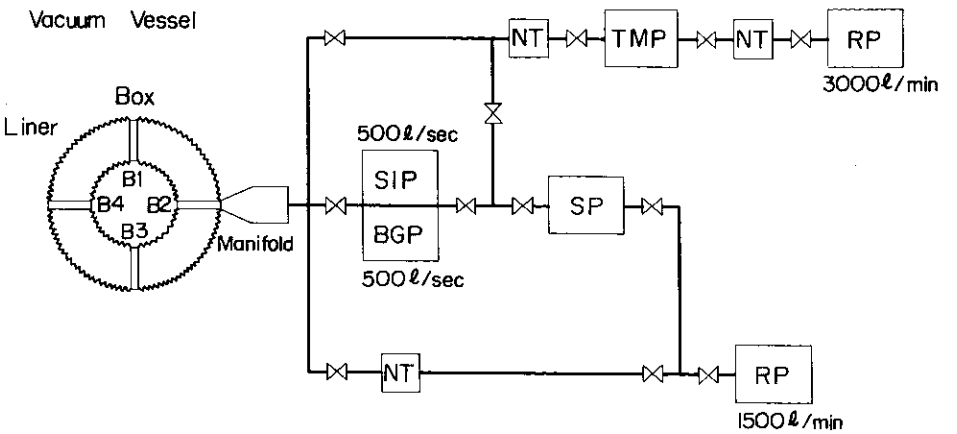

Fig. 26 JFT-2 vacuum system.

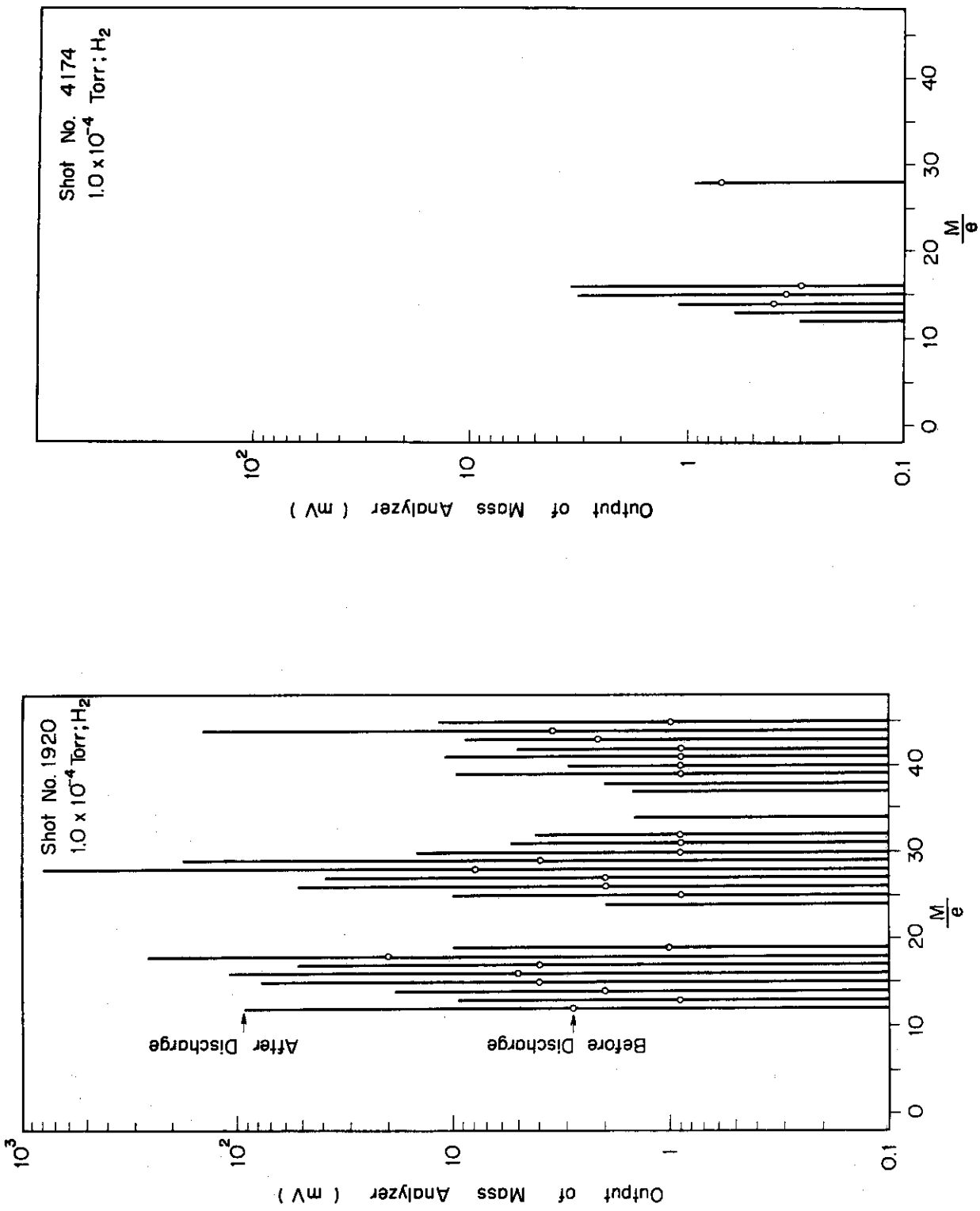

Fig. 27 Impurites with M/e from 1 to 50 at the 1920th and the 4174th shots.

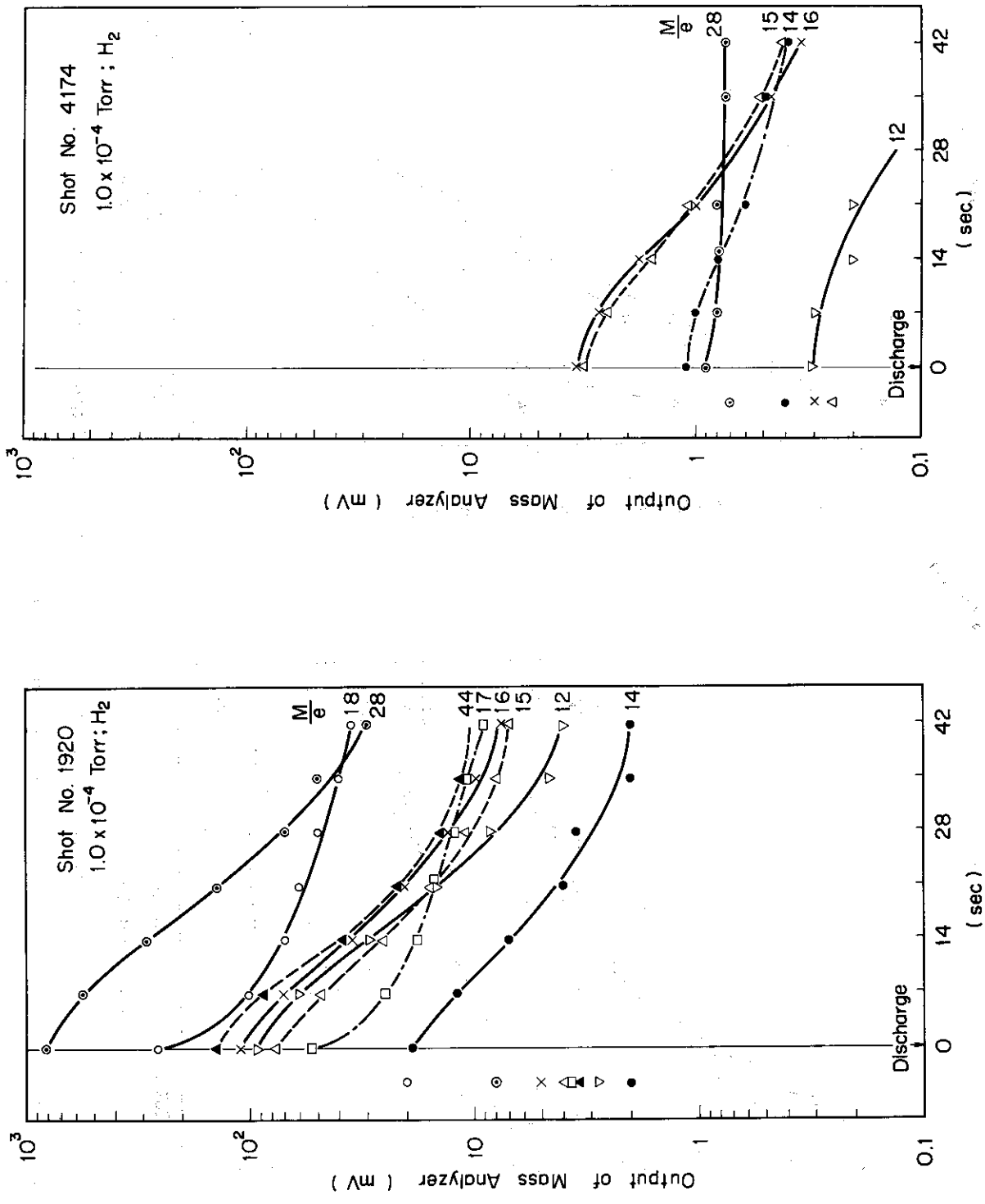

Fig. 28 Time evolution of impurities at the 1920th and the 4174th shots.

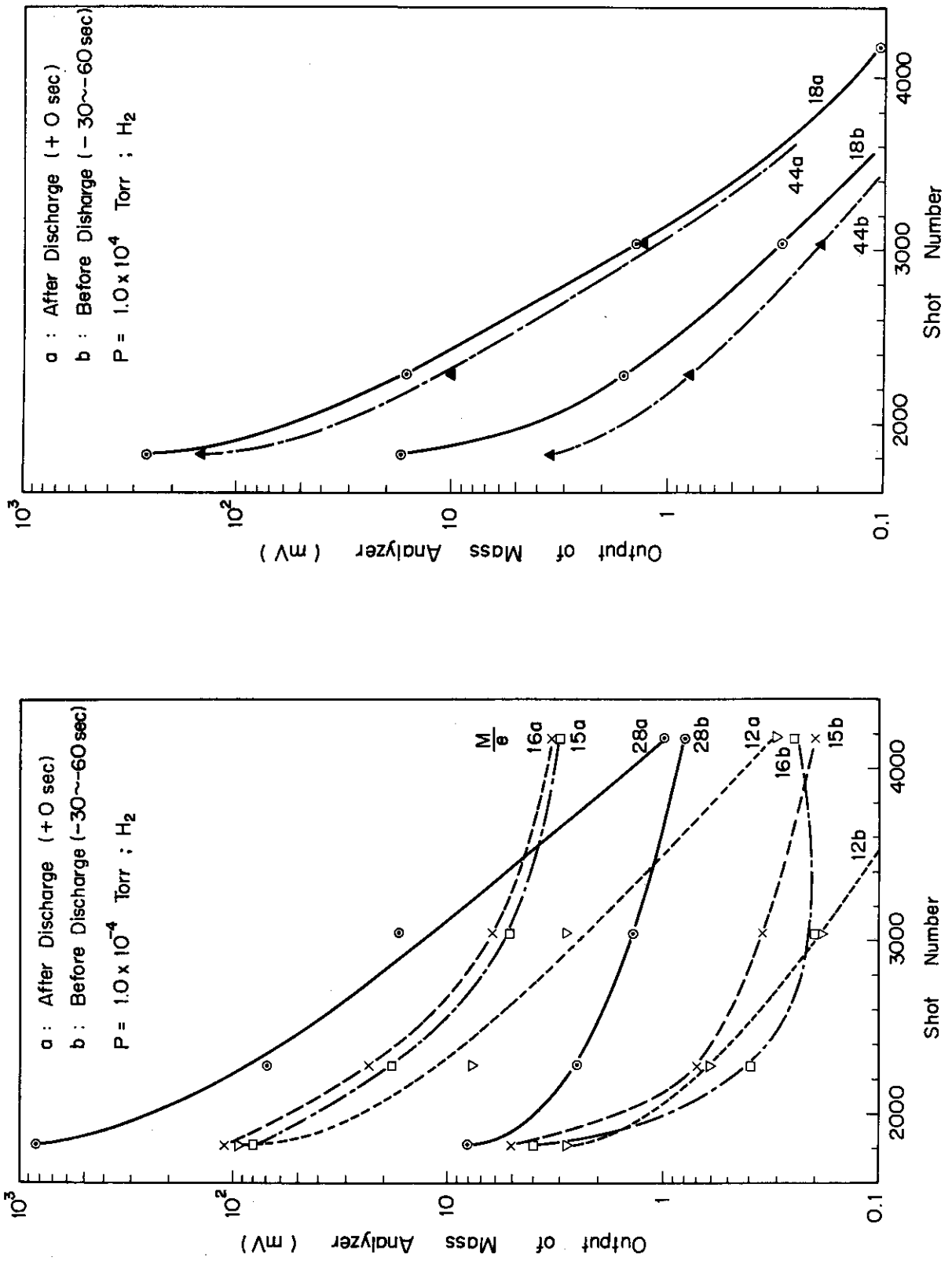

Fig. 29 Typical impurities before and after discharges versus shot numbers.

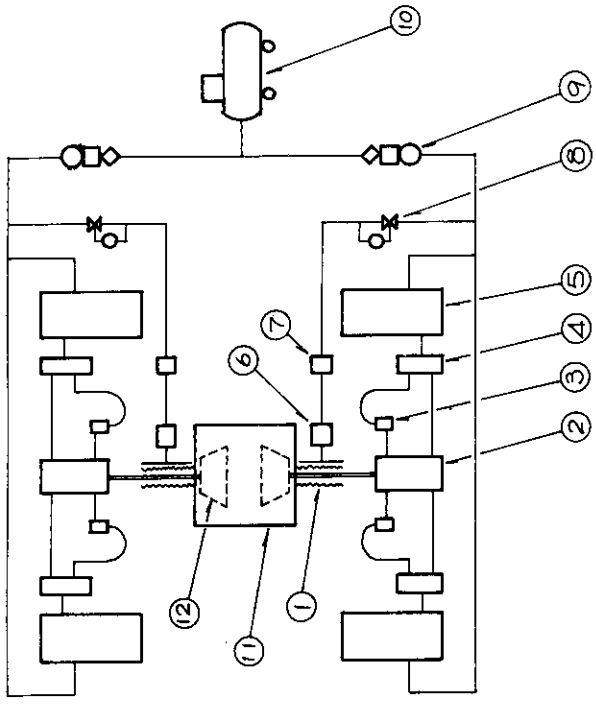

Fig. 31 The flow-sheet of driving mechanism of the dynamic limiter.
1) Welded bellows, 2) Air-cylinder, 3) Quick-exhausting valve, 4) 4-way valve, 5) Pressure tank, 6) Small air-cylinder for preventing bellows from vibration, 7) 3-way valve, 8) Reducing valve, 9) Pressure regulator, 10) Compressor, 11) Limiter box, 12) Parallel limiter.

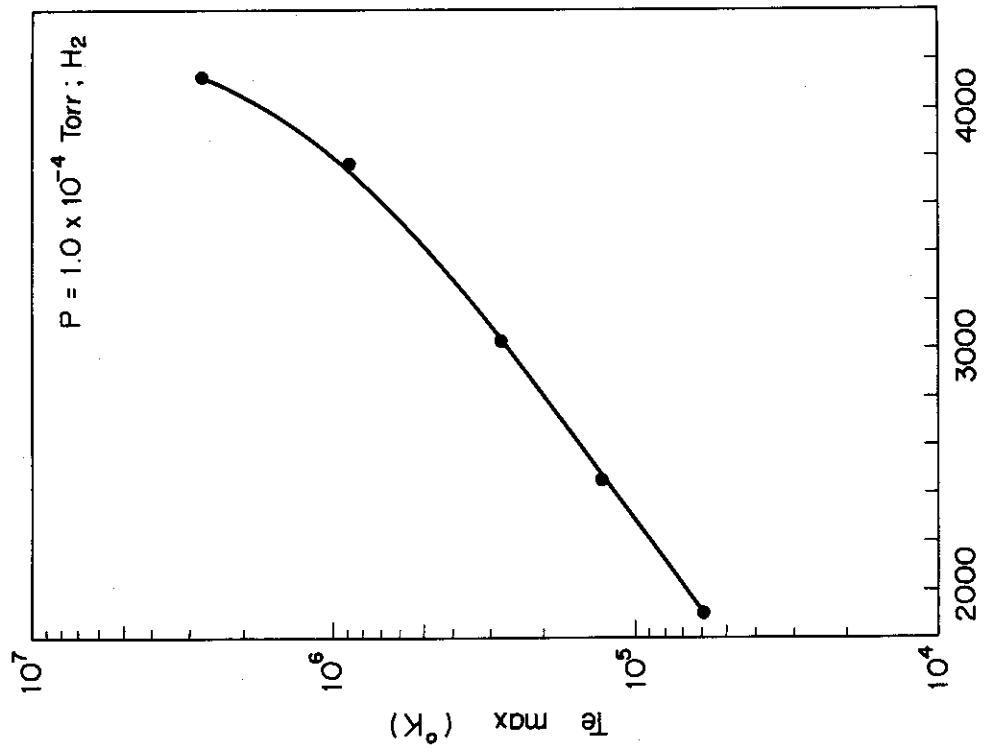

Fig. 30 Relation between the electron temperature and the shot number.

3. JFT-2a (DIVA)

A. Kitsunezaki, H. Maeda,
Y. Shimomura and M. Yoshikawa

3.1 Introduction

Significant progress made recently in plasma confinement in tokamaks suggests that two lines of research be undertaken in parallel to reach the goal of nuclear fusion research at an early date. One is to construct tokamaks of a large size in which scaling laws of confinement are extended to higher temperatures and densities. The other is study of tokamaks with specific objectives in which new concepts in tokamak confinement are tested.

The device described here[1] belongs to the second classification. The objective of the experiment is to study plasma confinement in tokamaks with a noncircular cross-section which possess higher stability properties than tokamaks with a circular cross-section and to investigate the operation of an axisymmetric divertor and its effect on plasma confinement. Conceptual design of the device is made under the following considerations: (1) The size of the device is large enough to allow comparison of experimental results with those in existing tokamak devices. Specifically plasma temperature of hundreds of eV is sought. (2) Plasma confinement can be studied with and without the divertor. (3) It is not intended to extend scaling laws of confinement to higher temperatures. Specifically no neutral injection heating is planned.

There are two types of noncircular cross-sections with better stability properties than the circular: the letter D-like cross-section and the teardrop-like cross-section.

A choice is made in favour of the latter for the present experiment. The reason is that the latter is capable of carrying higher current density than the former and consequently raising the plasma temperature to higher values. These features could be verified experimentally. The major merit of the former, a higher magnetohydrodynamic limit in β, cannot be tested experimentally without a help of powerful supplementary heating, since β attainable in the present-day tokamak experiments is determined by a thermal balance between heat input and losses and is kept to a value much lower than the above-mentioned magnetohydrodynamic limit.

There exists a limitation in the usefulness of conventional limiters which undergo severe surface damage and thermal loading in large tokamak devices

of the future. An axisymmetric divertor or magnetic limiter is one of the possible means in need to replace the conventional metallic limiters. Such a divertor has been incorpolated in the present device to study magnetohydrodynamic equilibria of the confined plasma, thermal properties of the plasma, especially on the flux lines connected to the divertor, and the effectiveness of the divertor operation.

The design of the device JFT-2a (DIVA) has been made and completed in the present reporting period. A summary is given below on the device (3.2 and 3.3), theoretical studies (3.4 and 3.5), and engineering studies (3.6 and 3.7) made in designing the device.

(M. Yoshikawa)

3.2 Brief description of the device

The cross-sectional views and machine parameters of the device are shown in Figs. 1, 2 and Table I. The device has a teardrop-like cross-section with major radius of 60 cm and an average aspect ratio of 5.5. The toroidal field is 10 kG and the steady vertical field is 0.15 kG.

The electric fields to drive a plasma current and a current through the divertor hoop are applied by two separate transformers. A common capacitor bank is connected across a switch to the primary windings of the two transformers connected in series as shown in Fig. 3. By employing such a circuit the ratio of the plasma current and the hoop current can be kept constant during a discharge except in cases where the plasma resistivity remains extremely high during the discharge.

The equilibrium of the plasma is maintained by the divertor hoop, a copper shell covered by gold and a steady vertical field. A set of movable shell can be placed at two positions. For a plasma confinement without the divertor in operation, the movable shell is placed at the "closed" position as shown in Fig. 2. The operation of the divertor is studied by placing the movable shell vertically to the "open" position. Particles escaping from the confinement region are guided along flux lines to the divertor plate. The plate is made of titanium and is periodically refreshed by flushing titanium alloy wires. Limiters shown in Fig. 2 are manually movable. The plasma is produced by initiating a discharge in a gas puffed in from four fast-acting gas valves.

(S. Shimomura, A. Kitsunezaki, H. Maeda and M. Yoshikawa)

3.3 Divertor design

The device is so designed that experiments can be switched between the operations with the divertor and those without it. A set of movable shell may be placed at two positions. For plasma confinement without the diverter in operation the movable shell is placed at the "closed" position as shown in Fig. 2. The operation of the divertor is studied by moving the movable shell vertically to the "open" position. Particles escaping the confinement are guided along flux lines to the divertor plate. The plate is made of titanium and is periodically refreshed by flushing titanium alloy wires. Gold-plated limiters shown in Fig. 2 are manually movable.

We shall describe below considerations made in designing the divertor[2].

(1) Magnetic flux required between the plasma and the wall

The difference $\Psi_{wall}-\Psi_{plasma}$ in the flux function Ψ between the plasma and the wall should be large enough to ensure that the bulk of particles lost from the confinement reach the divertor region. An analysis is made by assuming a collisional loss along flux lines with a time constant $\tau = 1.03\,\tau_{ii}\log_{10}R_m = \alpha T_i^{3/2}/n$ and a diffusional loss across flux lines with a banana diffusion coefficient times an anomaly factor γ, that is, $D = \gamma D_{banana} = 1.12\,\gamma a_{ep}^2\,\varepsilon^{1/2}(1+T_i/T_e)/\tau_e = \gamma\,\delta n/T_e^{1/2}B_p^2$, where a_{ep} is the electron gyroradius in the poloidal magnetic field B_p, ε the inverse aspect ratio, and R_m the mirror ratio. The transport equation in the divertor flux surfaces is solved including the effect of a singularity in the flux volume $dV/d\Psi \propto (\Psi-\Psi_s)^{-1+2/m}$ near the separatrix $\Psi=\Psi_s$ with the multipolar order m. Figure 4 shows, for various values of m, $\Phi_{wall}/\Phi_{plasma}$ the ratio of particle loss flux to the wall to the total loss flux as a function of $\Psi_{wall}-\Psi_{plasma}$. The unit of Ψ is $\Psi_1 = \{2\sigma\delta\gamma T_{iav}^{3/2}/T_{eav}^{1/2}\}^{1/2} = 23\,\gamma^{1/2}A^{1/4}Z^{-1/2}\varepsilon^{1/4}(\log_{10}R_m)^{1/2}(1+T_{iav}/T_{eav})^{1/2}\cdot(T_{iav}/T_{eav})^{3/4}T_{eav}(eV)^{1/2}$ G-cm. Here A and Z are the mass and the charge number, respectively, of the ions. The figure shows that $\Psi_{wall}-\Psi_{plasma} > 2.5\,\Psi_1$ is required for $\Phi_{wall}/\Phi_{plasma} < 0.01$. When a Bohm-like diffusion is assumed instead in the divertor flux surfaces a similar treatment can be made. Table II lists the maximum values of $\gamma = D/D_{banana}$ and $\gamma' = D/D_{Bohm}$ allowable for $\Phi_{wall}/\Phi_{plasma} < 0.01$.

A simple orbit analysis shows that the maximum separation between the drift and the magnetic surface is given by $\Delta\Psi = \{(1-B_0/B_d)^{1/2}+(B_0/B)(1-B/B_d)^{1/2}\}(mv/e)$. Here B is the total magnetic field at the position where the separation is concerned, B_0 is the field at the intersection of the particle orbit with the median plane, and B_d the field at the divertor. The separation is the largest

for $B = B_0$ and is $(2mv/e)(2-B_0/B)^{1/2}$. For a typical case of $B_d = 2B_0$ and $B_p = 2000$ G the separation is 1 cm and 0.3 cm for hydrogen ions of 100 eV and 10 eV, respectively, in energy.

(2) Trapping efficiency of neutral particles at the divertor

The trapping probability on titanium of hydrogen ions with energies above 3 keV is over 0.9 up to a dose of 10^{19} cm^{-2}. Although no measurement has apparently been reported in the 100 eV range, the trapping efficiency should be substantial since the range of ions is more than a few lattice constants.

Trapping in the divertor of neutral particles backscattered at the divertor plate can be provided with a moderate sticking probability on titanium evaporated on the inner surfaces of the vacuum chamber. A Monte-Carlo calculation has been made on backstreaming process. The time-integrated influx N_{total} and backstreaming flux N_{back} to the plasma are shown in Fig. 5 as a function of time. Table III summerizes the backstreaming fraction for H, H_2, O, and CO. The fraction can be held below 10 %. The sputtering yield of titanium by 100 eV hydrogen ions is in the range of 10^{-3}.

(3) Backstreaming of neutral particles upon ionization near the divertor

The mean energy of neutral particles produced at the divertor plate by ion impact is in the range of 1-5 eV. These particles may be ionized when passing through the plasma near the divertor. A small fraction of those ions may enter the main bulk of the plasma. The plasma density near the divertor can be estimated as $n_d = (B/B_p)\cdot(S/2\,\tau_n v_i^* d)n_e$, where S is the cross-sectional area of the plasma, τ_n the particle confinement time, v_i^* the ion velocity at the electron temperature, d the width of the plasma sheet near the divertor, and n_e the plasma density of the confined plasma. The calculated probability of local ionization is shown in Table IV. Most of particles in the eV energy range can go through the local plasma and then are absorbed in the aforementioned way. At the thermal velocity the ionization probability becomes substantial as shown in Table IV.

(4) Methane problem

Titanium surfaces have practically no sticking probability with methane and worse can produce hydrocarbons upon interaction with hydrogen. The methane released from the surface at thermal velocity has a higher possibility of being locally ionized as seen in Table IV.

The methane production can be limited by the supply of carbon. The major

supply of carbon is the alloy wires which have carbon content of 150-300 ppm. A calculation shows that the total number of carbon atoms from the above source and others amounts to 20 % of that of hydrogen ions in the confined plasma. Since only a small fraction of carbon from the alloy wires would be available for the methane production and a small part of ions produced by local ionization will actually enter the plasma, the impurity level of the confined plasma would be much less than the above figure. Furthermore the Monte-Carlo calculation shows that the backstreaming fraction at 5 msec of methane molecules at the thermal velocity is less than 20 %, even if the sticking probability is assumed to be zero. This should help further reduce the backstreaming.

(M. Yoshikawa and Y. Shimomura)

3.4 Equilibrium of a noncircular cross-section tokamak

A study is made on the equilibrium of a noncircular tokamak and applied to the design of the JFT-2a (DIVA) device. The equilibrium equation of a toroidal plasma is expressed in a well-known form[3)]

$$R\frac{\partial}{\partial R}\left(\frac{1}{R}\frac{\partial \Psi}{\partial R}\right)+\frac{\partial^2 \Psi}{\partial Z^2}+a+bR^2=0 \qquad (1)$$

The solution of the type

$$\Psi = C_1R^2(R^2-4Z^2)+C_2R^2+C_3(R^2\ln R-Z^2)+C_4+aZ^2/2+bR^2Z^2/2 \qquad (2)$$

is used here. This is an exact solution of Eq. (1) and has four free parameters C_1-C_4. The four parameters are determined so that the curve of Eq. (2) of the plasma boundary intersects with a curve

$$\rho^2 = a^2(1+\varepsilon_1 \cos 2\theta + \varepsilon_2 \cos 3\theta)$$

at least at four points at $\theta = 0$, 60°, 120° and 180°, where ρ is the radius and θ the angle around the center point $R = R_0$, $Z = 0$.

The plasma equilibrium configurations expressed by Eq. (2) for various values of the shape parameters ε_1 and ε_2 are shown in Fig. 6. Equilibrium quantities such as safety factor q, magnetic shear and magnetic well depth are also calculated. Typical examples are shown in Figs. 7 and 8. The shear

and the well depth are improved in the teardrop-like cross-section as seen in the figures.

(A. Kitsunezaki, Y. Shimomura and H. Maeda)

3.5 Stability of a noncircular cross-section tokamak

The plasma stability against local instability is studied numerically by using the criterion given by Solov'ev[4]. The computational error in evaluating the stability criterion is examined by varying the number of nodes used in the numerical calculation. The calculated critical q-value for stability with the number of nodes between 100 and 2500 agree with the analytical result within 3 %. The result of the stability calculation for discrete values of ε_1 and ε_2 is shown in Fig. 9. The critical q-value can be made low in the teardrop-like cross-sections compared with the circular cross-section.

(A. Kitsunezaki, Y. Shimomura and H. Maeda)

3.6 Field configurations in vacuum

The magnetic field configuration in the vacuum outside a given axisymmetric plasma equilibrium should be determined so as to satisfy the boundary conditions at the plasma surface. The method employed here is based on Garabedian's[5], in which one of the variables of the elliptic differential equation of the vacuum magnetic field is converted into a complex variable and the analytical continuation is applied. The equation is then converted into a hyperbolic differential equation and the solution can be expressed in an integral form by finding the Riemann function of the field equation.[6),7)] The integral is evaluated numerically by an electronic computer.

The equilibrium solution, Eq. (2) given in 3.4, is written in a convenient form to apply the present method. A typical computed field configuration is shown in Fig. 10.

The computational error should be small since only numerical integration is involved in the computation. In fact, it was found that the equality $\oint B_s d_s = \mu I$ holds within an error of 0.5 % for a case where the number of integration steps is 30.

(H. Maeda, Y. Shimomura, A. Kitsunezaki and M. Yoshikawa)

3.7 Specific engineering tests

(1) Properties of gold films

It is essential in tokamak devices to reduce gas desorption from the surface of vacuum systems under the bombardment of plasma particles. An evaluation has been made on the treatment of the copper shells of the JFT-2a (DIVA) device which are exposed to the plasma. It is well-known that gold films plated on stainless steel provide an inert sorption-free surfaces[8], and that the gold films on stainless steel reduce the outgassing by a factor of 3 to 5 compared with the bare stainless steel surfaces against the electron bombardment in the energy range of 1 to 2 KeV[9]. Based on these results, it is decided to coat the copper shells by gold. Technical development and evaluation in the gold evaporation on copper plates were carried out under a contract with ULVAC Corporation, Chigasaki, Japan. Details of the work performed are presented in the contract report[10]. A brief summary is described here.

As a method known to provide clean gold films firmly bonded with the base metal, the ion plating method is chosen. The evaporation of gold is performed in a glow discharge in inert gas atomosphere. Two types of copper plates are used; one is single-crystalline oxygen-free copper plates of 5 mm x 10 mm x 3 mm (type A sample) and the other amorphous oxygen-free copper plates of 50 mm x 50 mm x 5 mm (type B sample).

i) The results with type A samples

1) Crystalline-to-amorphous transition of gold films

For the measurement of the critical temperature of crystalline-to-amorphous transition of gold films on Cu(1,1,1) surface, the low energy electron diffraction (LEED) and Auger electron microscopy (AES) studies were performed throughout the evaporation processes under a temperature control. An empirical equation between the thickness d of gold films and the critical transition temperature T_c was found as $\log d \propto \frac{1}{T_c}$, as shown in Fig. 11. It is found that the structure of the gold films cannot be made crystalline when the film thickness exceeds approximately 0.5 μm in the temperature range below 380°C.

2) Test of type A samples

Three kinds of 10 μm gold-coated samples were prepared at evaporation temperatures of 225°C, 315°C and 390°C, and the following tests were performed for each sample.

2.1) Observation of the surfaces of gold films

The observation of the film surfaces by an optical and a scanning electron microscopes shows that the grain sizes and the evaporation temperatures of the samples have a correlation.

The typical grain size in the 225°C, 315°C and 390°C samples are approximately 0.2 μm, 0.3 μm and 0.5 μm, respectively.

2.2) Test of mechanical strength of gold films

Two kinds of tests were performed on the mechanical properties of the gold films. In the first the samples were alternatively placed for two minutes in the baths of liquid nitrogen and boiling water. The observation by an optical nicroscope after three cycles shows that the gold film is peeled off from the copper based for none of samples. Then the samples were bent repetitively by 90 degrees with a radius of 4 mm.
No peeling of gold film was observed before the copper base was torn.
The results of both tests show that the ion-plating method provides gold films firmly bonded with copper base.

2.3) Anti-corrosion test of gold films

Anti-corrosion tests were performed by exposing samples to the saturated vapor of nitric acid. Several etched pits were observed over an area of 5 mm x 15 mm in the 225°C samples, while none were observed in the 315°C and the 395°C samples.

2.4) Pin holes in gold films

The observation of pin holes was performed on gold films peeled off carefully from each sample by an optical microscope.

Contrary to the test 2.3), it is found that there exist about twenty pin holes over the surfaces of 5 mm x 15 mm of all the gold films observed.

ii) The results with type B samples

The type B samples were prepared by depositing gold film of 10 μm in thickness on amorphous oxygen-free copper plates, held at a temperature varied between 130°C and 320°C. The tests made on those samples are the same as on the type A samples. Despite the difference in the crystalline structure the test results for both types of samples were quite similar.

Technical problems associated with obtaining a film uniform in thickness over a large area were studied. It is found that three evaporation sources are required to keep the thickness uniform with ±30 % over a circular area of 36 cm in diameter at a distance of 20 cm.

The effectiveness of various cleaning treatments in cleaning smeared gold film surfaces were examined by using an Auger electron microscope. The test shows that surface contamination by human fingers can be removed by none of the supersonic washing in alcohol bath, the wiping by tissue saturated by athetone, and the baking at 130°C in vacuum. It is found, however, that the glass bead blasting (GBB) treatment is quite effective in eliminating various contaminants from the gold surfaces.

We would like to express our gratitude to Mr. H. Otsu for the observations of gold films by a scanning electron microscope and Dr. K. Izui for valuable suggestions, both of Laboratory for Solid Chemistry in JAERI.

(H. Maeda and M. Yoshikawa)

(2) Design and engineering tests of a disjointable divertor hoop

One of the possible designs in which the whole device can be assembled and disassembled is to use a divertor hoop consisting of two semi-circular portions with two vacuum-tight connecting joints. The design of such a divertor hoop and the construction and engineering tests of connecting joints are awarded under a contract with Hitachi, Ltd. Details of the design and tests are presented in the contract report,[11] a short summary of which is given here.

It is assumed that the maximum plasma current is 100 kA, the maximum hoop current 60 kA, the steady vertical field 100 G, the interaction between the shell surface and the hoop current can be neglected, and the maximum heat flux onto the hoop from the plasma and the titanium evaporator wire is 190 watt. Then, the electromagnetic force acting on each conductor bar encased in the hoop is the sum of

1) The hoop force of the conductor bar
2) The force produced by interaction of the conductor current with the plasma current and the vertical field, and
3) The force produced by interaction with the currents through the neighboring conductor bar.

The first and the second force, which are directed radially outwards amount to 3400 kgW summed over all the conductor bars. The third force is not important and neglected. Under these specifications two types of feasible designs are made. The connecting joint of each design is shown in Figs. 12 and 13.

The designed maximum stress in the hoop and current density at the joint contact surface are 8.5 kg W/mm^2 and 75 A/mm^2, respectively, for the hoop shown in Fig. 12 and 1.9 kgW/mm^2 and 180 A/mm^2, respectively, for that shown in Fig. 13. The forced air cooling is chosen for the former and the circulated-

oil cooling for the latter. It is not difficult to keep the maximum temperature below 100°C in both designs.

In the test, 60 kAT is driven through the connecting joints in which the return winding is placed so that the stress larger than the design acts on the conductor bars. No damage is found in the conductor bars, contact surfaces and joint bellows. The pressurizing test of the bellows to the designed air pressure, insulation test at the working voltage, and measurement of the contact resistance yielded satisfactory results. An assessment over the choice of the designs shown in Fig. 12 and 13 indicated that the former is more reliable and simpler. Consequently, the former design is incorporated in the final design of the JFT-2a (DIVA) device.

(Y. Shimomura and M. Yoshikawa)

(3) Design and engineering tests of a toroidal coil with joints

Another way to make the device assemblable and disassemblable is to use toroidal coils with connecting joints where they can be separated into two halves (see Fig. 14). The coil design and the fabrication and tests of a piece of the joint are carried out under a contract with NAIG-Toshiba.[12)]

Design consideration is given to the stress distribution in the coil due to the toroidal magnetic field and poloidal field by the plasma and the divertor hoop current. Each coil consists of eight parallel copper plates 7 mm in thickness and 84-137 mm in width. For each coil, two interlocking joints are provided where the contact pressure is applied by a pair of holding plates (see Fig. 15).

A series of tests have been conducted on the joint test piece: the measurement of contact resistence, leakage current between the copper plates, deformation under a simulated mechanical load and the inspection of insulator (NOMEX) sheet used to provide insulation between interlocking copper plates, before, during and after applying a current of 15 kA lasting 1.5 sec for more than 500 times and a simulated mechanical load for more than 16,000 times, and repeating the assembling and disassembling procedures more than 10 times.

The result of the tests is satisfactory which showed no significant increase in the contact resistance and leakage current and no excessive deformation. The only technical problem is the wear observed on the Nomex sheets after a number of assembling and disassembling procedures, which took more time and work than expected. Possible improved designs over the original have been proposed by the manufacturer.

(M. Yoshikawa and Y. Shimomura)

References

1) A. Kitsunezaki, H. Maeda, Y. Shimomura and M. Yoshikawa : in Proceedings of Third International Symposium on Toroidal Plasma Confinement, Garching, March 26-30, 1973, Paper G2.
2) M. Yoshikawa, Y. Shimomura, H. Maeda and A. Kitsunezaki : in Proceedings of Sixth European Conference on Controlled Fusion and Plasma Physics, Moscow, July 30- August 4, 1973, Vol. I, p. 173.
3) T. Ohkawa : Kakuyugo-kenkyu 22, 99 (1968).
4) L.S. Solov'ev : Soviet Phys. JETP 26, 400 (1968).
5) P.R. Garabedian : J. Math. Phys. 36, 192 (1957).
6) K.J. Harker : J. Math. Phys. 4, 993 (1963).
7) M. Tanaka, T. Tuda and M. Azumi : J. Phys. Soc. Japan 34, 1641 (1973).
8) S. Komiya, T. Narusawa and C. Hayashi : J. Vac. Sci. Tech. 9, 302 (1972).
9) Y. Ishibe : Private communication.
10) M. Mizuno, et al. : Report on technical development and evaluation on gold evaporation method, ULVAC Corporation, 1972 (in Japanese).
11) Report on the design, fabrication and test of a disjointable divertor hoop, Hitachi, 1973 (in Japanese).
12) Report on the design, fabrication and test of a toroidal coil with joints, Tokyo Shibaura Electric Co., 1973 (in Japanese).

Table I Dimensions of JFT-2a and plasma parameters

Flux of iron core		0.29	vsec
Toroidal magnetic flux density		10	kG
Vertical flux density		150	G
Shell	inner radius	105 x 145	mm
	major radius	600	mm
	thickness	20	mm
Main condenser energy		90	kJ
Plasma	major radius	600	mm
	average aspect ratio	5.5	
	maximum current	100	kA
Maximum divertor hoop current		60	kA

Table II Requirement for the diffusion coefficients in the divertor flux surfaces for particle flux to the wall to be less than 1 % of the total loss flux.

Assumed parameters in 1) hydrogen (A=Z=1), $\Psi_{wall} - \Psi_{plasma} = 2000$ G-cm, $\varepsilon = 0.2$, and $R_m = 1.7$

Assumed parameters in 2) hydrogen (A=Z=1), B=10kG, wall-plasma distance 2cm, τ_n=3msec minor radius 11 cm, and $R_m = 1.7$

Cases	Case I T_e=300eV, T_i=100eV	Case II T_e=100eV, T_i=100eV	Case III T_e=30eV, T_i=10eV
	Plasma thermally well insulated from the wall	Electrons in the divertor flux surfaces cooled	Plasma poorly insulated from the wall
$\gamma = D/D_{banana}$ 1)	$\gamma < 90$ 1)	$\gamma < 30$ 1)	$\gamma < 900$ 1)
$\gamma' = D/D_{Bohm}$ 2)	$\gamma' < 0.01$ 2)	$\gamma' < 0.03$ 2)	$\gamma' < 0.6$ 2)

Table III Time-integrated fraction N_{back}/N_{total} of backstreaming particles (see Fig. 5)

Species	Sticking probability	Time		Species	Sticking probability	Time	
		5 msec	∞			5 msec	∞
H at 323°K	0.1	0.200	0.20	O at 323°K	0.1	0.095	0.20
	0.2	0.095	0.10		0.2	0.070	0.10
	0.3	0.070	0.07		0.3	0.060	0.07
H_2 at 323°K	0.05	0.25	0.35	CO at 323°K	0.1	0.080	0.20
	0.1	0.15	0.20		0.3	0.050	0.07
	0.2	0.10	0.10		0.5	0.025	0.01

Table IV Probability of local ionization of atoms emitted from the divertor plate Assumed parameters are $n_e=3.10^{13}cm^{-3}$, $\tau_n=3$ msec, hydrogen(A=Z=1), and $B/B_p=2.85$

Electron temperature		300eV		100eV		30eV	
Energy of atoms		5 eV	323°K	5 eV	323°K	5 eV	323°K
Species of atoms	H	0.02	0.13	0.03	0.19	0.004	0.02
	O	0.10	0.57	0.13	0.65	0.040	0.23

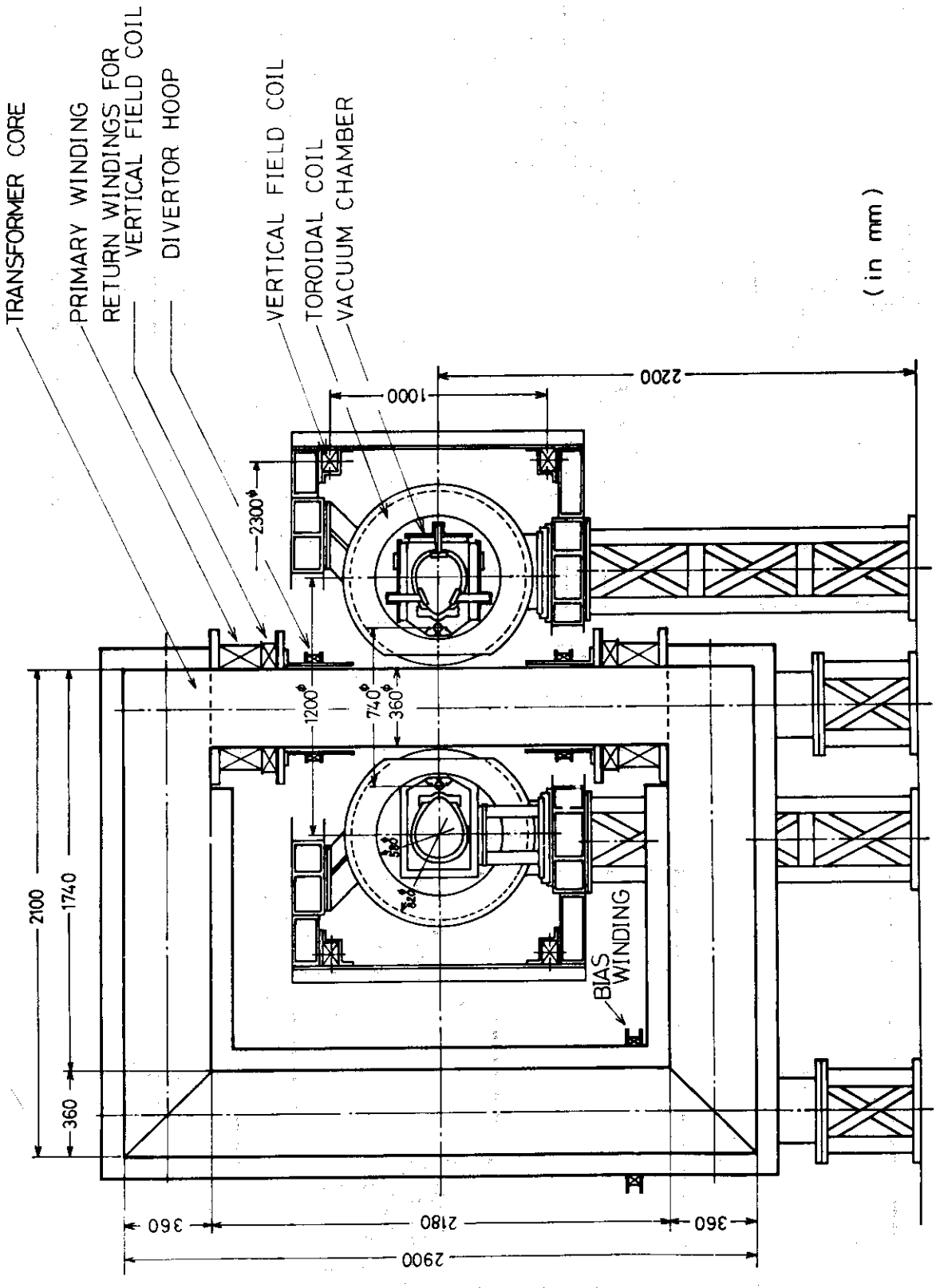

Fig. 1 Cross-section of JFT-2a.

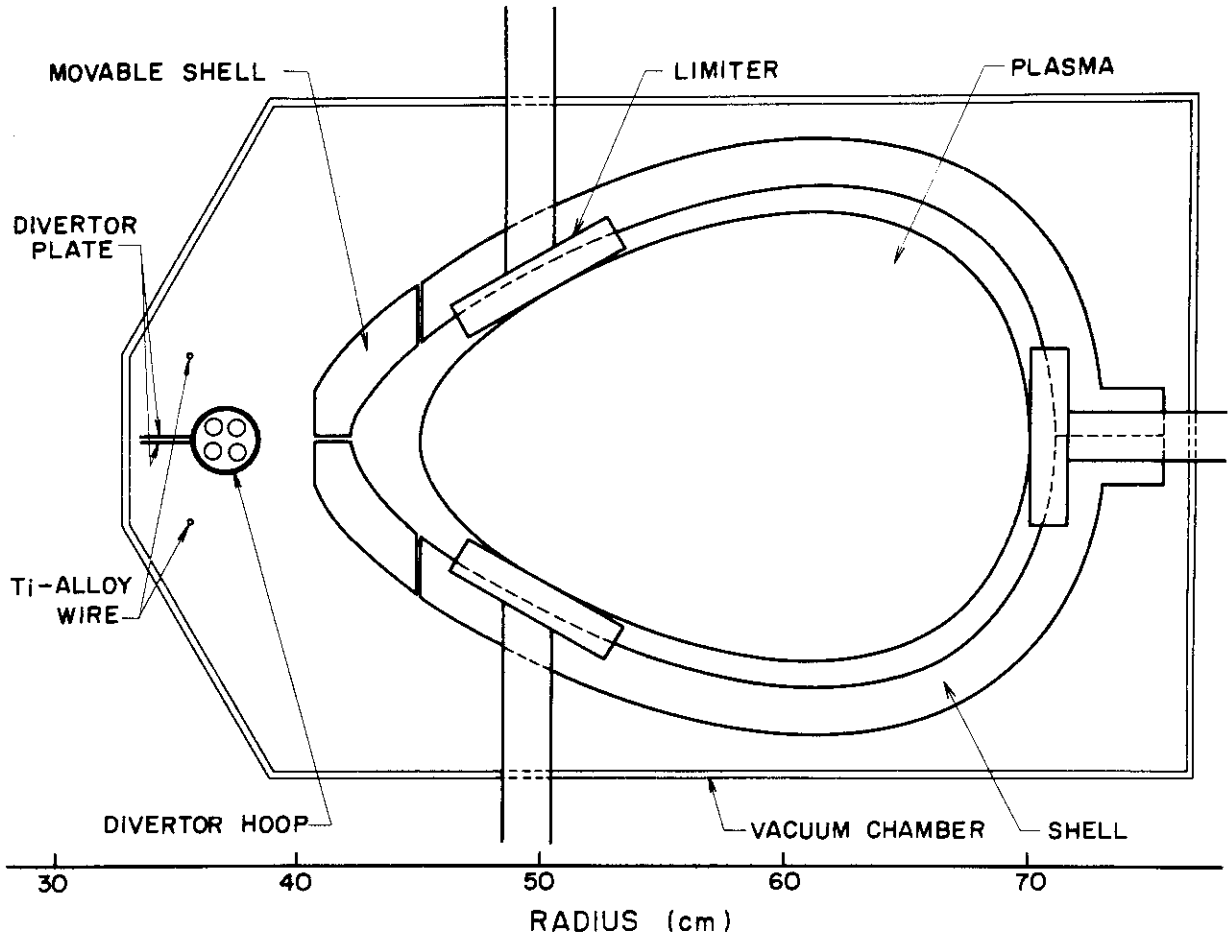

Fig. 2 Cross-section of the vacuum chamber.

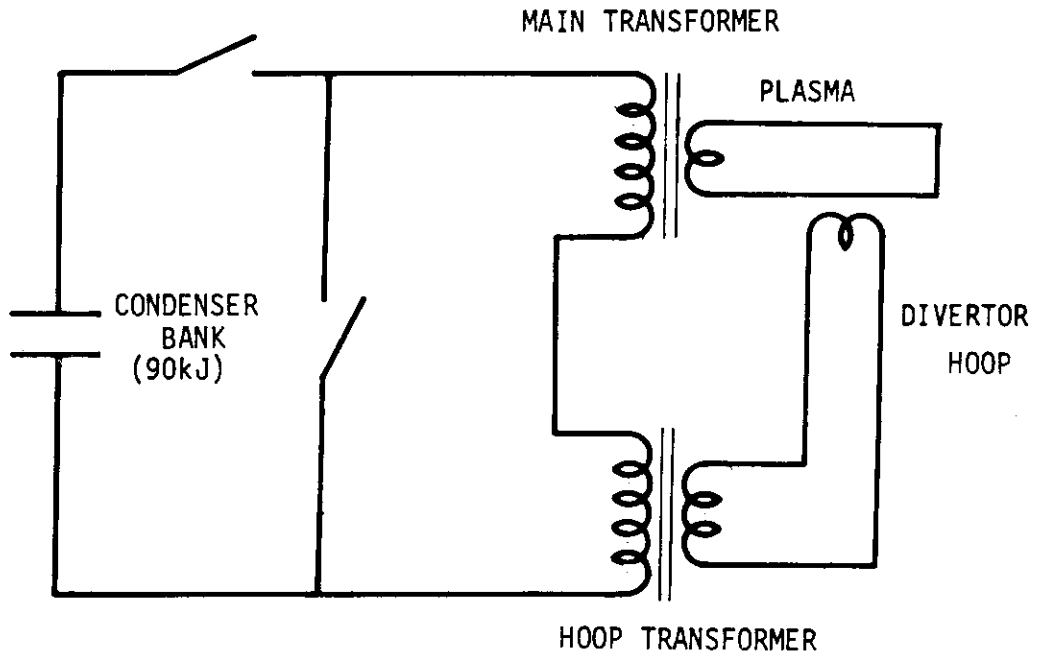

Fig. 3 Circuit diagram of power supply for plasma and divertor hoop.

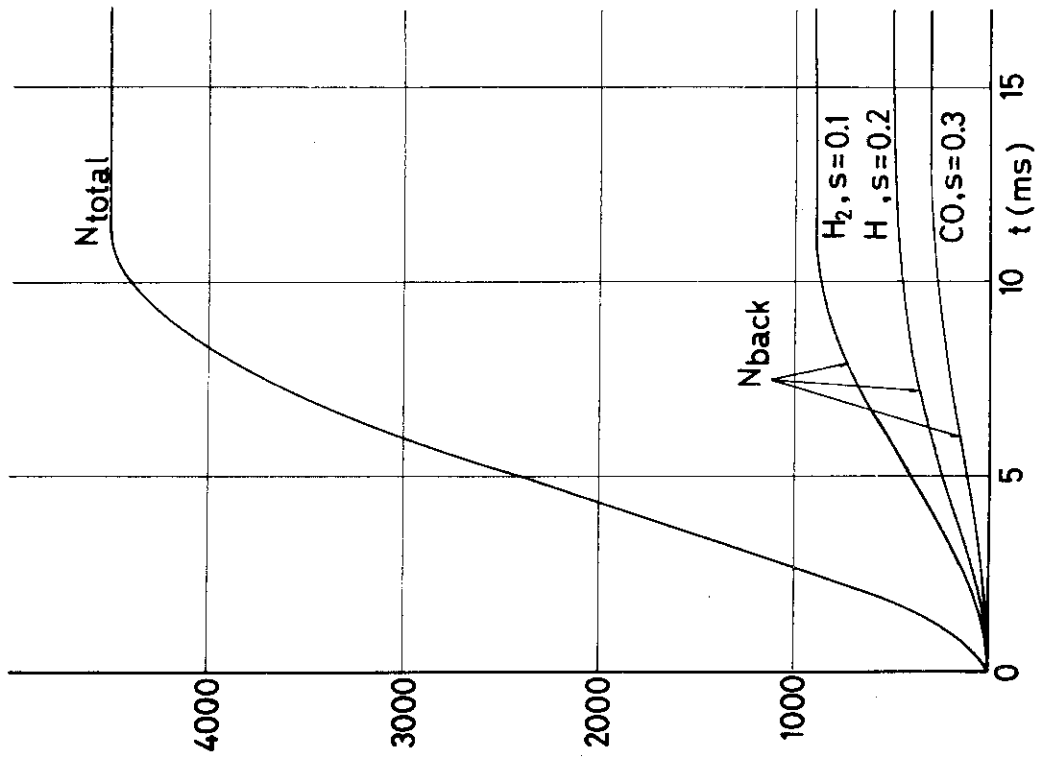

Fig. 5 Time-integrated influx and backstreaming flux to the plasma.

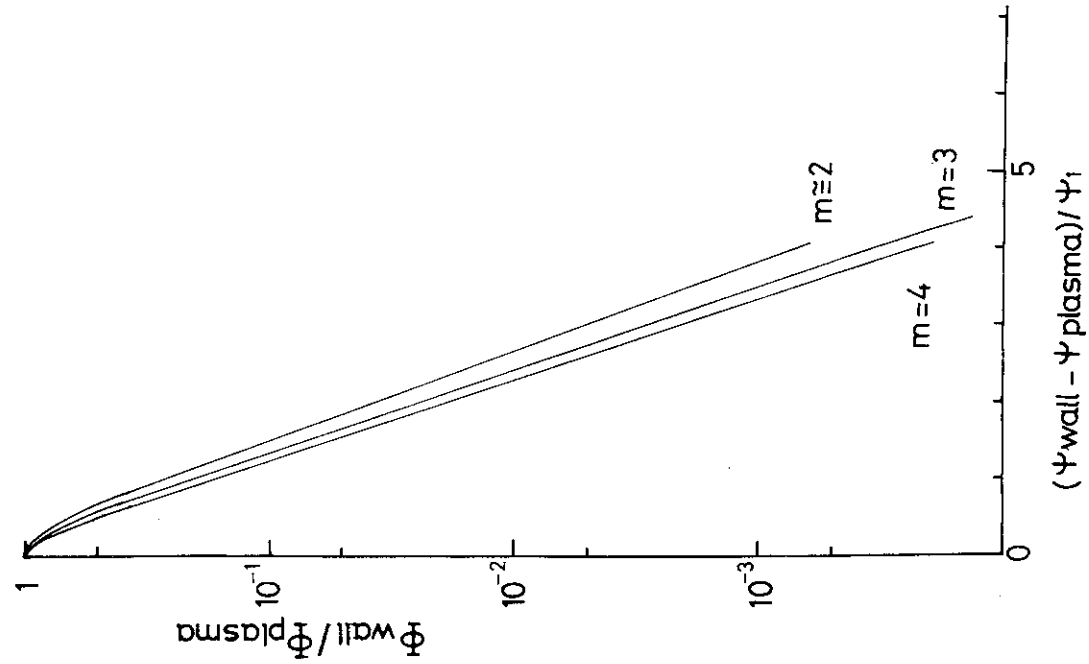

Fig. 4 Ratio of particle flux to the wall to total particle loss flux.

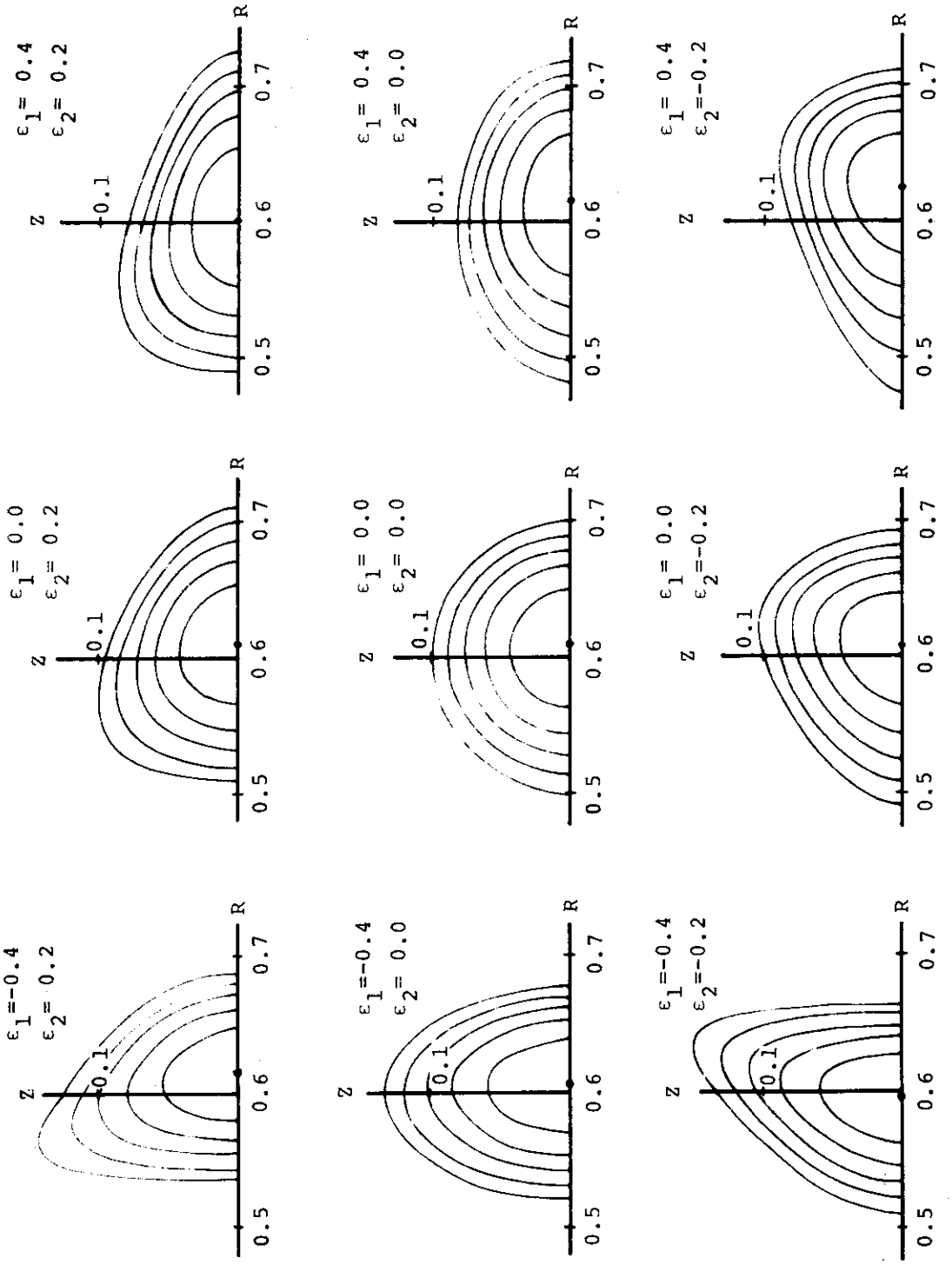

Fig. 6 Equi-psi lines of Eq. 2.

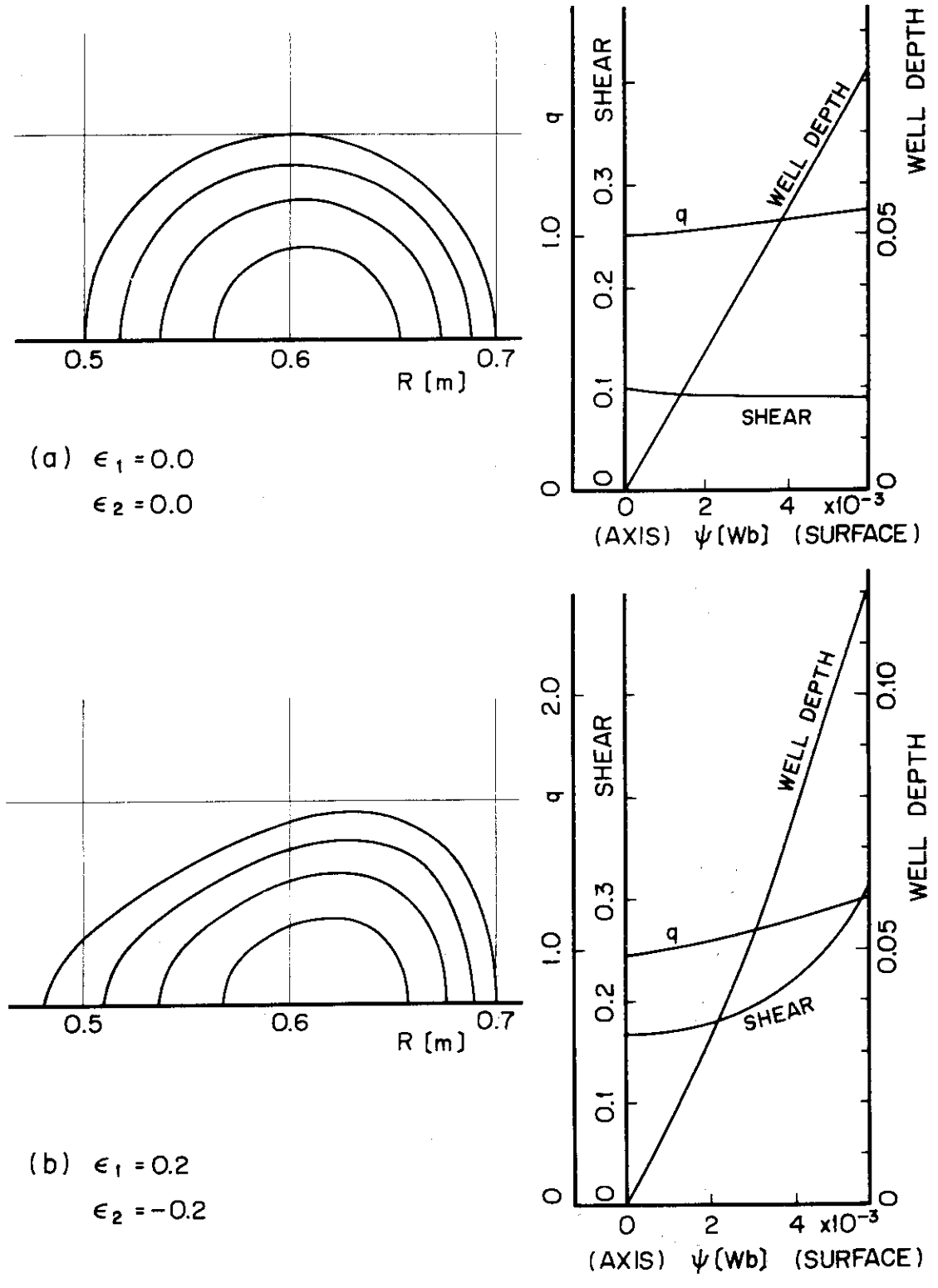

Fig. 7 Typical results of plasma equilibrium calculation.

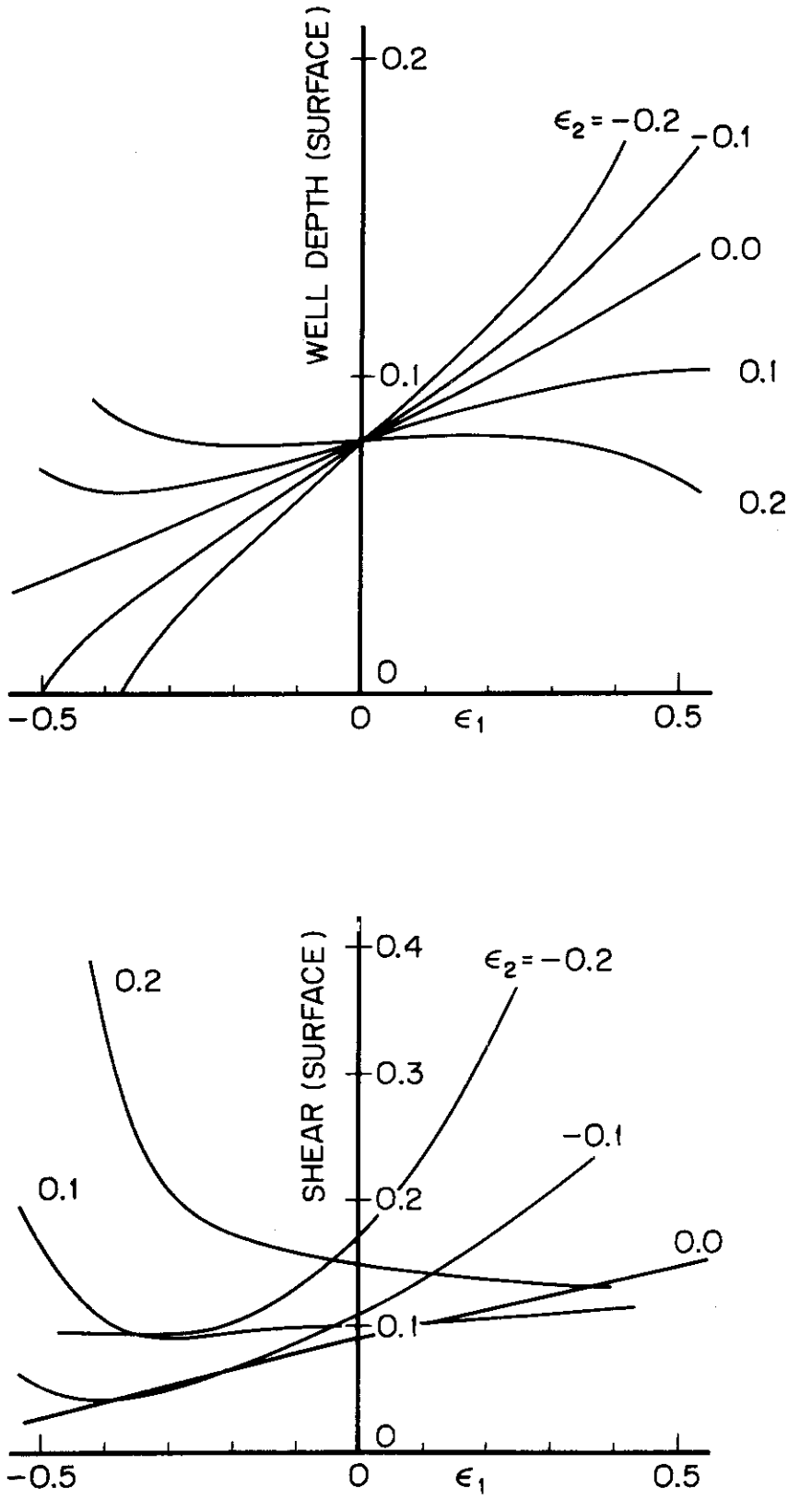

Fig. 8 Magnetic well depth and shear.

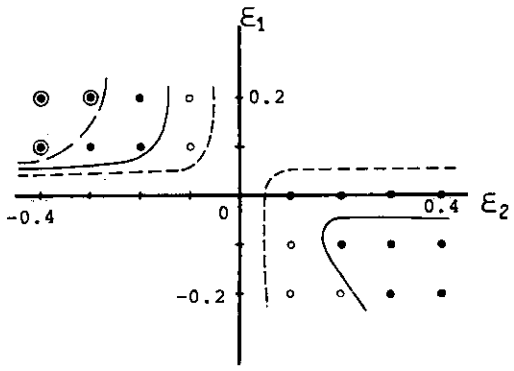

Fig. 9 Stability for discrete values of shape parameter ε_1 and ε_2.
◎ stable for q=1, β_p=2.0, 1.0, 0.5.
○ stable for q=1, β_p=1.0, 0.5.
● stable for q=1, β_p=0.5.

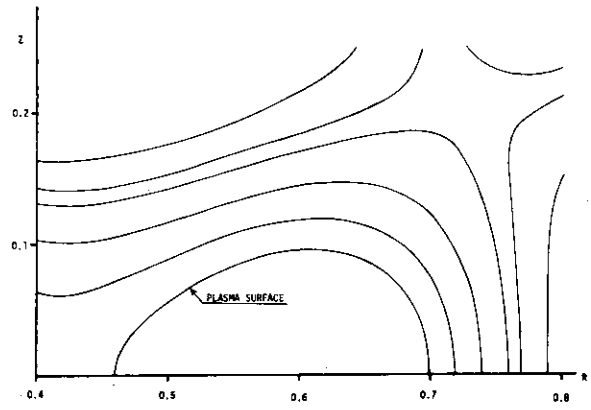

Fig. 10 Equi-psi lines of vacuum magnetic field.

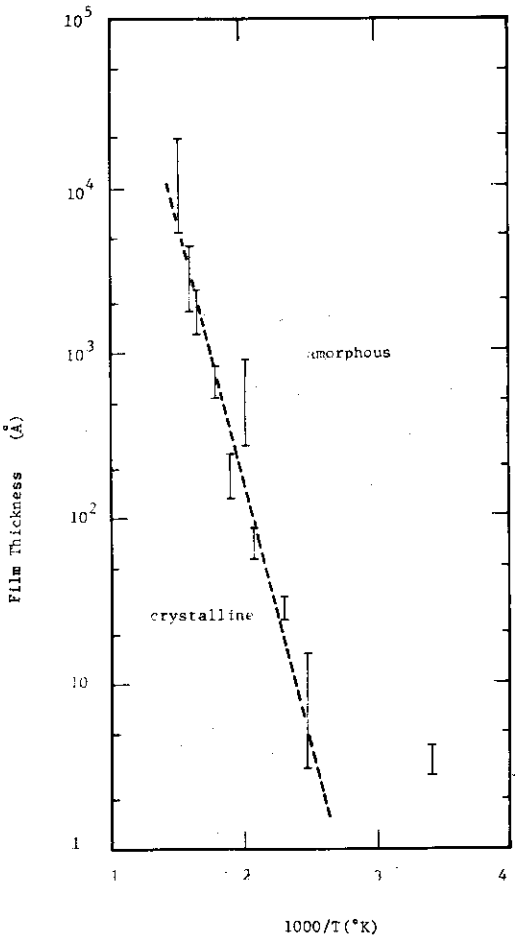

Fig. 11 Crystalline-to-amorphous transition observed by LEED.

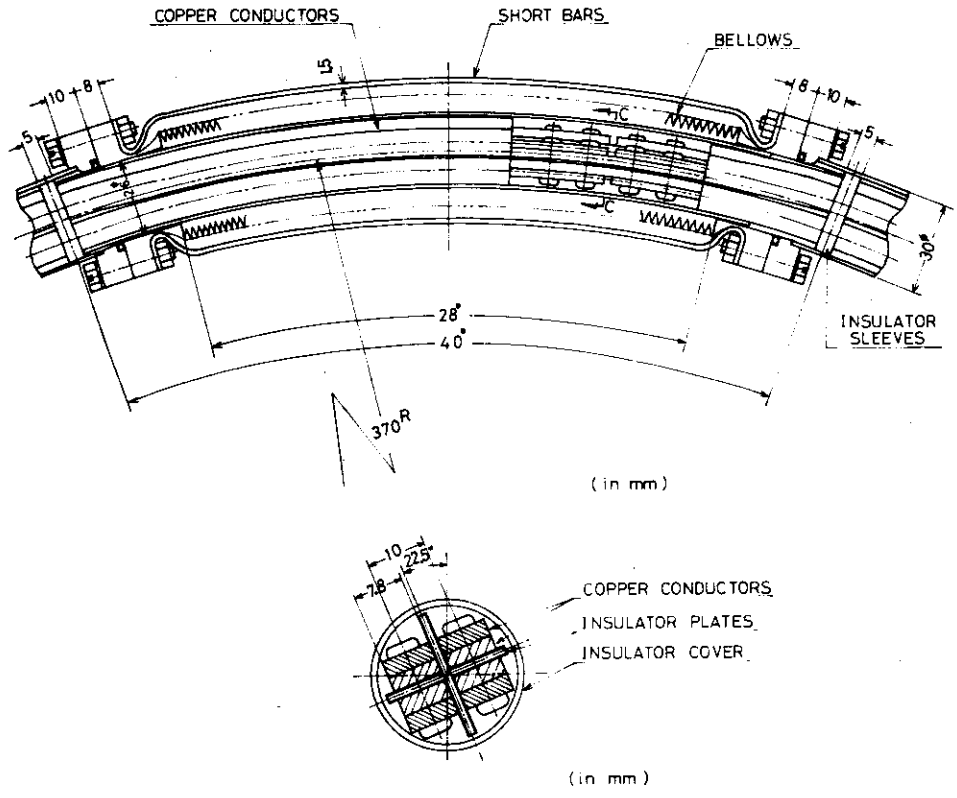

Fig. 12 Connecting joint of divertor hoop.

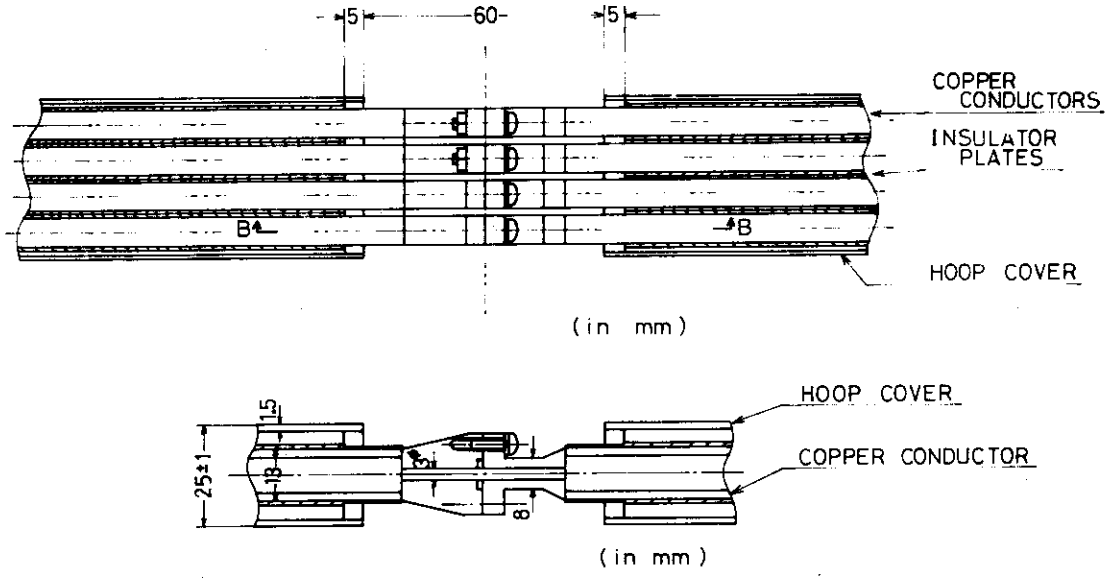

Fig. 13 Another type of divertor hoop joint.

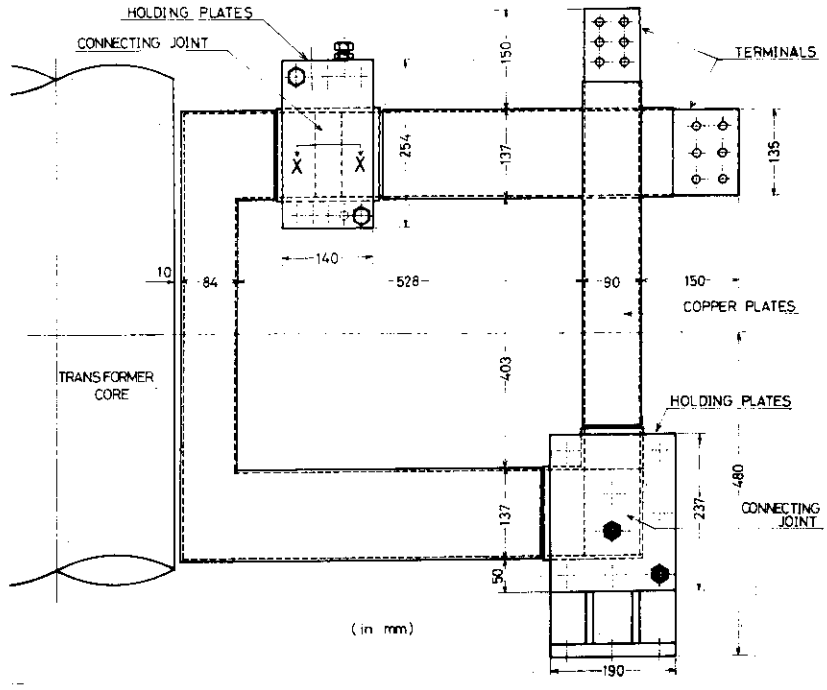

Fig. 14 Toroidal coil with joints.

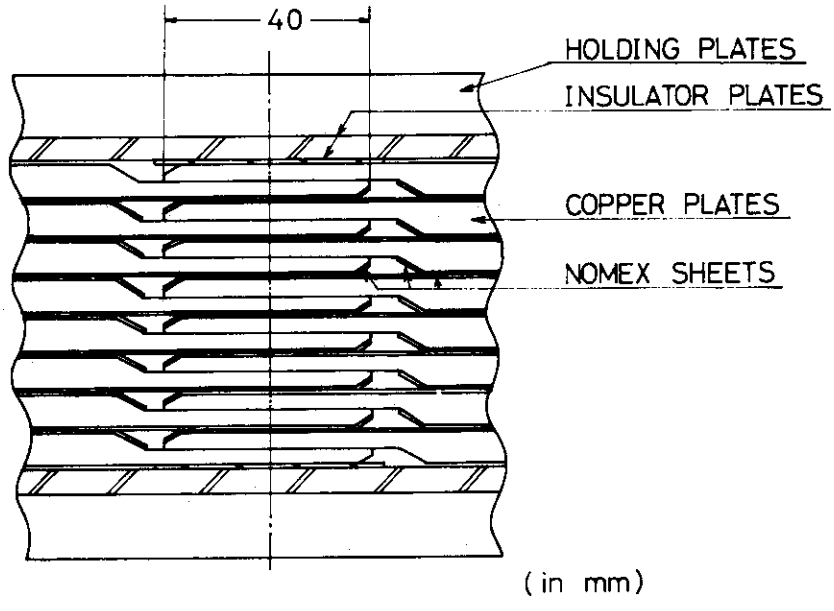

Fig. 15 Connecting joint (X-X section).

II. THEORY

1. Numerical analysis of properties of the axisymmetric plasma equilibrium

The computer code is developed to study the mhd equilibrium and the local stability condition of the axisymmetric plasma column with an arbitrary cross-section. The homogeneous distribution of the toroidal plasma current is assumed.

The calculation of the equilibrium is made using the general solution for the azimuthal magnetic flux function Ψ in the toroidal coordinate system[1]. The coefficients of this solution are numerically determined so that Ψ = constant on the given boundary of the plasma column and $\Psi = 0$ at the magnetic axis for a given value of the poloidal beta β_J. The critical plasma current is obtained by evaluating numerically Solov'ev's expression of the local stability[2].

The dependences of the equilibrium properties and maximum plasma current on the agree ratio and the poloidal beta were investigated in detail for the case of the circular cross-section and compared with the analytical calculation. They agree well in general. When the total plasma current J_φ, which is measured with the effective safety factor $q_a=(r_o/R_o)^2 I_o/J_\varphi$, is fixed, the safety factor at the magnetic axis q_{axis} decreases appreciably with the decrease of the aspect ratio and/or the increase of the poloidal beta. The maximum value of the total plasma current for the local stability is restricted because of this decrease of q_{axis}/q_a rather than the deformation of the magnetic surfaces near the magnetic axis.

The effects of the deformation of the cross-section are also investigated. The critical current can be increased by the deformation of the type $\varepsilon_2 \varepsilon_3 > 0$, as expected analytically[3], where the cross-section is assumed to be s: $(1+\varepsilon_2)(R-R_0)^2 + (1-\varepsilon_2)Z^2 - \varepsilon_3(R-R_0)^3 + 3\varepsilon_3(R-R_0)Z^2 - r_0^2 = 0$. The triangular deformation ε_3 was shown to be restricted by the appearance of the second magnetic axes at the sharpened edges of the boundary off the torus plane.

The results are shown in Figure 1 (for the circular cross-section) and Figure 2 (for the elliptic and/or triangular cross-section).

(M. Azumi, T. Tuda and M. Tanaka)

References

1) V. D. Shafranov: Soviet Phys. JETP 10, 775 (1960).
2) L. S. Solov'ev: Soviet Phys. JETP 26, 400 (1968).
3) M. Tanaka and T. Tuda: JAERI-M 4532 (August, 1971).

2. Singularities of the vacuum magnetic field around a noncircular plasma cylinder*

The vacuum magnetic field outside a particular class of cylindrical plasma equilibria with noncircular cross-sections are examined on the basis of a method due to Kerner, et al.[1] The exterior field which fits the boundary conditions on a prescribed plasma surface is obtained using complex functions, and the singularities of the resultant field are investigated.

(M. Tanaka and G. Iwata**)

References

1) W. Kerner, D. Pfirsch and H. Tasso: Nuclear Fusion 12, 433 (1972).

---

* Plasma Physics 15, 712 (1973).

** Department of Physics, Ochanomizu University.

3. The equilibrium of an axisymmetric torus with an elliptical cross-section*

A method is described to obtain a free boundary equilibrium of an axisymmetric torus with a noncircular plasma cross-section. An elliptic equation describing the vacuum magnetic field can be continued analytically into the complex plane to yield a normal hyperbolic equation. Then the exterior vacuum field around a given plasma equilibrium are expressed in terms of an integral along the plasma boundary. As an example the vacuum field outside an elliptical torus of high aspect ratio is constructed explicitly and its singularities are examined.

(M. Tanaka, T. Tuda and M. Axumi)

* J. Phys. Soc. Japan 34, 1641 (1973).

4. Long wavelength helical plasma equilibrium with a free boundary*

A method obtaining a straight free boundary equilibrium of helical symmetry is presented. The exterior vacuum field which fits the boundary conditions is determined using complex functions. The long wavelength m-fold ($m \geq 2$) helical equilibrium slightly distorted from a circular cylinder is obtained as well as m=1 fold equilibrium of finite amplitude.

(M. Tanaka, M. Azumi and T. Tuda)

* J. Phys. Soc. Japan 34, 1645 (1973).

5. Drift dissipative instabilities in tokamaks

Drift instabilities driven by the finite electrical conductivity in the tokamak configuration[1) 2)] are investigated on the basis of the two fluid model. The basic equations are; the continuity equations for ions and electrons, the equation of motion of the fluid and Ohm's law along the magnetic field (the perpendicular motion of ions and electrons is described by the guiding center drift due to the fluctuating electric field, pressure gradient, and toroidal curvature), and finally conservation equations of energy for ions and electrons. Linear stability analysis is done under the several assumptions (charge neutrality, absence of radial electric field in equilibrium, no radial localization of perturbations etc.).

For a strongly localized mode at the outer side of the torus along the field line the eigen function and corresponding eigenvalue (frequency and growth rate) are obtained analytically. In addition to the ion parallel viscosity, the electron thermal force is stabilizing when $\nabla T \cdot \nabla n > 0$. Also examined are the mode periodic along the field line. The fourth order differential equation which describe the variation of the perturbation along the field line is solved using the Fourier series. The resultant recurrence relations yield the dispersion equation, which was solved numerically. Typical examples of the unstable eigen functions are shown in Fig. 3, where $\omega_M/\omega_* = 0.3$, $\omega_*/D_e k^2 = 0.027$, $\nu k^2/\omega_* = 0.058$. Here $k = (qR)^{-1}$, D_e is the parallel diffusion coefficient of electrons, ν the ion parallel viscosity, and other notations are conventional. We find that the growth rate of the unstable mode increases as the perturbation is localized near the unfavourable region.

(M. Tanaka and T. Tuda)

References

1) B.B. Kadomtsev and O.P. Pogutse, Soviet Phys. JETP 31, 898 (1970).
2) C.W. Horton and R.K. Varma, Phys. Fluids 15, 620 (1972).

6. Behavior of impurity ions in a tokamak plasma

The steady-state distributions of oxygen impurity in various states of ionization and related energy losses in a tokamak plasma are studied numerically. An axisymmetric cylindrical mhd model is used to solve the steady-state coupled equations for the oxygen impurity concentrations taking account of neoclassical diffusion and successive ionization and recombination processes.

$$\frac{1}{r}\frac{d}{dr}r\left(D_k\frac{dO_k}{dr} - W_kO_k\right) + n_e\left(\alpha_{k-1}O_{k-1} - \alpha_kO_k\right) - n_e\left(\beta_{k-1}O_k - \beta_kO_{k+1}\right) = 0$$

$$k = 1,2,3, \ldots\ldots, 9$$

where O_k is the oxygen density, D_k is the neoclassical diffusion coefficient,[1] W_k the pinch velocity[1) 2)], α_k and β_k are the ionization and recombination rates[3)], respectively.

The energy losses due to the presence of impurity ions such as the ionization loss P_i, excitation loss P_{ex}[4)] and Bremsstrahlung loss P_{Br} are estimated using the following approximate formulae.

$$P_i = 1.6\times10^{-19}\sum_{k=1}^{8}\left[\chi_k n_e \alpha_k O_k + \frac{3}{2}T_e\beta_k O_k\right]$$

$$P_{Br} = 1.5\times10^{-38}\bar{Z}\, n_e^2\, T_e^{\frac{1}{2}}$$

$$P_{ex} = 3.2\times10^{-33}\chi_H\left(\frac{\chi_H}{T_e}\right)^{\frac{1}{2}}n_e\left[O_2e^{-15/T_e} + O_3e^{-16/T_e} + O_4e^{-16/T_e} + O_5e^{-20/T_e} + O_6\left(e^{-12/T_e} + e^{-83/T_e}\right) + 2O_7e^{-575/T_e} + 2O_8e^{-655/T_e}\right]$$

where χ_k and χ_H are the ionization potential for oxygen and hydrogen, respectively, and the other notations are standard.

In comparing with an experiment, the plasma parameters of an ST experiment[5)] are adopted. Some computed results are shown in Figs. 1 and 2. Figure 4 shows that the plasma axis is surrounded by the shells of oxygen ions in various states of ionization which is in qualitative agreement with the experimental observation[5)]. Figure 5 shows that near the plasma boundary the energy losses due to the ionization and excitation of oxygen impurity are the same order of magnitude as the power input by joule heating even though the total oxygen concentration amounts to only 2~4 %. This suggests a significant influence of

impurity ions on the energy balance of the tokamak discharge.

This work is a continuation of a preliminary consideration reported earlier[6], where the analytical results are obtained assuming a uniform background plasma.

(T. Tazima, M. Tanaka, M. Yoshikawa and K. Inoue)

References

1) F. L. Hinton, et al.: Phys. Rev. Letters 29, 698 (1972).
2) A. A. Ware: Plasma Physics and Controlled Nuclear Fusion Research, 1971, Vol. II, p. 411 (IAEA, Vienna 1971).
3) E. Hinnov: MATT-777 (1970).
4) D. F. Düchs: NRL Report 7340 (1971).
5) D. Dimock, et al: Plasma Physics and Controlled Nuclear Fusion Research, 1971, Vol. I, p. 451 (IAEA, Vienna, 1971).
6) M. Tanaka, et al: JAERI-M 4961 (September, 1972) (in Japanese).

7. Study of a gas-insulated plasma

The gas insulation of a high temperature plasma column initially suggested by Alfvén and Smårs[1] is now under study. The idea of the gas insulation has certain advantages: 1) the mhd instabilities are eliminated[2] or at least the growth rates are reduced[3], 2) it is possible to reduce the impurities in the plasma since the plasma is isolated from the wall by high pressure neutral gas,[1) 4)] 3) thus the wall might be free from the damages due to the radiation and charged particles, 4) the neutral gas blanket could play a role both in the injection of fuels and in carrying off reaction products, 5) the blanket system could be simple since the energy is converted by leading directly hot neutral gas, which is heated by the charged particles and radiation emitted from the plasma, to the heat exchanger.

Several authors[5) 6)] have investigated recently the energy balance and equilibrium of a plasma in the presence of surrounding neutral gas. However further investigations, especially concerning the effect of neutral gas on the energy balance and equilibrium in detail, are required to clarify the feasibility

of the gas blanket. With a mind to apply the gas insulation to tokamak-like devices by using a neutral gas vortex shown schematically in Fig. 6, the numerical study of the energy balance and equilibrium of the system is initiated.

(T. Tazima)

References

1) H. Alfvén and E. A. Smårs : Nature 188, 801 (1960).
2) A. G. Elfimov: Soviet Phys. Tech. Phys. 17, 592 (1972).
3) G. S. Murty: Arkiv Fysik 19, 511 (1961).
4) E. A. Smårs and R. B. Johansson: Phys. Fluids 4, 1151 (1961).
5) B. Lehnert: Nuclear Fusion 8, 173 (1968).
6) S. G. Alikhanov, I. K. Konkashbaev and P. Z. Chebotaev: Nuclear Fusion 10, 13 (1970).
7) G. K. Verboom and J. Rem: Plasma Physics 11, 703 (1973).

8. Thermal stability in an inhomogeneous D-T fusion plasma

The thermal stability is discussed in a radially inhomogeneous plasma in a D-T fusion reactor, solving the diffusion and the heat conduction equations numerically and analytically. When the injection of fuel is uniform, the plasma can be unstable only for the zeroth order mode, that is, the mode in which the temperature deviations increase over the entire plasma radius and higher order modes are always stable. This fact is clearly shown when perturbations of various mode numbers are applied. The stability criteria are similar to those found previously in the uniform plasma. The critical temperature, above which the plasma is stable, is shown in Table I.

It is shown that the feedback stabilization discussed previously can also be applicable. In the nonuniform injection of fuel, especially in the surface injection, temperature and density distributions are obtained. The results obtained so far seem to suggest the stable equilibria of the distribution may be possible in the surfac injection.

(H. Yamato* and M. Ohta)

* On leave from the Research and Development Center, Tokyo Shibaura Electric Co. Ltd.

Table I Critical temperature at the plasma center

D, K	Computer calculation		Analysis**
	$A_2 = 0$*	$A_1 = 0$*	
const.	29 keV	32 keV	38 keV
Bohm	22	19	18
classic	55	50	54

* $A_2=0$; The particle loss is dominant among the energy loss.
$A_1=0$; The thermal conduction loss is dominant.

** Density and temperature distribution are assumed to be parabolic.

Fig. 1 (a)

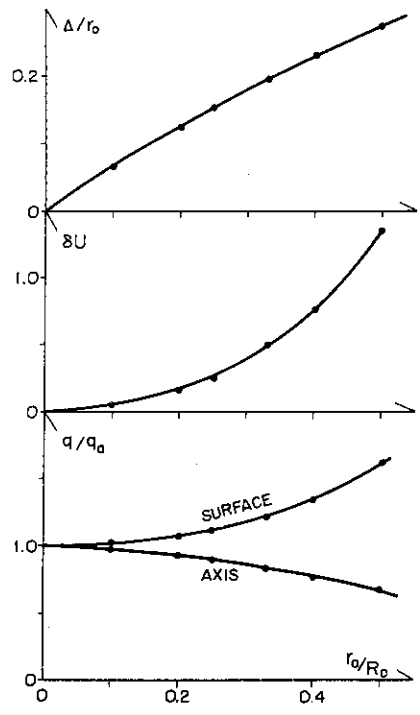

Fig. 1 (b)

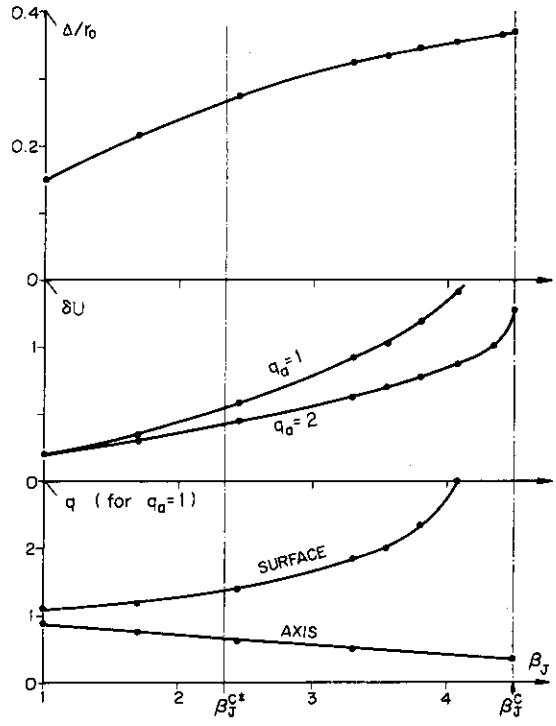

Fig. 1 (c)

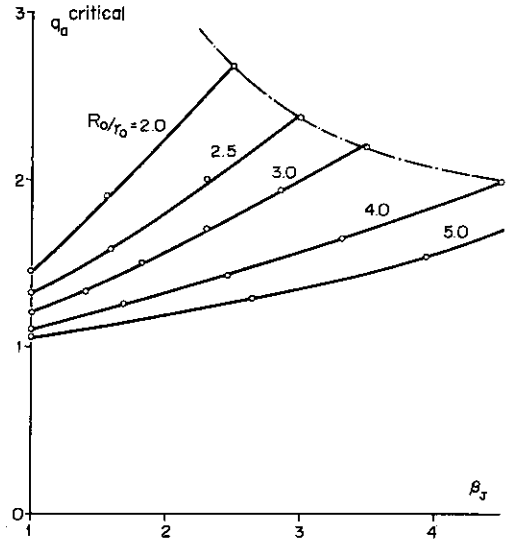

Fig. 1 Dependences of the equilibrium properties and the critical value of q_a on the aspect ratio R_0/r_0 and the poloidal beta β_J for the case of the circular cross-section (Δ: displacement of magnetic axis, δU: average magnetic well depth, q: safety factor, q_a: effective safety factor ($=(r_0/R_0)^2 I_0/J_\varphi$)). Fig. 1(a) is for $\beta_J=1.0$, and Fig. 1(b) is for a fixed value of $R_0/r_0=4.0$.

Fig. 2 (a)

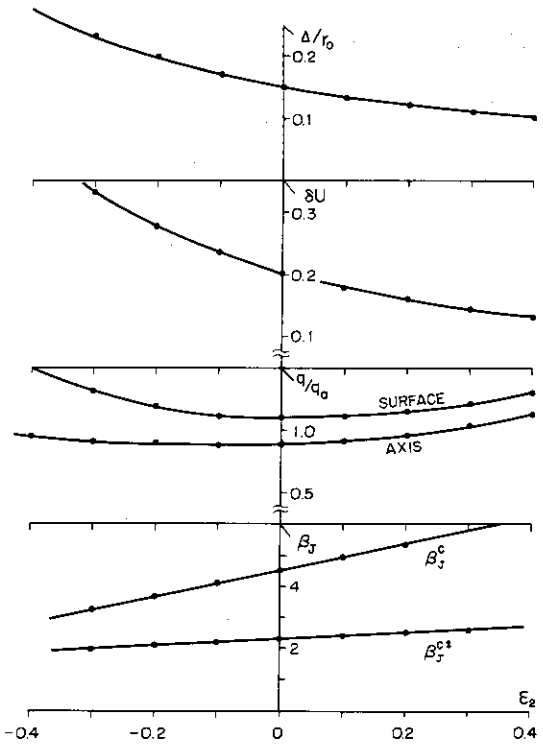

Fig 2 (b)

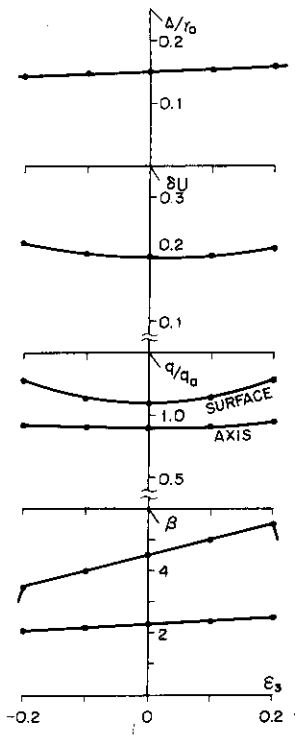

Fig. 2 (c)

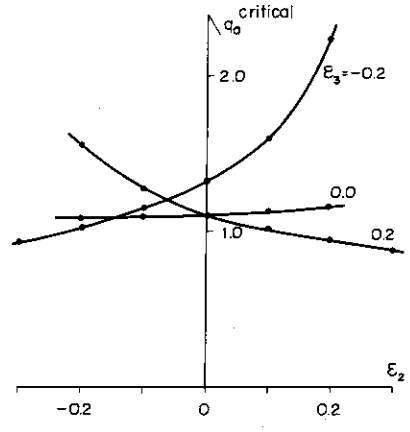

Fig. 2 Dependences of the equilibrium properties and the critical value of q_a on the elliptic and/or the triangular deformation where $R_0/r_0=4.0$ and $\beta_J=1.0$ except for the critical value of β_J (β_J^c and β_J^{c*} are the critical value of β_J on the appearance of the second magnetic axis and of the reverse current, respectively). Fig. 2(a) is for $\varepsilon_3=0$ and Fig. 2(b) is for $\varepsilon_2=0$.

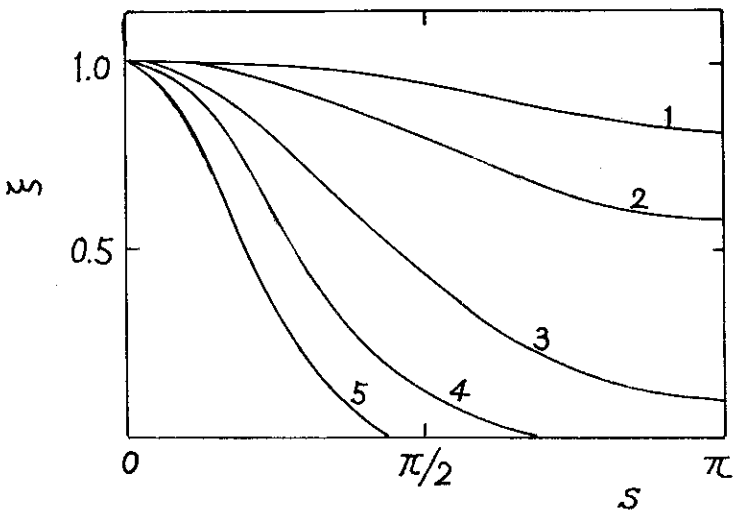

Fig. 3 Amplitudes of the density perturbation along the magnetic lines of force. A dimensionless quantity $B=(1+\lambda)c_s k/\omega_*$ is taken as a parameter, where $\lambda = T_i/T_e$, $k=(qR)^{-1}$, c_s is the sound velocity. Also $s=kz$, where z is the distance along field lines measured from the outer side of the torus. The values of B, frequencies and growth rates corresponding to the eigenfunctions of the figure are; 1) 1, $0.997\ \omega_*$, $4.62 \times 10^{-3}\omega_*$, 2) 0.5, $0.987\omega_*$, $1.21 \times 10^{-3}\omega_*$ 3) 0.225, $0.956\omega_*$, $3.26 \times 10^{-2}\omega_*$, 4) 0.1, $0.927\omega_*$, $4.77 \times 10^{-2}\omega_*$, 5) 0.05, $0.913\omega_*$, $5.09 \times 10^{-2}\omega_*$.

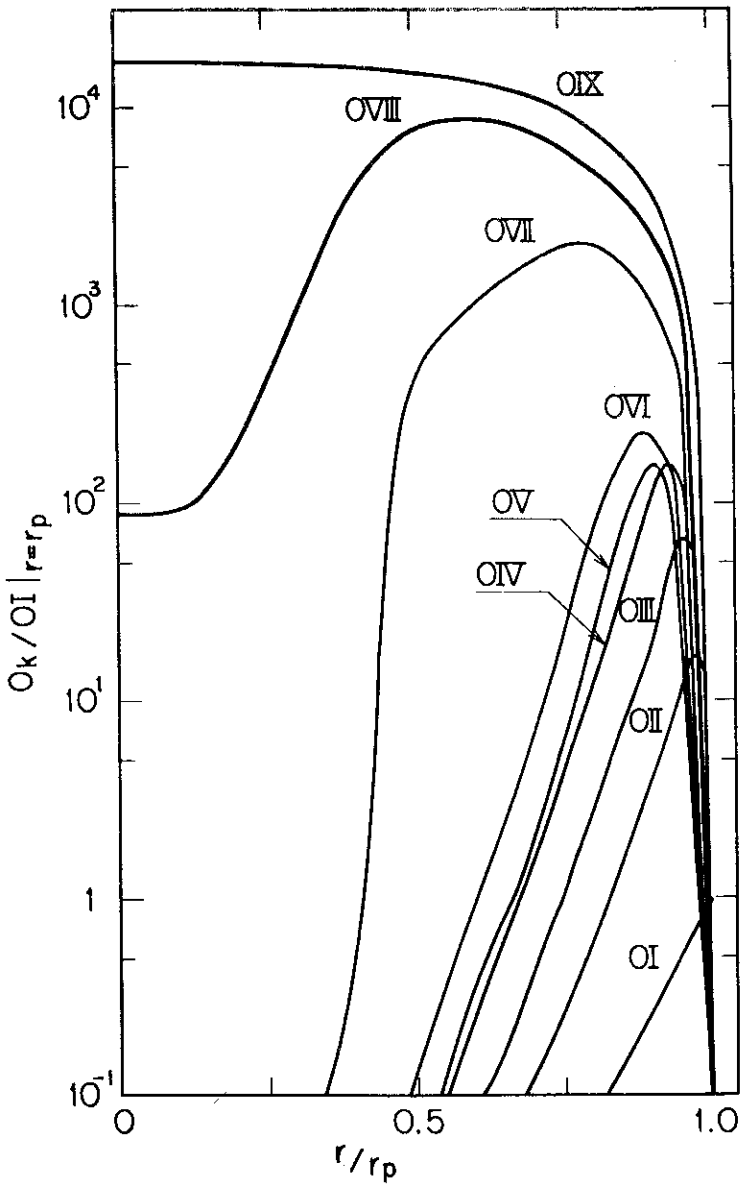

Fig. 4 Radial distributions of the neutral and ionized oxyzen densities normalized by $O_1(r=r_p) = 2 \times 10^{13}$ (particles/m^3)..

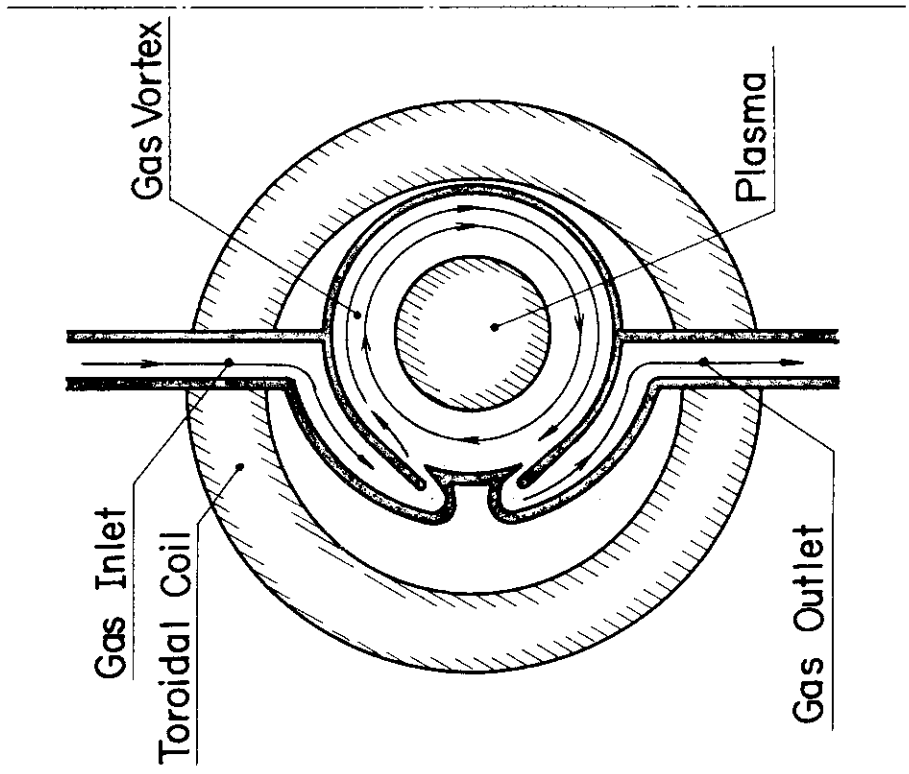

Fig. 6 Schematic drawing of a gas-insulated tokamak.

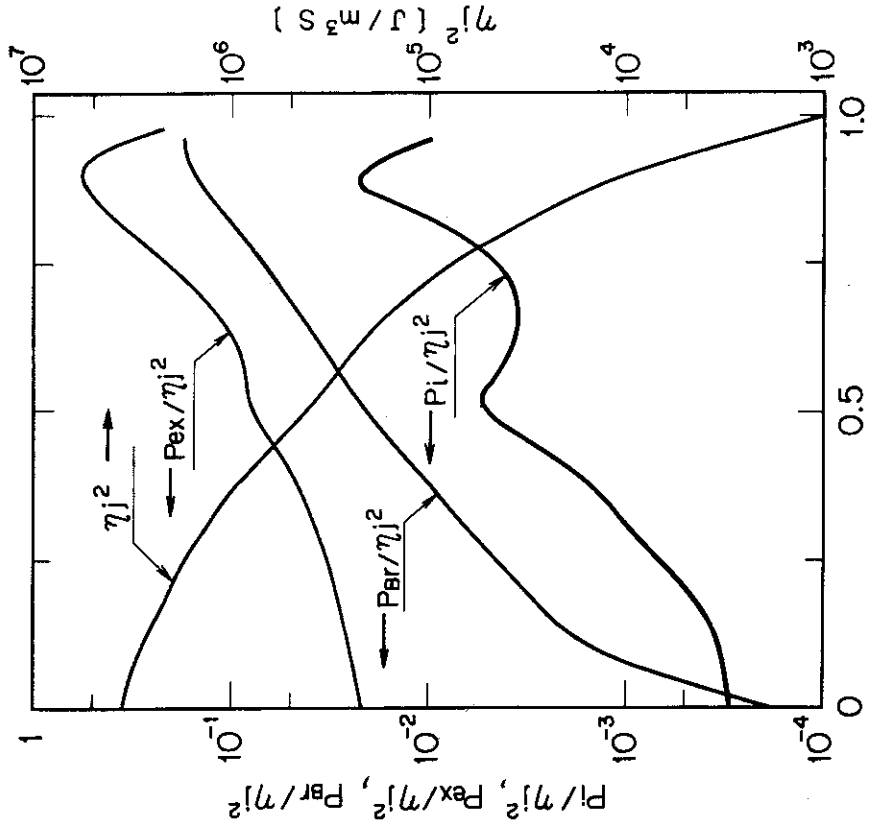

Fig. 5 Radial distributions of the energy losses due to oxygen impurity: P_{ex} (excitation losses), P_i (ionization losses) and P_{Br} (Bremsstrahlung losses) are normalized by the power input by joule heating ηj^2 (J/m^3·s).

APPENDICES

1. Publication list

Ohta, M., Shimomura, Y. and Takeda, T.: Analysis of hydromagnetic plasma stability by the finite element method, Nuclear Fusion 12, 271-272 (1972).

Takeda, T., Shimomura, Y., Ohta, M. and Yoshikawa, M.: Numerical analysis of magnetohydrodynamic Instabilities by the finite element method, Phys. Fluids 15, 2193-2201 (1972).

Ohta, M., Fujisawa, N. and Itoh, S.: Analysis of magnetic fields by the finite element method, J. Inst. Elec. Engrs Japan 92-A, 233-240 (1972). (in Japanese).

Sometani, T.* and Itoh, S.: The field distribution near a gap formed by sectionalized shells of a tokamak type apparatus, Japan. J. Appl. Phys. 11, 1181-1186 (1972).
(*Shizuoka University)

Kawasaki, S.* and Inoue, K.: Alpha-particle probing of current distribution in an axisymmetric plasma column, Nuclear Fusion 12, 387-389 (1972).
(*Guest scientist on leave from Kanazawa University)

Yamato, H.*, Ohta, M. and Mori, S.: Thermal stability of a spatially nonuniform plasma in a D-T fusion reactor, Nuclear Fusion 12, 604-606 (1972).
(*on leave from Tokyo Shibaura Electric Co., Ltd.)

Tanaka, M.: Two dimensional wave motion near the magnetic neutral line, J. Phys. Soc. Japan 32, 1377-1379 (1972).

Tanaka, M., Tuda, T., Fujisawa, N. and Takeda, T.: Major radius oscillation of a plasma column, J. Phys. Soc. Japan 32, 1680 (1972).

Tanaka, M., Tuda, T. and Takeda, T.: Stability effect of a resistive liner on kink instabilities, Nuclear Fusion 13, 119-120 (1972).

Itoh, S., Ohta, M., Fujisawa, N., Takeda, T., Maeno, M., Funahashi, A., Inoue, K., Kunieda, S., Matsuda, S., Tazima, T., Suzuki, N., Ohga, T., Matoba, T., Kasai, S., Sugawara, T.*, Toi, K. and Mori, S.: Tokamak apparatus (JFT-2) in JAERI, in Proceedings of Fifth European Conference on Controlled Fusion and Plasma Physics, Grenoble, France, August 21-25, 1972, Vol. I, p. 3 and Vol. II, p. 231.
(* on leave from Tokyo Shibaura Electric Co., Ltd.)

Itoh, S., Fujisawa, N., Funahashi, A., Kunieda, S., Takeda, T., Matoba, T., Kasai, S., Sugawara, T.*, Toi, K., Suzuki, N., Maeno, M., Inoue, K., Ohta, M., Matsuda, S., Ohga, T., Arai, T., Yokokura, K. and Mori, S.: Tokamak Experiment at JAERI, in Proceedings of Third International Symposium on Toroidal Plasma Confinement, Garching, West Germany, March 26-30, 1973, Paper B4.
(*on leave from Tokyo Shibaura Electric Co., Ltd.)

Kitsunezaki, A., Maeda, H., Shimomura, Y. and Yoshikawa, M.: Design of a tokamak device with an axisymmetric divertor, in Proceedings of Third International Symposium on Toroidal Plasma Confinement, Garching, West Germany, March 26-30, 1973, Paper G2.

Tamura, S., Yamato, H.*, Nagashima, T., Ohtsuka, H., Arizono, S., Shiina, T., Yoshikawa, M. and Mori, S.: Confinement and fluctuation studies in the JAERI hexapole, in Proceedings of Fifth European Conference on Controlled Fusion and Plasma Physics, Grenoble, France, August 21-25, 1972, Vol. I, p. 94 and Vol. II, p. 240.
(*on leave from Tokyo Shibaura Electric Co., Ltd.)

Nagashima, T., Arizono, S., Yamato, H.*, Ohtsuka, H., Tamura, S., Shiina, T., Yoshikawa, M. and Mori, S.: Observation of collisionless drift waves in the JAERI hexapole, in Proceedings of Third International Symposium on Toroidal Plasma Confinement, Garching, West Germany, March 26-30, 1973, Paper C5.
(* on leave from Tokyo Shibaura Electric Co., Ltd.)

Ohta, M., Yamato, H.* and Mori, S.: Summary of tokamak system, in Proceedings of International Working Sessions on Fusion Reactor Technology, Oak

Ridge, U.S.A., June 28-July 2, 1971, CONF-710624, 350-351.
(* on leave from Tokyo Shibaura Electric Co., Ltd.)

Yamato, H.*, Ohta, M. and Mori, S.: Numerical analysis of thermal stability in an inhomogeneous D-T fusion plasma, in Proceedings of Texas Symposium on the Technology of Controlled Thermonuclear Fusion Experiments and the Engineering Aspects of Fusion Reactors, Austin, U.S.A., November 20-22, 1972, Paper Session I-4.
(* on leave from Tokyo Shibaura Electric Co., Ltd.)

Matoba, T., Funahashi, A. and Itoh, S.: Scattering measurement in JFT-2 tokamak with a ruby laser, in Proceedings of Japan-U.S. Seminar "Laser Interaction with Matter", Kyoto, Japan, September 24-29, 1972, 413-419.

Matoba, T.*: Measurements of laser-produced plasmas from lithium targets by retarding potenial probe, Japan. J. Appl. Phys. 11, 770-771 (1972).
(* Kyoto University, now at JAERI)

Toi, K.*, Hayase, K.** and Okuda, T.**: Radial distributions of Z-current and electron density in a screw-pinch discharge, J. Phys. Soc. Japan 33, 1500 (1972).
(* Nagoya University, now at JAERI, ** Nagoya University)

Azumi, M.* and Mohri, A.**: Plasma confinement in toroidal ringless quadrupole, Phys. Letters 42A, 81-82 (1972).
(* Kyoto University, now at JAERI, ** Kyoto University)

Takeda, S.* and Funahashi, A.**: Three-body recombination and its transition to dissociative recombination, in Proceedings of Seminar on Gas Breakdown and Its Fundamental Processes, Tokyo, Japan, October 3-6, 1972, 17-20.
(* Nagoya University, ** Nagoya University, now at JAERI)

Yoshikawa, M.*, Gilleland, J.**, Ohkawa, T.**, Tamano, T.**, Meade, D.*** and Jernigan, T.***: Effect of field errors on the plasma confinement in the d.c. octopole, Gulf-GA-A-12006 (September, 1972) 41 pp.
(* Gulf General Atomic Inc., now at JAERI, ** Gulf General Atomic Inc., ***University of Wisconsin)

Suzuki, N., Funahashi, A. and Itoh, S.: Fundamental quantities and data of plasma physics for the experiments in JFT-2, JAERI-M 4726 (February, 1972) 98 pp.

Matsuda, S. and Yoshikawa, M.: Influence of the error field on the plasma confinement in the tokamak device, JAERI-M 4842 (June, 1972) 39 pp. (in Japanese).

Takeda, T., Shimomura, Y., Ohta, M. and Yoshikawa, M.: Numerical analysis of the magnetohydrodynamic instabilities of cylindrical and toroidal plasma by the finite element method, JAERI-M 4890 (July, 1972) 44 pp.

Thermonuclear Fusion Laboratory (JFT-2 Group): Plans for the experiments in the JFT-2 tokamak with emphasis on confirmation of the available data, JAERI-M 4923 (August, 1972) 31 pp. (in Japanese).

Tazima, T., Takeda, T. and Itoh, S.: Numerical calculation of the space-time evolution of tokamak discharge plasmas, JAERI-M 4941 (August, 1972) 53 pp. (in Japanese).

Tanaka, M., Yoshikawa, M., Inoue, K. and Tazima, T.: Behavior of impurity ions in a tokamak plasma, JAERI-M 4961 (September, 1972) 13 pp. (in Japanese).

Matsuda, S., Ohga, T., Suzuki, N. and Fujisawa, N.: Measurements of vertical magnetic fields in JFT-2, JAERI-M 5021 (October, 1972) 27 pp. (in Japanese).

Thermonuclear Fusion Laboratory: Annual report of JAERI Thermonuclear Fusion Laboratory (for period ending March 31, 1972), JAERI-M 5029 (October, 1972) 65 pp.

Matsuda, S.: Effect of the dynamic limiter on plasma diffusion, JAERI-M 5035 (November, 1972) 14 pp. (in Japanese).

Study Committee on Thermonuclear Fusion Research, Tokai, JAERI, Report of the Tokai meeting on toroidal experiments, JAERI-M 5135 (February, 1973) 127 pp. (in Japanese).

Kawasaki, S.*, Inoue, K. and Takeda, T.: Measurement of the plasma current distribution in a tokamak device by alpha-particles injected transverse to the toroidal magnetic field (Numerical calculations of the particle orbits and experimental arrangement), JAERI-M 5146 (February, 1973) 31 pp.
(* Guest scientist on leave from Kanazawa University)

Maeno, M., Matoba, T., Fujisawa, N. and Itoh, S.: Electromagnetic diagnostic instruments for JFT-2, JAERI-M 5204 (March, 1973) 52 pp. (in Japanese).

2. Budget and personnel

Budget

(in unit of million yen)

	FY 1970[1]	FY 1971	FY 1972	FY 1973
Scientific program (excluding staff & administration cost)	(550.)[2] 170.25[3]	305.12[3]	408.696[3]	433.946
Building & Establishment	(273.)[4] 82.[5]	90.[5]	101.[5]	26.369

(1) From April 1970 to March 1971,

(2) Financial obligation from FY 1970 to 1972 to construct JFT-2 including a DC power supply,

(3) Including cash of the financial obligation for each year,

(4) Financial obligation from FY 1970 to 1972 of a building for JFT-2,

(5) Cash of the building of the financial obligation for each year.

Number of staffs of the Laboratory

	FY 1970	FY 1971	FY 1972	FY 1973[4]
Regular staff[1]	21	27	32	42
Staff on loan	2	1	2[2]	3[2]
Guest scientist	1	2	2[3]	3[3]

(1) Including scientists, technicians, secretaries and managers. Numbers in the table are at the end of each fiscal year.

(2) On loan from the Research and Development Center, Tokyo Shibaura Electric Co., Ltd. (FY 1972) and from the same and the Atomic Energy Research Laboratory, Hitachi Ltd. (FY 1973).

(3) From Kanazawa and Kyoto University (FY 1972) and Ochanomizu, Tokyo and Kanazawa University (FY 1973).

(4) Expected.